Marine Physical Laboratory

Observations of the 1 Hz - 10 kHz Acoustic Ambient Noise Field Near the Surf Zone in the 1995 Adaptive Beach Monitoring Experiment

G. L. D'Spain, L. P. Berger, W. S. Hodgkiss,
W. A. Kuperman, and W. K. Melville

Supported by the
Chief of Naval Research
Contract N00014-93-D-0141 (DO#10)

MPL Technical Memorandum 454

MPL-U-11/96
October 1996

University of California, San Diego
Scripps Institution of Oceanography

REPORT DOCUMENTATION PAGE

Form Approved OMB No. 0704-0188

1. Agency Use Only (Leave Blank).

2. Report Date. November 1996

3. Report Type and Dates Covered. Technical Memorandum

4. Title and Subtitle.
Observations of the 1 Hz - 10 kHz Acoustic Ambient Noise Field Near the Surf Zone in the 1995 Adaptive Beach Monitoring Experiment

5. Funding Numbers.
N00014-93-D-0141
(DO#10)

Project No.
Task No.

6. Author(s).
G. L. D'Spain, L. P. Berger, W. S. Hodgkiss, W. A. Kuperman, and W. K. Melville

7. Performing Monitoring Agency Names(s) and Address(es).
University of California, San Diego
Marine Physical Laboratory
Scripps Institution of Oceanography
San Diego, California 92152

8. Performing Organization Report Number.
MPL-U-11/96
MPL TM-454

9. Sponsoring/Monitoring Agency Name(s) and Address(es).
Chief of Naval Research
Department of the Navy
800 North Quincy Street
Arlington, VA 22217-5660
Code 321US

10. Sponsoring/Monitoring Agency Report Number.

11. Supplementary Notes.

12a. Distribution/Availability Statement.
Approved for public release; distribution is unlimited.

12b. Distribution Code.

13. Abstract (Maximum 200 words).

The ABM '95 experiment was conducted in May and June of 1995 on the Camp Pendleton Marine Base in Southern California. Several institutions participating in the experiment deployed various types of sensor systems. Data collected by two bottom hydrophone arrays, the moored sonobuoys, and the land-based air acoustic array are presented. An extensive set of environmental and ancillary data were also collected to support these measurements. Observations of the properties of the background sound field from 1 Hz to 10 kHz are presented. Signals generated by shs, amphibious craft, and aircraft, although prevalent in the data, are excluded from the discussion.

14. Subject Terms.
Envioronmental and ancillary data, near-shore environment, ambient noise field, air acoustic fields

15. Number of Pages. 77

16. Price Code.

17. Security Classification of Report.	18. Security Classification of This Page.	19. Security Classification of Abstract..	20. Limitation of Abstract.
Unclassified	Unclassified	Unclassified	None

Observations of the 1 Hz - 10 kHz Acoustic Ambient Noise Field near the Surf Zone in the 1995 Adaptive Beach Monitoring Experiment

G. L. D'Spain, L. P. Berger, W. S. Hodgkiss, W. A. Kuperman, and W. K. Melville

Marine Physical Laboratory
Scripps Institution of Oceanography
San Diego, CA 92152

ABSTRACT

The purpose of this paper is to present observations from underwater and air acoustic measurements near the surf zone, a region where few results have been reported. The measurements were made along the Southern California coast in early summer of 1995. Underwater acoustic sensors included two 64-element, bottom hydrophone arrays 3.4 km offshore in 20-m water, and moored sonobuoys, containing either an omnidirectional broadband hydrophone or a directional "DIFAR" sensor, at distances of 1.2 km to 4.5 km offshore. Air acoustic measurements were made by a six-element microphone array on land. Complementing these acoustic measurements were various types of environmental measurements. Examination of the data reveal spectral lines generated by the operation of 21 land-based water pumps up to 16 km inland, as well as by two sanitation pumps on an offshore island 77 km distant. The underwater spectral levels from 50 Hz to 1 kHz are, on average, 20 to 30 dB higher at night than during the day due to the unusual chorusing behavior of fish, believed to be members of the croaker (Sciaenidae) family. Another, as yet unidentified, biological source(s) existing seaward of the arrays, generates 50-250 Hz pulses at regular 4-8 sec intervals intermittently throughout the experiment. A broad spectral peak occurs at 3.5 kHz in sonobuoy data collected 1.5 km from shore and decays with distance offshore. Rather than coming from the surf zone, this energy, whose spectral shape agrees closely with published measurements of snapping shrimp noise, emanates from a kelp bed region. Biological sounds dominate the underwater noise field and can be easily misinterpreted as surf noise. Efforts to detect surf noise in the 250-400 Hz band by endfire beamforming with the bottom hydrophone array oriented perpendicular to shore are inconclusive -- although the landward endfire spectral levels generally are higher than those from the seaward direction during periods when no obvious interfering sources are present, the correlation with environmental data is weak. Reasons why the underwater sensors may not have detected surf noise, in addition to the fact that biologics dominate the noise field, are that the water depth decreases too slowly with distance offshore, the presence of a kelp bed 1-2 km offshore attenuates both incoming ocean surface waves and the underwater surf-generated sounds, and deep water swell from the west and northwest are shielded by offshore islands. In contrast, the air acoustic data are dominated by surf noise. The shape of the ratio of the spectrum during wave breaking to that during a quiet period shows a broad peak centered around 4 kHz, coincidentally similar to the broad 3.5 kHz peak in the near-shore sonobuoy data. The spectral ratio shape, rather than being a property of the source, is dictated to a large extent by air acoustic propagation conditions. Correcting the received spectrum for propagation effects yields a surf "source" spectrum with a 5-6 dB/octave roll-off from 1-1.3 kHz and 5-10 kHz.

Observations of the 1 Hz - 10 kHz Acoustic Ambient Noise Field near the Surf Zone in the 1995 Adaptive Beach Monitoring Experiment

G. L. D'Spain, L. P. Berger, W. S. Hodgkiss, W. A. Kuperman, and W. K. Melville

Marine Physical Laboratory
Scripps Institution of Oceanography
San Diego, CA 92152

INTRODUCTION

The near-shore environment represents the confluence of three complicated media, the atmosphere, the ocean, and the solid earth. Processes such as the saturation of the sandy seashore by ocean water, sediment transport by wave action and longshore currents, entrainment of air by breaking waves, and the ejection of sea spray into the air blurs the boundaries between these media. Understanding the generation of mechanical wave energy, both from deterministic manmade sources as well as naturally-occurring ambient noise sources, and the propagation of this energy within, and the coupling between, these three media, provides both scientific and ocean engineering challenges.

Few measurements of the seismoacoustic fields in this environment have been made. Those of the underwater sounds produced by breaking surf made in the early 1980's [1] are a notable exception. More recent measurements (e.g., [2]) are beginning to fill the void. The purpose of this paper is to present some observations of the underwater and air acoustic fields from measurements made in the near-shore Adaptive Beach Monitoring pilot experiment (hereafter referred to as ABM 95).

The ABM 95 experiment was conducted in May and June of 1995 on the Camp Pendleton Marine Base in Southern California. Several institutions participating in the experiment deployed various types of sensor systems; these are listed in Appendix I. In this paper, data collected by the two bottom hydrophone arrays, the moored sonobuoys, and the land-based air acoustic array are presented. An extensive set of environmental and ancillary data, listed in Appendix II, were also collected to support these measurements.

The general location of the experiment in the Southern California area is shown in Fig. 1. The small box in the figure indicates the position of the Camp Pendleton base, on the coast at 33.3° N 117.5° W between the cities of Oceanside and San Clemente. In Fig. 2, the part of the Camp Pendleton operations chart where most of the experiment was conducted is shown. The offshore locations of the two bottom arrays are plotted as two straight lines, and the moored sonobuoy positions are plotted as solid triangles and circles. On shore, the solid square at the northwest end of Red Beach signifies the approximate position of the 6-element microphone array.

Observations of the properties of the background sound field from 1 Hz to 10 kHz are presented in this paper. Signals generated by ships, amphibious craft, and aircraft, although prevalent in the data, are excluded from the discussion. Sect. I provides a description of the sensor systems' hardware, followed by a summary of the environmental observations in Sect. II. In Sect. III, general observations of the underwater noise field, including land-based cultural sounds and underwater biological sounds, are presented. The data processing results for identification and examination of the acoustic fields generated by breaking surf appear in Sect. IV. Finally, a list of conclusions from this work is given in Sect. V.

I. DESCRIPTION of the HARDWARE

This section describes the hardware used to make the underwater and air acoustic measurements presented in this paper. Appendix I contains a list of all the sensor systems deployed during the ABM 95 experiment.

A. Two Hydrophone Line Arrays

The two bottom hydrophone line arrays used in the experiment are large-dynamic-range, digital, line arrays. The large dynamic range is provided by 24-bit A/D converters located adjacent to each hydrophone element at the wet end, thereby reducing the possibility of cross-talk and other electronic self noise. The arrays are constructed in modular fashion of from one to four interchangeable subarrays. Each subarray contains 16 low-frequency hydrophone channels (1 to 750 Hz) spaced at equal intervals of 1.875 m (equal to half-wavelength spacing at 400 Hz). These data acquisition channels have been calibrated in amplitude, with an uncertainty of ± 0.5 dB, and in phase. Included in each subarray are four additional, equally-spaced hydrophones whose outputs are fed into nine narrowband filters (the filters' center frequencies occur in 0.5-kHz increments from 9.0 kHz to 13.0 kHz) to provide acoustic element localization (AEL) capability. Additional information on the array design and hardware are provided in [3].

During the ABM 95 experiment, two arrays, each composed of 4 subarrays, 64 low-frequency elements, and 118.125 m total aperture, were placed on the ocean bottom in 20 m of water about 3.4 km offshore of Las Pulgas Beach, Camp Pendleton. Both arrays were nearly straight, with the first being parallel to the coastline and the second nearly perpendicular to it. Data from the arrays were sent back by fiber-optic cable to a data acquisition van on shore where it was recorded almost continuously over a 2.5-week period, from 24 May - 14 June, 1995.

To localize the array elements, 11 kHz and 12 kHz acoustic pings were transmitted to the arrays' AEL phones from a surface ship at ranges of about 0.5 km and at various azimuths [4]. Once the AEL phone positions were determined, interpolation was used to obtain the 64 low-frequency element locations for each array. Fig. 3 is a plan view of the element positions. As an independent verification of the AEL results, predictions were made of the pulse arrival times across a given array using the AEL-derived element positions. These predictions were compared to cross-correlations between the data from a given low-frequency hydrophone in the array and all other phones in that array during periods when the underwater sound field was dominated by a single, broadband source of known position [4].

B. Moored Sonobuoys

Standard Navy sonobuoys of two types were modified for long-term, moored deployment, following suggestions in previous work [5, 6]. These sonobuoy types were omnidirectional, broadband (10 Hz - 40 kHz), AN/SSQ 57B sonobuoys and AN/SSQ 53D DIFAR (DIrectional low Frequency Analysis and Recording) buoys with a bandwidth of 10 Hz - 2.4 kHz [7]. The sonobuoy sensor was suspended inside a bell-shaped flow shield to improve the low frequency performance. The flow shield rested on the ocean bottom and the sensor's analog data were cabled up to a surface float containing the sonobuoy radio frequency transmitter and antenna. Also inside the surface float were battery supplies sufficient for up to 5 days of continuous operation for the DIFAR sonobuoys and up to 8 days for the omnidirectional buoys [8]. The radio frequency signals were received at the data acquisition van on land where they were low-pass filtered, digitized at 50 kHz for the DIFAR data and 84 kHz for the omnidirectional data, and recorded onto tape.

DIFAR sonobuoys simultaneously measure the east-west and north-south components of acoustic particle velocity, along with acoustic pressure, to provide information on the directional properties of the sound field in the horizontal plane. These three time series are frequency-multiplexed into a single broadband (up to 17.5 kHz) signal at the wet end and sent to the transmitter for broadcasting. A software package [9] was used to demultiplex these signals after digitization.

C. 6-Element Land Microphone Array

Land-based air acoustic measurements just off the beach were made during three non-overlapping time periods by three different sensor systems (re Appendix I). Discussed in this paper are those made by a 6-element array, whose elements were inexpensive lapel microphones [10]. The 6 microphones, of two different types, were mounted equidistant from the intersection of three orthogonal metal rods, as shown in Fig. 4. This assembly was erected on a dirt road about a third of the way up the side of the 3-m-tall bluff on which the data acquisition van was situated. The microphone outputs, after being fed through standard audio amplifiers, were written onto DAT tape, and re-digitized after the experiment with the same data acquisition system used to acquire the moored DIFAR sonobuoy data.

The two microphones mounted on the vertical rod have a nominal sensitivity of −165 (±3) dB re 1 V/μPa and a flat response from 70 Hz to 4 kHz, with a steadily increasing sensitivity up to 16 kHz, whereas the response of the other four microphones is flat from 30 Hz to 10 kHz at a sensitivity of −172 (±4) dB re 1 V/μPa. The self noise floor of the array data acquisition system places the upper limit of the data usefulness at 10 kHz.

Both impulsive and continuous sound signals were generated at several known azimuths from the microphone array to provide phase calibration for beamforming. However, for the purposes of this paper, beamforming was not necessary because the air acoustic signal of interest, that of breaking surf, is the predominant sound source in a single microphone's data (re Sect. IV.B).

II. ENVIRONMENTAL SETTING

This section contains a summary of the general environmental conditions during ABM 95. Additional environmental data are presented in the later sections in support of the acoustic data. Appendix II contains a complete list of all the environmental and ancillary data collected during the experiment, and a more complete discussion of these data is given in [11].

A typical sound speed profile at the hydrophone array location, derived from one of the CTD (conductivity, temperature, depth) casts is shown in Fig. II.1. A set of these profiles was used in the acoustic propagation modeling discussed in Sect. IV. The profile shows a surface mixed layer extending to 8 m depth. Below that, the 6-m-thick thermocline, with a maximum sound speed gradient of 1.5/sec, creates downward refracting acoustic propagation conditions typical of summertime shallow water environments.

The temporal variations in the underwater sound speed during the hydrophone array recording period are shown in Fig. II.2a. This plot was created by calculating an average sound speed profile for each day on which CTD casts were taken, and then plotting the average speeds at 1, 5, 10, 15, and 20 m depth versus time. The horizontal axis of this plot is the same as in all other time series plots in this section, as well as in Figs. IV.A.3.a-g. A crossover of the 1-m and 5-m lines occurs between JD 145 and 153, indicating the formation of a surface duct. The rapid increase in sound speed at 15 m depth signifies a thickening of the surface mixed layer. The plot in Fig. II.2b shows the corresponding temporal variations in air temperature. The general increase in daily average air temperature associated with the onset of summer is correlated with the increase in sound speed of 6-10 m/sec at all depths. Therefore, even though the sound speed profile in Fig. II.1 displays a surface mixed layer, air temperature changes have an impact throughout the whole water column.

As for ocean surface wave activity, Figs. IV.A.3e,f display the significant wave height (average height of the highest one-third waves) and a gray-scale plot of the ocean surface wave spectrogram. Three notable wave events occur in this time period, but only during the event on JD 155-159 were data recorded by both bottom arrays. Corresponding plots over time of the ocean wave peak period band (the period band in which the wave energy is greatest) and the significant wave angle (the weighted average of the wave directions in each of 8 period bands, with the weighting equal to the band's percentage of the total wave energy) are shown in Figs. II.3a and II.3b. The direction normal to the coastline is indicated by a horizontal dotted line in the significant wave angle plot. Inspection of these time series shows that the first and third wave events are long period in nature, whereas the middle event is short period. Also, changes in the

peak period band are strongly correlated with changes in the significant wave angle; longer period waves propagate towards a more northerly direction than short period waves. In general, long period swell tends to arrive at directions closer to normal incidence on the coastline, probably because of refraction due to bottom interaction. In addition, as shown in Fig. II.4, deep water swell from the west and northwest is shielded from the experiment site by the offshore islands of San Clemente, Santa Catalina, and San Nicolas, and by the California coastline. Short period waves travel towards a more easterly direction, in the predominant direction of local winds. However, as comparison with the wind speed versus time in Fig. IV.A.3.g shows, ocean wave activity is only weakly associated, at best, with local wind speed. The large wind speed spike on JD 160 results in a very small, very short period event. Examination of the wind and wave activity over a longer time period suggests that high local wind speeds must be sustained over periods greater than a half day to have an appreciable effect on wave activity.

In summary, the ocean wave activity was quite small and varied little (only by a factor of two in significant wave height) over the course of the experiment.

In most of the data recorded during ABM 95, the predominant component of temporal variability is diurnal. To illustrate this property, the plot in Fig. II.5a shows the tide height variations recorded by the deep oceanography sensor at the site. In Fig. II.5b are the hourly vehicle counts for both northbound (solid line) and southbound (dashed line) traffic along Highway 5, the major San Diego-to-Los Angeles freeway that passes within 0.5 km of the Red Beach experiment site. Traffic noise is a significant component of the background noise field measured by the geophone array on land [12]. The the vehicle counts in both directions reach a minimum of a few hundred vehicles per hour in the early morning hours between 2-4 am local time, and have spikes later in the morning in the northbound direction and in the evening in the southbound direction, representing the rush-hour commuter traffic to jobs in the Los Angeles area. A weekly component of variation is visible, with a large number of vehicles heading southward on Fridays and Saturdays and a large northbound spike on Sundays. Coherence squared estimates between the tide heights and the traffic counts indicate that 90 % of the variability at 1 cycle/day in one of the time series is linearly related to the variability at this frequency in the other time series. As discussed in the next section, predominant components of the background underwater noise field, i.e., land-based water pump signals and fish-generated sounds, also display a strong diurnal component of variability.

III. GENERAL OBSERVATIONS

The major features of the underwater background sound field are presented in this section. These features include land-based cultural noise and various types of underwater biologics. Although the data also contain numerous recordings of nearby passing ships, helicopters and other aircraft, and amphibious vehicles, these signals will not be discussed in this paper.

Figure III.1 shows a 30-min spectrogram from a single element of the bottom hydrophone array. The predominant aspects of the figure are the four vertical lines (three at the harmonically-related frequencies of 85, 170, and 255 Hz, and the fourth at 100 Hz), the broadband horizontal stripes occurring at regular 30-35 sec intervals, and the short-duration events at very low frequencies. These latter infrasonic signals are non-acoustic in nature. Most are due to the coupling of direct pressure fluctuations associated with the passage of ocean surface waves over the array element. In addition, the ocean surface wave surge appears at times to have caused small relative motions between the array elements and the ocean bottom, generating glitches at very low frequencies, e.g., the one at about 12 min in Fig. III.1. The other features of the spectrogram now will be discussed in turn.

A. Land-Based Pump Signals

The dark vertical lines at 85, 170, and 255 Hz in Fig. III.1 are prominent features of the underwater acoustic spectrum, with received levels at the bottom hydrophone array as high as 110 dB re 1 μPa. They were discovered within a day or two after the start of data recording, and immediately became the focus of investigation. Concern that they were the result of self noise disappeared when they were also seen in simultaneously-recorded sonobuoy data. Subsequent examination of half-hour spectrograms covering the

whole 2.5-week array recording period revealed that the signals were clearly present only at night. Their typical pattern of occurrence was to begin appearing at sunset with their levels ramping up to maximum values over a half-to-one hour period. The levels remained fairly constant throughout the night until sunrise, when the signal levels ramped down in mirror image to the pattern seen at sunset (re Fig. III.8). At times, the harmonically related lines were broader than at other times, and sometimes split into a pair of harmonically-related line sets.

Interviews with Camp Pendleton personnel revealed that the source of these spectral lines are 21 land-based water pumps at various locations on the base [13]. The pumps are used to keep a reservoir filled to aid in fighting wildfires. They are operated mostly in the spring and summer months (fire season in Southern California) and mostly at night, when the electrical use is otherwise low. They are vertical turbine pumps driven by motors located above ground operating in the 1700 to 1800 rpm (28 - 30 Hz) range. Whereas spectral lines at these fundamental frequencies are not apparent in the underwater acoustic data, they do appear in the land-based geophone array spectra [12]. Piping extends to depths of 60 to 90 m below ground where the pumps' impellers are located in water-bearing formations. Since the impellers are below the water table, they are probably the source of the signals in the underwater acoustic data.

Fig. III.3 presents a frequency-versus-angle plot obtained with data from both bottom hydrophone arrays collected near midnight local time (06:51 GMT, JD 148). The water pump signals appear as horizontal ridges with dark peaks at 85, 170, and 255 Hz. The other main features are the 50-329 Hz vertical ridges at - 60° and 120°; these are believed to be of biological origin and will be discussed later. After the experiment, the differential GPS position fixes of each of the 21 water pumps on the base were obtained. The headings from the array location to the pumps then were calculated and are plotted as vertical black lines on Fig. III.3. Significant offsets in azimuth occur between the true pump headings and the beamforming results, indicative of the complex propagation conditions (predominantly in the solid earth) affecting these signals.

The result in Fig. III.3 was created using a fixed elevation angle of 5° above the horizontal plane. However, the signals can be expected to arrive at steeper angles with respect to horizontal due to the higher elastic wave velocities in the solid earth. Therefore, a single frequency, 170 Hz, was chosen and white-noise-constrained adaptive beamforming was performed over both azimuth and elevation angle. These results are given in Fig. III.4. The vertical arrival structure of the water pump signals, at azimuths around 10° and at 75°, are symmetric about 0° elevation angle due to multipathing in the water column. However, the two vertical arrival structures otherwise differ. Whereas the higher-level arrivals near 10° have peaks at $\pm$ 15° elevation angle, the weaker arrivals at 75° azimuth show peaks at $\pm$ 25° elevation angle. The weaker arrivals are from pumps at greater distances from the array location. Given that the properties of the medium vary greatest in depth and that the speed of propagation increases with increasing depth, then the angles of arrival are steeper for more distant sources since their ray paths penetrate deeper into the earth.

In addition to the Camp Pendleton water pumps, signals from another type of pump appear in Figs. III.1 and III.3. The narrowly-focused, 100 Hz peak coming from the west at - 80° (280° T) in Fig. III.3 is believed to be generated by two large saltwater pumps at Avalon Harbor on Santa Catalina Island (re Fig. 1), 77 km distant. These pumps transport saltwater from within the bay - the suction inlet is located in 5-m-deep water - to holding reservoirs to be used for sanitary flushing water [14]. They operate at rpm values similar to the pumps on Camp Pendleton. Since the sound source of these pumps is in water, the propagation path is restricted within the water column, and the arrival angle is much closer to horizontal than with the Camp Pendleton pump arrivals. The lower-frequency harmonic lines from the pumps probably are not seen because of mode cutoff.

In summary, near-shore underwater acoustic sensors can clearly detect land-based cultural noise. The arrival structure of those signals with predominantly earth-borne propagation paths are more complicated than those from water-borne signals. Numerical modeling of these signals will be the focus of future study.

B. Underwater Biological Sounds

1. Croaker (Sciaenidae) Choruses

To provide a closer look at the properties of the horizontal broadband stripes in Fig. III.1, five min of data from a single hydrophone array element were used to create the spectrogram in Fig. III.5. These data were collected on a different day; i.e., JD 152 versus JD 147. Also, since they were collected early in the evening, at 01:43 GMT (18:43 local PDT), compared to Fig. III.1, 06:51 GMT (23:51 PDT), they do not contain the pump-generated spectral lines. However, the broadband stripes show a similar behavior. That is, they last for 20 sec or so and occur at regular 30-35 sec intervals. Spectral energy is concentrated in the 300-550 Hz band and peaks between 400 and 450 Hz.

Fig. III.6 shows five 2D spectral density curves and illustrates the changes in levels more clearly. The uppermost plot, labeled "Knocks", was estimated during the particularly loud event 1.75 min into Fig. III.5 and will be discussed shortly. The second highest curve, called "Chorus", was calculated during the height of the broadband stripe starting just after 1 min into Fig. III.5. Peak spectral densities exceed 90 dB re 1 $\mu Pa^2/Hz$ between 400-450 Hz and reach levels above 80 dB at a secondary peak between 600-700 Hz. These levels are extremely high compared to shallow water wind-generated ambient noise levels [15]. The "Between Choruses" curve was estimated during the relatively quiet period around 1.5 min after the start of Fig. III.5. Spectral levels decrease by 4-6 dB over the 250-750 Hz band, resulting in the cycling nature of the levels in Fig. III.5.

For comparison, the lower two spectral density curves in Fig. III.6 were estimated from data not collected during the period in Fig. III.5. The curve labeled "Background" was recorded during a quiet period earlier in the same day. This spectrum is nearly flat at a level of 70-75 dB re 1 $\mu Pa^2/Hz$ from 100 to 500 Hz. The night-time broadband stripes significantly raise the background sound levels over those recorded during the day; by almost 20 dB around 400 Hz and by 10-15 dB at other frequencies above 75 Hz. Occasionally, the increase in levels can be as much as an additional 10 dB when events labeled "Knocks" occur. However, even the lower daytime levels in ABM 95 are fairly high. The lowermost "SWX-2" curve in Fig. III.6 shows the background spectral density estimate from data collected during another experiment in Southern California, away from the shoreline, where the water depth was 460 m. (The spectral lines at 175 Hz and 350 Hz in this lowermost curve are calibration signals that were broadcast during the experiment). Clearly, the underwater near-shore region is a noisy place in this frequency band, particularly at night.

The bandwidth of the array hydrophones goes up to about 720 Hz, so that the highest-frequency portion of the transient sequences and broadband stripes is not recorded. Examination of the broader-band moored sonobuoy data collected at night shows that the spectral energy in these features extends up to about 1 kHz.

The single element time series corresponding to the "Knocks" curve in Fig. III.6 is shown in Fig. III.7. It is composed of 10 impulsive arrivals each separated by 0.7 sec. Other transient sequences such as this typically contain 7 to 13 impulsive transients. The received peak-peak pressure level of the transients in Fig. III.7 is about 156 dB re 1 μPa (equal to 64 Pa). Their source level can be estimated by using the data from adjacent array elements to calculate the source range. The ranges are quite small, varying from 1.9 m to 2.2 m for the set of 10 transients, suggesting that knock sequences are readily apparent in the time series only when the source is very near a given array element. With a transmission loss given by spherical spreading, the average peak-to-peak source level for the 10 transients in Fig. III.7 is 162 dB re 1 μPa @ 1 m. The source level variation for the 10 transients is about ± 0.5 dB.

The sound produced when a set of impulses is played back through a D/A converter and speaker system is very much like that of someone knocking on a table or a carpenter hammering a nail into a hollow log. The broadband stripe immediately following these knocks in Fig. III.5 sounds similar to hand clapping from a crowd of people at some distance. This "applause" lasts for 15-20 sec and then dies off. After a delay of 10-20 sec, the clapping, or chorusing, begins again. Often, individual knocks are discernible.

This pattern of repeated choruses, punctuated by periods of lower spectral levels, persists all through the night. Near sunrise, the time interval between the choruses begins to increase. Fig. III.8 shows a three-hour spectrogram from a single hydrophone. The start time of the plot is 10:33 GMT, or 03:33 PDT.

Local sunrise occurs between 105 and 120 min after the start of the plot. Around sunrise, most of the land-based water pumps begin to cease operation. Simultaneously, the time interval between the broad-band choruses also begins to increase, to a period of more than 1.5 min an hour after sunrise. This interval continues to increase and the chorus amplitude continues to decrease for a few hours, until they no longer are discernible.

The diurnal pattern of the choruses is very regular over the 2.5-week array data recording period. A qualitative assessment of the chorusing behavior obtained from visual observations of consecutive, half-hour, single-element spectrograms is presented in Fig. III.9. Each line of the figure represents a given day during the data recording period. The background spectral levels begin to increase and the cycling nature of the choruses becomes evident starting three to four hours before sunset. Shortly after sunset on every day except the first, the chorusing behavior abruptly changes to an acoustic field with a continuous, high-level, and temporally stationary character, almost as if the "audience" breaks into continuous "applause". During this time, the received spectral levels increase to over 100 dB re 1 $\mu Pa^2/Hz$ in the 400-450 Hz band. This continuous sound lasts for a half-hour or so, and then abruptly reverts back to its cycling nature. The cyclic chorusing continues for the remainder of the night, until sunrise when the time interval between choruses begins to grow and the chorus amplitudes decay.

These unusual nighttime choruses also have been detected in other recent underwater acoustic experiments conducted 12 km west of San Diego [16, 17]. However, due to the significant offshore distance of this experiment site, the chorus levels were much lower and individual knocks were not discernible. In addition, the horizontal directionality of the choruses was strongly anisotropic, coming predominantly from the regions south of San Diego harbor and to the north of the experiment site, where the water depth shoals and the ocean bottom is sandy. None of the sounds came from the kelp beds east-northeast of the site. In contrast, the horizontal directionality in ABM 95 was nearly isotropic, with different sequences of knocks being apparent in the time series of widely separated (greater than a water depth) array elements. The much higher spectral levels, the presence of knocking sequences with significant spatial variation over the array aperture, and the nearly isotropic nature of the horizontal directionality strongly suggest that the arrays in ABM 95 were located in the same area as the acoustic sources.

The character of these sounds corresponds to that found in year-long, single-hydrophone measurements made from a shallow water (18 m) tower off the San Diego coast in the early 1960's [18]. Because of the diurnal and seasonal variability of the sounds, they are believed to be biological in origin. The author of Ref. 18, referring to work by Johnson [19], attributes the "continuous applause" just after sunset (dubbed the "sunset chorus") to two species of fish from the croaker (Sciaenidae) family, the spotfin (Roncador stearnsi) and the yellowfin (Umbrina roncador). The source of the night-long cycling sound remains unidentified, but is probably due to at least one other species of croaker. Evidence presented later in this section suggests that the queenfish (Seriphus politus) may be one of the contributors.

Several species of fish are well known to be producers of high levels of underwater sound [20, 21, 22]. Many members of the Sciaenidae family generate sound by twitching muscles attached to their air bladders, causing the air bladders to vibrate. In many species, only the males have the required musculature to generate loud sounds [23]. Because of this fact, and the fact that the sounds occur predominantly in the late spring and summer months and are weak or absent in the fall and winter [18], they are probably associated with some sort of mating behavior. That is, the males are trying to "out-knock" one another to attract females, who deposit their eggs in the water column to be fertilized by the males [24]. Clapp presents evidence that the period between choruses in the cycling sound is a function of background noise level, with shorter inter-chorus periods occuring during higher background levels. This observation further supports the idea of acoustic competition among males.

An interesting aspect of these cycling choruses is their similarity to the pattern of light flashes from a certain species of North American fireflies, Photinus carolinus [25, 26]. One or two male fireflies start to flash, apparently stimulating other males into synchronous flashing. An individual male generates a sequence of 5 to 8 flashes, each separated by about 0.5 sec. Synchronous group flashing continues for 4 sec, and then suddenly stops. After a quiescent period of 8 to 12 sec, the group flashing begins anew. This type of behavior is categorized as "discontinuous synchrony" [25, 26]. Controlled studies have examined the attempts of single individuals to synchronize their flashing to an artificial light stimulus. Future studies

will examine if synchronous knocking within a croaker chorus occurs.

Croakers serve as prey to several types of marine mammals. Therefore, the choruses may occur at night because of the protection afforded by darkness. In addition, the temporal variations and the spectral content, at least for the majority of the energy centered about 400-450 Hz, is strikingly similar to that of surf-generated noise [1]. So similar, in fact, that the group chorusing behavior may have evolved to mimic the sounds of other naturally-occuring phenomena. In other words, the chorusing croakers are an acoustic analog of chameleons. Although this conjecture is highly speculative, it is certainly true that these biological sounds can be easily confused with surf-generated noise. The significant diurnal variability of the fish sounds is a useful discriminant between the two sources.

Some of the knock sequences show an interesting feature in their arrival structure. One such sequence is plotted on an expanded time scale in Fig. III.10. Time increases from left to right and from top to bottom in the figure. The first arrival of relatively high frequency (8 to 10 cycles at 400-460 Hz) is followed by a low frequency oscillatory tail. Arrivals of this type give rise to the broad spectral peak around 60 Hz seen in the "Knock" spectrum in Fig. III.6. Near the end of the knocking sequence in Fig. III.10, the first arrival is decreased in amplitude and the oscillatory tail arrives at a later time. This tail represents a Scholte interface wave generated by a calling fish at the ocean-sediment interface. Supporting this interpretation is a weak, secondary, higher-frequency arrival about 26 msec after the first arrival, that appears as a notch in the peak of the second cycle of the tail. It is most clearly seen in expanded plots of individual knocks. Its travel time equals that of the two-way travel time of an ocean-surface bounce path in 20-m-deep water, the water depth at the array location. The acoustic source, therefore, is at, or very near, the ocean bottom.

On weekends and holidays, Las Pulgas Beach is opened to the public. Examination of the catch by surf fishermen late one afternoon during the experiment revealed that it was primarily composed of queenfish. Interviews with these fishermen affirmed their success in catching queenfish in late afternoon and early evening periods during the spring and summer months. Queenfish (Seriphus politus) are abundant along the Southern California coast in summer [22]. They are found in shallow water (usually less than 10 m), sandy bottom areas, and tend to congregate in schools, often with white croakers (Genyonemus lineatus). A fish that schools may be more likely to demonstrate some social organization to its calling behavior. At nighttime, they migrate into deeper waters. They also feed on the bottom, which might explain the existence of Scholte wave arrivals in certain knock sequences. For these reasons, the queenfish may be one of the participants in the night-time choruses during ABM 95. Future studies of the calling behavior of captive fish may help to make a more definitive species identification.

2. Biological Pulses of Unknown Origin

Another acoustic source apparently of biological origin contributed to the low-frequency sound field during ABM 95. Fig. III.11 shows a 5-minute spectrogram of single-element array data starting in early afternoon, 13:36 local PDT (20:36 GMT), JD 154. Four croaker-generated transient features over the 250-650 Hz band are present, but are much lower in level than those presented in the previous section. Of greater amplitude are the short-duration pulses from 50 to 250 Hz that occur at regular 4-to-8 sec intervals.

The complete time series and the spectrum of the first arrival for one of the pulse types in Fig. III.11 are plotted in Fig. III.12. Delay-and-sum beamforming was used to separate out this pulse type from the others occurring in the figure. The time series of the signal, shown in the upper plot, actually is composed of a pair of pulses. The first pulse contains three arrivals of approximately equal amplitude, each separated by 0.25 to 0.35 sec, followed by a fourth arrival with half the amplitude. The spectrum of the first arrival, in the lower plot, diplays a "picket-fence" structure with peaks every 25 Hz from 50 to 250 Hz. When played back through a speaker, the sound of the four arrivals in this first pulse is something like "rhoomm-rum-rump". The second pulse of the pair arrives 1.4 sec later and is followed by a weaker secondary arrival. The pair of pulses repeats regularly at 5.5-sec intervals over a minute or so period within the 5-min period in Fig. III.11.

The diurnal variability in the occurrence of the pulses over the course of the experiment is displayed in Fig. III.13. The information in this figure was obtained by examination of single-array-element

spectrograms, similar to Fig. III.9. The pulses are present predominantly in the mid-morning and mid-afternoon periods. The gaps in occurrence at night do not necessarily indicate the absence of the pulses, but rather that they may be obscured by the croaker-generated sounds. In fact, the vertical, broadband ridge of energy around –60° azimuth (300° T) in Fig. III.3, recorded near local midnight, is due to the pulses. (The ridge at 120° azimuth in Fig. III.3 does not show a pulse-like behavior in time. Rather, it is associated with the "sunset chorus" discussed in the previous part of this section). During a few nighttime periods, e.g., the one shown in Fig. III.5, the pulses are sufficiently loud to be discernible above the croaker din in single-element spectrograms.

Unlike the isotropic nature of the croaker sounds, the pulses arrive predominantly from given directions in the horizontal. Results from time-delay-and-sum beamforming with one of the bottom hydrophone arrays, to be discussed in the first part of Sect. IV, clearly show that the pulses are coming from the seaward direction (re Figs. IV.A.1a and b). That is, the source(s) of these pulses must be more than 3.4 km off the coast. This seaward directionality of the pulses is a consistent feature over the course of the experiment. Additional beamforming will be performed in the future to examine the temporal evolution in directionality and the nighttime occurrence of the pulses.

The arrival structure and spectral content of the pulses is similar to sounds of several species of fish [20]. Although the source appears to be biological, its identity otherwise remains unknown.

3. Snapping Shrimp

The four moored omnidirectional sonobuoys, whose deployment positions are plotted as solid circles in Fig. 2, provided underwater acoustic data with bandwidth up to 40 kHz. The results up to 10 kHz are discussed here.

Data from the two moored buoys closest to the coast, at offshore ranges of 1.2 km and 2.3 km in Fig. 2, were used to estimate the spectral density functions plotted in Fig. III.14. Three spectral estimates were created for each sonobuoy to illustrate the temporal variations. The time periods for these estimates were 15 min in duration, taken at the same time of day on three consecutive days. The spectra have been corrected for the prewhitening in the sonobuoy data acquisition system [27]. However, they are otherwise uncalibrated because the data are clipped, and so provide only qualitative information on major spectral features. Below 1 kHz, the spectral levels are greater for the sonobuoy farther from shore because it is closer to the biological sound sources just discussed. Above 1 kHz, the reverse is true; the levels are higher closer to shore. The spectra have a broad peak centered around 3.5 kHz. This bimodal nature of the inshore buoy spectra is similar to that seen in underwater acoustic spectra from laboratory breaking waves, where the higher frequency energy is attributed to sound radiated by single bubble oscillations [28]. On the other hand, the underwater sounds generated by snapping shrimp display a broad spectral peak from 2 to 15 kHz [29], much like the one seen in Fig. III.14.

To determine whether the inshore sonobuoy's spectral peak was generated by breaking surf or possibly another biological source such as snapping shrimp, data from the moored DIFAR sonobuoys were processed to obtain the horizontal directional properties of the acoustic field. Although the DIFAR data only have bandwidth up to 2.4 kHz, the 3.5 kHz peak is sufficiently broad that significant energy exists between 1 kHz and 2.4 kHz. The time period chosen was just after the deployment of the omnidirectional and DIFAR sonobuoys at their nearest-to-shore locations. Fig. III.15 shows the track of the deployment ship during the data processing period as it departed to the west-southwest, along with the positions of the sonobuoys. The processing results for the DIFAR sonobuoy closest to the coast, at 1.2 km offshore range, are shown in Fig. III.16. Since these data do not suffer significant clipping, the spectra have been fully calibrated. The upper plot in the figure is the pressure autospectrum from the omnidirectional channel of the DIFAR sensor. Most of the spectral energy below 1.3 kHz is generated by the deployment ship. In contrast, the spectrum above 1.3 kHz is relatively featureless and represents the lower-frequency portion of the 3.5 kHz energy. In the lower plot of Fig. III.16 is the horizontal projection of the active acoustic intensity spectrum over the same frequency band. The length of the vector in each frequency bin is equal to the magnitude of the net acoustic energy flux in that bin, and the direction of the vector points in the direction that the acoustic energy is flowing *to* [30]. The vectors below 1.3 kHz show acoustic energy flowing away from the deployment ship, from the southwest to the northeast. Above 1.3 kHz, the energy flow is

overwhelmingly to the southeast, in a direction somewhat parallel to the coast, and so is not associated with breaking surf.

The data from the moored DIFAR sonobuoy farther from shore in Fig. III.15 (2.4 km distance offshore) can be used to obtain additional information on the position of the 3.5 kHz energy source. First, the pressure spectral density above 1.5 kHz is about 20 dB lower farther from shore than at the inshore site. Assuming a 4 to 6 dB per double distance transmission loss [29], the inshore site is 10 to 32 times closer to the source. Since the two DIFAR buoys are separated by 1360 m, then the distance of the 3.5 kHz source from the inshore buoy is somewhere in the 40 to 150 m range. Second, the horizontal directionality from the offshore DIFAR buoy, although more variable because of the lower received levels, provides a cross-fix on the source location. The dotted lines emanating from each of the DIFAR buoy positions in Fig. III.15 indicate the range of directions of the active acoustic intensity vectors in the 1.3-2.4 kHz band. The region where they intersect, just to the west-northwest of the inshore site, defines the area within which the source exists. A source location in this area is consistent with the 20 dB difference in pressure autospectral levels. It also explains why the inshore omnidirectional sonobuoy's data are clipped; the buoy may have been deployed in close proximity to, or possibly on top of, the source of the 3.5 kHz energy.

Because of the similarity in spectral shape to published data taken off San Diego [29], it is likely that the source of the 3.5 kHz energy are snapping shrimp. These animals generate high levels of sound (and a focused water jet) by snapping closed their large, major frontal chela (fighting claw) [31]. They are found on stationary, rough ocean bottoms such as those covered by rocks or shells, in coral reefs, along pier pilings and jetties, and other areas where they can be protected, and not over mobile, sandy bottom regions. Comparison of Fig. III.15 and Fig. 2 shows that the 3.5 kHz source appears to exist at the southeast edge of the kelp canopy coverage. Giant kelp (Macrocystis) also requires stationary ocean bottom conditions to establish their holdfasts. A listing of the species commonly found in California kelp beds, given in Ref. 32, contains members of the genus Alpheus, one of the genera of vigorously snapping shrimp. The presence of the kelp bed therefore introduces an environment in which snapping shrimp can thrive.

Much of the work on the worldwide distribution and underwater acoustics of snapping shrimp was published in the late 1940's [19, 29, 31]. Recent work extending the measurements to frequencies above the sonic band [33, 34] has shown that snapping shrimp sounds contain energy up to 200 kHz and can have peak-to-peak source levels as great as 189 dB re 1 μPa @ 1 m. Also, colonies of snapping shrimp (Synalpheus regalis) that dwell in the interstices of sponges in Caribbean coral reefs recently have been discovered to display eusocial behavior, with a single reproductive female in each colony, much like a beehive or an anthill [35]. They are the first marine animals found to show this cooperative breeding behavior.

IV. SURF NOISE PROCESSING

A. Endfire Beamforming Towards and Away from the Coast

To determine the contribution, if any, of the sounds from breaking surf to the underwater noise field in the 10-400 Hz band, time-delay-and-sum beamforming was performed with a 35-element subarray of the bottom hydrophone array oriented perpendicular to the coast. Fig. 3 shows the element positions in plan view of this 35-element subsection. Endfire beams were formed towards and away from the coast. The directions of maximum response (33.9° T) and the 3-dB down points at 195 Hz and 370 Hz for the landward endfire beam are plotted in Fig. 2. Due to the significant offshore distance of the bottom arrays and the thickness of the main lobe at endfire, several wave breaking events, each with spatial scales in the alongshore direction of order tens of meters at most, can occur in the few-hundred meter distance spanned along the surf zone by the array beam pattern. Therefore, the landward endfire data cannot be expected to show jumps in spectral levels associated with individual wave breaking events. To identify surf noise, processing over sufficiently long time scales to permit significant variations in ocean surface wave activity, e.g., at least a week, is required.

Five minutes of array data were extracted once an hour over the full 2.5-week array recording period to provide a long-duration time series. For each 5-min period, spectrograms of single element data, and rms time series and averaged spectra for all elements, were plotted to verify data quality and provide indications of the presence of loud, interfering sound sources. A subset of these 5-min data periods were selected, restricting them to daytime hours (07:30 - 16:30 local PDT) to reduce contributions from biological sounds (re Sect. III). Endfire beams were formed using a phase speed of 1500 m/sec and a Kaiser-Bessel spatial-weighting window with $\alpha = 1.5$. Their spectrograms were calculated and plotted.

The calibrated spectrogram for a single element's data during a typical 5-min period in daytime (13:36 local PDT, JD 154) was presented previously in Fig. III.11. The two endfire beams during this same period of time are shown in Figs. IV.A.1a and b. Many of the features seen in these spectrograms, e.g., the infrasonic fluctuations, the 50-250 Hz pulses, and the 95 Hz energy on the landward endfire spectrogram from land-based water pump noise, were discussed in the last section. Also mentioned previously were the weak croaker knocking sequences from 250 to 700 Hz. It is important to note here that, although these data were collected in the early afternoon and so do not display the croaker chorusing behavior, individual knocking sequences are still apparent. An additional feature on the seaward gram is the broad hump of energy from 30 Hz to nearly 100 Hz, reaching a peak just over 75 dB re 1 μPa^2/Hz at 70 Hz. It is probably related to distant shipping. The rise in spectral levels above 390 Hz on the seaward spectrogram are the result of spatial aliasing from the landward endfire beam.

The set of endfire spectrograms were used to identify several 12-sec periods when loud interferers and anomalous spectral features were absent. Landward spectral densities and landward/seaward spectral ratios were estimated for these selected periods. Assuming the noise field is stationary and is Gaussian distributed, then sufficient averaging of statistically independent samples was done to yield a 90 % confidence interval of + 1.4 dB to – 1.2 dB for the spectral density estimates [36]. For the spectral ratios, their values are statistically different from zero at the 95 % level of confidence when the ratio exceeds 2.5 dB (using a one-tailed F-test [37]). Figs. IV.A.2a,b show plots of the landward beam spectral density and the landward/seaward spectral ratio for a 12-sec period indicated in Figs IV.A.1a and b. Also shown are the linear regression fits to these data across the 250-390 Hz band. The parameter values obtained from the regression fits provide a convenient 2.5-week time series for comparison of the temporal dependence of the spectral levels and ratios with fluctuations in environmental parameters.

Figs. IV.A.3a-g present the linear regression time series results along with the corresponding time series of the important environmental parameters. The upper two panels show the variations in the linear regression level at 300 Hz and slope, respectively, for the landward endfire spectral density. The next lower two panels show the corresponding two time series for the landward/seaward spectral ratios. Below that, in the fifth, sixth, and seventh panels, are the ocean surface wave significant wave height, the ocean surface wave spectrogram (to investigate the possibility that the 250-390 Hz acoustic energy is correlated with a certain period band in the ocean wave spectrum rather than the total wave height), and the wind speed at 10 m height. The ocean surface wave spectrogram shows clear evidence of the dispersive nature of deep water swell propagation. Also, as mentioned in Sect. II, the one large significant wave height event on Julian Days 156-159 which occurred during the array data recording period is short period in nature. Although the dip in landward spectral levels around Julian Day 161 may be related to the decrease in the significant wave height at the same time, the overall correspondence between fluctuations in the underwater acoustic data and those in the environmental parameters is weak. However, as the data in the third panel clearly illustrates, the landward spectral levels at 300 Hz were almost always higher, by an average of 6 to 8 dB, than those in the seaward direction.

Therefore, the beamformed data are inconclusive as to whether or not surf-generated noise in the 250-400 Hz band was detected by the bottom arrays 3.4 km offshore. The data presented by Wilson, Wolf, and Ingenito [1] indicates that underwater surf noise was measurable at least out to 9 km offshore. Several reasons exist for why surf-generated noise at the ABM site might be more difficult to detect than in Monterey Bay. One reason is discussed in Sect. III, i.e., the underwater sounds generated by fish totally dominated the background noise field over the 50 Hz - 1 kHz band in ABM 95, at least at night. A residual component of these biological sounds also may be present during the day (re Figs. IV.A.1a and b), even though individual knocks are not visible in the time series used to create Figs. IV.A.3a-d, and it may be

coming predominantly from the landward direction.

A second reason for the possible difference in contribution of surf noise is that the wave activity during ABM 95 was much lower than in [1]. The three asterisks in the fifth panel of Fig. IV.A.3a-g show the significant wave height for the three time periods discussed in [1]. Given that total wave energy is proportional to the square of the wave height, that the acoustic energy generated by wave breaking scales with the amount of energy dissipated in wave breaking [38], and assuming that the same fraction of total wave energy is dissipated during breaking in the two studies, then the acoustic source levels of the surf in [1] are order 6 dB greater than in ABM 95. In addition, the lack of correlation between the array data and the ocean wave activity in ABM 95 may be due to the small degree of ocean wave variability; the significant wave height only changed by a factor of two over the array recording period.

The lower ocean surface wave activity in ABM 95 may be partially a result of the experiment site. As shown in Fig. III.4, the offshore islands in the Southern California Bight region and the central California coastline shield the site from deep water swell coming from the west and northwest. In addition, the main lobe of the landward endfire beam points directly at the area of kelp canopy coverage, as Fig. 2 illustrates. The presence of the kelp bed not only introduces an environment that supports soniferous animals, but its canopy acts like a filter for ocean surface waves. The impact of the canopy filtering may be particularly pronounced in the data considered here given the fact that the only large wave event during the array recording period was short period in nature. The effect of the kelp bed is compounded by the fact that once a wave breaks and generates sound, its acoustic energy must pass through the kelp, which introduces additional attenuation, to arrive at the array site.

Given an incident ocean surface wave whose wave slope is not too steep, then the wave breaker type is spilling for very gentle-sloping beach bottoms, and, as the bottom slope becomes progressively steeper, the breakers become plunging in nature [39]. Laboratory studies [28] have shown that the character of the sound produced by breaking surf is determined to a large extent by the breaker type and, therefore, by the slope of the ocean bottom in the wave breaking region. Plunging breakers are much more efficient at generating acoustic energy below 1 kHz than spilling breakers. In Fig. IV.A.4, the bottom bathymetry out to 5 km offshore is plotted for both the ABM 95 site and the Monterey Bay site [1]. The bottom bathymetry appears to be significantly steeper in the near-shore region in Monterey Bay, thereby resulting in a site that has greater potential for producing low-frequency acoustic energy during surf breaking than at Las Pulgas Beach.

The comparison of the bottom bathymetries in Monterey Bay and off Las Pulgas Beach also suggests that surf-noise interactions with the ocean bottom are significantly greater at the latter site. Numerical acoustic propagation modeling at both sites using a parabolic equation code [M. Collins, RAM PE] clearly illustrates this effect. Results show that the received levels offshore for an inshore source at the ABM 95 site can be made to be greater than, or less than, those at Monterey Bay by decreasing, or increasing, respectively, the ocean bottom attenuation [L. Pautet, private communication]. Therefore, the attenuation properties of the ocean bottom at a gently sloping bottom site is an important factor in determining the contribution of surf noise to the offshore underwater acoustic field. Although the increase in water depth with distance from shore at the ABM location is not signficantly different from that at the site of the DUCK 94 experiment (re Fig. IV.A.5), where experimental evidence for the detection of surf-generated noise has been presented [2], the bottom array in DUCK 94 was only 0.55 km offshore, as opposed to the 3.4 km offshore distance of the arrays in ABM 95.

In summary, the beamformed bottom array data are inconclusive as to the contribution of surf-generated sounds in the 250-400 Hz band to the ambient noise field 3.4 km offshore during the ABM 95 experiment. It *may* not have been detected because:

1) The background noise levels were otherwise too high, due to biologics;

2) The breaking-surf source level was too low, and varied too little, due to shadowing of deep ocean swell by offshore islands and the central California coastline, to ocean surface wave filtering by the kelp bed canopy, and possibly to the gently-sloping nature of the near-shore bottom topography;

3) Propagation conditions for the surf noise to the arrays were too unfavorable, due to attenuation of sound by the kelp bed, possibly the gentle slope of the attenuating ocean bottom, and the distance offshore of the arrays.

B. Air Acoustic Measurements

In contradistinction to the underwater acoustic data, the air acoustic data collected by the 6-element microphone array are clearly dominated by breaking surf noise. A spectrogram from 0 - 10 kHz over a 5-min period from the data collected by a single microphone element is shown in Fig. IV.B.1. Wind noise effects are visible as impulsive "glitches" from near DC up to a few hundred hertz, particularly over the period from 0.5 min to 1.75 min. However, the most predominant feature are the broadband jumps in spectral levels occurring three to five times per minute, the result of individual wave breaking events. The duration of the events is determined by the character of breaking. At gently sloping beaches, such as that at Las Pulgas Beach during ABM 95, the spilling character of breaking is more prolonged in time than the initial, impulsive nature of plunging breakers. However, for plunging breakers, once the wave breaks, a turbulent bore is formed which travels shoreward [39], constantly generating sound. In either case, the effect of the progressively decreasing range of the acoustically active part of the breaker from a near-shore, land-based sensor tends to compensate for the decrease in sound-producing turbulence and degassing of the water column after breaking, thereby maintaining higher sound levels than otherwise.

The data in Fig. IV.B.1 were averaged over a 1.2-sec period, indicated by the lower arrow in Fig. IV.B.1, to obtain the calibrated spectral density estimate plotted as a solid curve in Fig. IV.B.2. For comparison, the spectral density estimate from a second microphone's data over the same time period are plotted with a dotted curve. The offset in spectral levels is due to the variation of the microphones' sensitivities from the nominal value provided by the manufacturer. The ripples in the spectra below 2 kHz, and seen as parallel light and dark bands running down the gray-scale plot in Fig. IV.B.1, are the result of multipath interference of the surf noise arriving at the microphones; it changes character as the microphone's position with respect to the ground changes.

To measure the character of the acoustic field due to breaking surf alone, the spectra estimated during a wave breaking event were normalized by those estimated just prior to wave breaking. This measure has the added benefit of removing the effects of uncertainties in channel calibration. A plot of the spectral ratio for the two time periods marked by arrows in Fig. IV.B.1 is given in Fig. IV.B.3. Individual wave breaking events can lead to jumps in the received field of up to 20 dB between 3-6 kHz. The curve fits to these spectral ratio data are discussed later in this section.

The shape of the wave breaking spectral ratio curves is surprisingly similar to that of the 3.5 kHz peak in the nearest-to-shore omnidirectional sonobuoy data (re Fig. III.14). So similar, in fact, that one initial hypothesis was that both the underwater and air acoustic energy around 3-4 kHz were generated by the same source, i.e., breaking surf. However, the horizontal directional properties of the sound field near this band, from the DIFAR sonobuoy measurements, eliminates this hypothesis.

The bandpass nature of the breaking-wave spectral ratios also is quite similar to that seen in other ocean acoustic data sets. For example, the surface dipole source spectra for deep water breaking waves, derived from a parametric spectral estimation scheme [40], have a bandpass character over a large variation in sea conditions; re Fig. 3 of [41] and Figs. 4 and 5 of [42]. However, these source spectra have a much lower center frequency, i.e., between 400-800 Hz, versus that of 4 kHz in the air acoustic results. Kennedy *et al* have argued that the center frequency is related to the characteristic length of whitecapping along the wave crest during breaking [41]. In shallow water, the wave breaking spectral ratios from bottom hydrophone measurements at 200 m outside the surf zone in Monterey Bay also have a bandpass character. Fig. IV.B.4, calculated from the two spectra in Fig. 4 of [1], shows a jump in spectral level due to wave breaking of order 15 dB between 200 - 700 Hz, with a center frequency around 500 Hz. If the center frequency in the air acoustic data bears the same relationship to the characteristic length of whitecaps in the breaking process as that in water, the whitecap length during this time period in ABM 95 is nearly an order of magnitude smaller than in these other two data sets. However, the offset in center frequencies may be the result of the difference in physical mechanisms generating the breaking wave sounds in the two media;

the underwater signature is due to bubble oscillations (both singly and collectively [28]), whereas that in air must be the result of initial wave impact (for plunging breakers) and bubble bursting at the sea surface during degassing.

An alternative explanation for the shape of the air acoustic spectral ratios in Fig. IV.B.3 is now presented. This shape is that measured at the receiver and does not necessarily represent the spectral shape at the source. That is, the shape may be determined to some extent by propagation effects. The important variables dictating sound propagation in the atmosphere are 1) the sound speed, which is mainly a function of wind velocity and air temperature, 2) the attenuation due to absorption, predominantly a function of sound frequency and relative humidity, 3) attenuation due to interaction with the ground, which is a function of sound frequency, the source and receiver height, and the type of ground, and 4) the range from the source to receiver [43]. Each of these variables now will be addressed in turn.

Fig. IV.B.5 shows a plot of wind speed and direction from the 10-m weather station over the duration of a data tape recording period, with the vertical dotted lines indicating the time when the data in Figs.IV.B.1-3 were recorded. The horizontal dashed line in the wind direction plot (lower panel) signifies the direction normal to Las Pulgas Beach. The wind was light and blowing onshore during data recording. Given that the wind speed increases with height above the ground/sea surface (e.g., a logarithmic profile is often assumed in the calculation of wind stress, e.g., [44]) and that the air temperature does not decrease too rapidly with increasing height to counteract the wind effects, then downward refracting conditions exist for sound propagating from an offshore source to an onshore receiver. These wind conditions meet the criteria for "meteorological conditions which are favorable to propagation" in clause 5 of [45].

The absorption of sound in the atmosphere is a function of the relaxation frequencies for oxygen and nitrogen, the primary components of air [46]. These relaxation frequencies are, in turn, primarily functions of acoustic frequency and relative humidity, secondarily of air temperature, and only very weakly of atmospheric pressure [43]. Unfortunately, the relative humidity sensor in the 10-m weather station malfunctioned during the experiment. Along the shoreline, the humidity can be expected to be fairly high, except in weather conditions where the wind is strong and coming from land. During the data recording period, the sky was cloudy, but clear visibility conditions existed, with no presence of fog or heavy haze. Therefore, in the estimation of attenuation due to atmospheric absorption, values of both 70 and 90 percent relative humidity are used. As for air temperature, the 10-m weather station measurements indicate that it was fairly constant at 17° C.

In the estimation of the attenuation of sound due to ground interaction, the ground surface is classified into three categories; 1) hard ground, including water with a smooth surface, 2) soft ground, and 3) very soft ground, composed of very porous surfaces [43]. Whereas wet sand is probably in the first category, the stretch of dry sand near the receiver location most likely falls into the third category. Also, the scattering losses from the rough ocean surface inside the surf zone must certainly classify this part of the propagation path as effectively soft or very soft. For propagation distances of 100 m or less, Table 3.2 in [43] can be used to estimate the losses due to ground interaction. Because of the uncertainty in type of ground, attenuation values for both soft ground and very soft ground are used in the comparison with the air acoustic spectral ratios. Also, the values in Table 3.2 are given at three different source heights, 0.01 m, 0.3 m, and 1.2 m. Since the effective acoustic source height for breaking surf is unknown, the attenuation-versus-frequency curves for all three source heights are presented. In addition, the values in the table pertain to a receiver height of 1.8 m, which is appropriate given that the microphone array was placed about a meter or so up the side of the bluff next to the beach and that most of the microphones were mounted nearly a half-meter or more above the ground support.

The final step in modeling the propagation characteristics of surf noise is the estimation of the source/receiver range. Simple theoretical arguments and experimental results indicate that for shoaling waves, the ratio of wave height to water depth at breaking is between 0.7 and 1.2 [39]. Therefore, if measurements of the ocean surface wave directional spectrum at a given location outside the surf zone and the near-shore water depth profile are available, then the use of this ratio and a suitable ocean surface wave propagation model permit the calculation of the water depth, and hence the offshore range, at which wave breaking occurs. One model that can be used is a simple steady-state, linearized shoaling wave model whose expression for the evolution of wave height in the near-shore region is based on the conservation of

ocean wave energy [39]. For simplicity and as a first approximation, the range to the breaking surf is estimated here by setting $h = H/0.8$, where h is water depth (including tides) and H is the significant wave height. Fig. IV.B.6 shows a plot of the resulting estimated range of the breaking surf from the mean low level water mark as a function of time over a 4-week period in the experiment. For this calculation, the water depth profile from a July, 1994 Navy SEAL (SEa, Air, Land) team survey off Las Pulgas Beach (re Fig. IV.A.5) is used along with the directional ocean surface wave spectrum and tidally-induced water depth changes obtained from the oceanography mooring at 300 m offshore. As Fig. IV.B.6 illustrates, the range of breaking surf from a fixed sensor varies by a few hundred meters over a half-tidal cycle period. Whereas these range changes represent a small fraction of the total range to the bottom arrays at 3.4 km offshore, they are a significant proportion of the range to fixed sensors in and near the surf zone, and must be incorporated into any analysis of temporal variations. Taking into account the distance of the microphone array from the mean low level water mark, the estimated range from the breaking surf to the receivers during the data recording period is close to 100 m.

The resulting predictions of the attenuation due to atmospheric absorption and to interaction with the ground at 100 m range are shown with the air acoustic spectral ratio in Fig. IV.B.3. The fits of these propagation estimates to the spectral ratios is surprisingly good. The high-frequency roll-off in the ratio appears to be dictated by atmospheric absorption, whereas the low-frequency roll-off seems to be the result of ground interaction. The best fit at the low-frequency end is provided by an assumed source height of 0.3 m and a very soft ground type, although the result is not too sensitive to the latter variable. The behavior of the low frequency roll-off may be affected by contamination due to wind turbulence; however, its impact at these low wind speeds should be restricted below a few hundred hertz.

The effects of propagation on the received spectrum from a breaking wave now can be removed, at least to some extent, to obtain an estimate of the equivalent point source pressure spectral level of a breaking wave. The air absorption curve for an air temperature of 20° C and a relative humidity of 70 % is combined with the ground attenuation curve for a 0.3 m source height and very soft ground to create a frequency-dependent "calibration" curve. Applying this "calibration" curve to the received spectra in Fig. IV.B.2, along with simple spherical loss to account for geometrical spreading, the equivalent source pressure spectrum plotted in Fig. IV.B.7 is obtained. The upper plot shows the results on a linear frequency axis, as in Fig. IV.B.2, and the horizontal axis of the lower plot is on a log-frequency basis from 1 kHz to 10 kHz. Examination of the lower plot shows that the spectral slope has an average value of about 7.5 dB/octave over the whole 1 - 10 kHz band. However, in the band from 1-3.3 kHz and from 5-10 kHz, the rolloff is about 5-6 dB/octave. This rolloff value is the same as that given by the Knudsen curves describing the underwater ambient noise field above a few hundred hertz [15]. The much larger slope of about 12 dB/octave in the 3.3-5 kHz band may be the result of the peak in the "propagation calibration" curve being at too high a frequency. Additional work, including calibrated acoustic propagation measurements, will be required to firmly establish the frequency dependence of the rolloffs in the various bands in this equivalent breaking wave "source" spectrum.

In summary, the air acoustic data clearly are dominated by surf noise. However, rather than being a function of breaking wave source properties, the shape of the spectral ratio measurements probably is dictated by propagation effects. The 4 kHz peak in the ratios may represent an optimal frequency of propagation in the atmospheric waveguide which is formed above by refraction due to the increase with height of the onshore wind speed and reflection from the ground below.

V. CONCLUSIONS

The purpose of this paper has been to provide a broad, qualitative overview of the properties of the near-surf-zone background sound field in the 1 Hz to 10 kHz band. All of the major features in the air and underwater acoustic data collected over a 2.5-week period in early summer, 1995, off the Southern California coast have been identified and discussed.

Interesting features in the underwater acoustic data include the land-based cultural noise generated by the operation of water pumps. The pump sounds may have been readily detectable offshore because their sound sources are below the water table, thereby providing efficient coupling to the medium. The arrival structure of these signals, traveling mostly in the solid earth, is fairly complex, being smeared in azimuth and elevation angle. Predicting these arrivals will be the focus of future propagation modeling work. In contrast, the waterborne arrivals from pumps on Santa Catalina Island, 77 km to the west of the site, appear to be much simpler in structure.

The nighttime underwater acoustic data reveal the strange chorusing sounds of fish, believed to be members of the croaker (Sciaenidae) family. These sounds totally dominate the field at night from 50 Hz to more than 800 Hz. The cycling nature and frequency content of the choruses permit them to be easily confused with surf-generated sounds. Often, an individual fish was sufficiently close to a hydrophone array element that its knocking sequence was clearly discernible. These sequences are typically composed of 7 to 13 knocks, each separated by 0.7 sec, and having peak-peak source levels of around 160 dB re 1 μPa @ 1 m. Work is in progress in quantifying the variations in interknock periods during the experiment, information that will be useful in making a species identification. Some of the knock arrivals have 50-70 Hz oscillatory tails that represent the dispersive arrivals of interface waves propagating along the ocean-sediment interface. These Scholte wave arrivals can be used to invert for the shear wave properties of the uppermost part of the ocean bottom, another future area of research.

Another, as yet unidentified, biological sound source(s) created 50 - 250 Hz pulses intermittently throughout the experiment. In addition, it appears that the broad peak around 3.5 kHz in the nearest-to-shore moored sonobuoy data is generated by snapping shrimp, as it emanates from a kelp bed. Biological sounds were the dominant contributor to the underwater noise field in this experiment. In future underwater acoustic experiments designed to study surf-generated sounds, an understanding of the contribution from the biologics of the area is critical to correct interpretation of the data.

The evidence is weak that the underwater acoustic sensors detected surf noise. Although the spectral levels from 250-400 Hz in time-delay-and-summed beams in the landward direction are almost always higher than those in the seaward direction, the temporal variations in the landward spectral levels and the landward-to-seaward spectral ratios show little correlation with significant wave height or other surface wave parameters. The low correlation may be due to the fact that wave activity varied only a small amount (e.g., the significant wave height changed only by a factor of two) during the experiment. Alternatively, surf noise *may* not have been a measurable contributor to the offshore underwater sensor data. Several reasons why the latter might be true is that biological sounds dominated the noise field, the ocean surface waves never got to be very high due to shielding of westerly/northwesterly deep water swell by offshore islands and filtering by a kelp bed canopy, the kelp bed attenuated surf-generated sounds propagating through it to offshore sensors, water depth decreased too slowly with distance offshore, and the underwater sensors were placed too far from the surf zone.

However, in air, the acoustic field adjacent to the beach is clearly dominated by surf noise, with individual wave breaking events being easily distinguishable in air acoustic spectrograms. The ratio of the spectrum during wave breaking to that from a quiet period just prior to breaking shows a broad peak centered near 4 kHz. The shape of this peak appears to be determined by the air acoustic propagation conditions in the atmospheric waveguide formed by refraction above due to the prevailing onshore winds and reflection from the ground below. Future experimental work will include the broadband calibration of this waveguide using controlled air acoustic sources.

ACKNOWLEDGEMENTS

Bill Gaines of the Marine Physical Lab provided most of the logistics support and acted as the military liason for the experiment. His ideas and hard work greatly improved the quality of the data. Fruitful discussions were held with, and data processing results were provided by, Grant Deane and LeRoy Dorman, two other principal investigators in MPL's Adaptive Beach Monitoring program. Critical support was provided by other people at the Marine Physical Lab, notably Jim Murray, Pam Scott, Dave Ensberg,

Dick Harriss, Paula Hodgkiss, Greg Edmonds, Megan McArthur, Jui-Yuan Chang, Martin Olivera, and Katherine Kim.

Thanks are due to the Range Scheduling Office, Marine Corps Base, Camp Pendleton for giving permission to conduct this pilot experiment on Red Beach. Lieutenant Colonel Settle, Terry Finch, and Warrant Officer Cooper provided the support required to get the operations underway. Without the support of the Commander, Amphibious Group Three, this experiment would not have occurred. A special acknowledgement is due to Commander Craig Madsen of Amphibious Group Three, whose recognition of the potential advantages to Amphibious Warfare of the Adaptive Beach Monitoring system and his support for the experiment were instrumental in allowing MPL to stage this experiment. Special thanks also are extended to Ms. Ann Rosenberry, Code 232, Southwest Division, Naval Facilities Engineering Command, for her valuable assistance in ensuring compliance with State and federal environmental regulations. Her assistance was invaluable to the success of this pilot experiment. In addition, the cooperation of the Commander, U. S. Third Fleet is appreciated.

The cost of conducting ABM 95 was kept lower than otherwise posssible due to the generous loan of equipment from the Naval Command, Control, and Ocean Surveillance Center, RDT & E Division (NRaD). This equipment includes the towed HX 29 underwater source, ARR 52A sonobuoy receivers, a portable CTD, a differential GPS setup for use during deployment, an OTDR to check the fiber optic cable integrity, and 3.7 km of fiber optic cable. Additional thanks are due the Commander, Naval Air Warfare Center and the Commander, Naval Surface Warfare Center Division Crane for the gift of many of the sonobuoys used in this experiment.

Dean Carlson of the R/V Fisherette and Robert Mitchell ("Mitch") and Mike Kyle who crewed the Harbor Chief provided valuable support in the sea-going operations. Robert J. Triplett, the Traffic Census Coordinator at CalTrans, provided us with the Highway 5 vehicle count data.

The Adaptive Beach Monitoring program is sponsored by the Office of Naval Research, Code 32, under contract number N00014-93-D-0141 (DO #10).

Some of the work in this paper was presented at the Fall, 1995 [47] and Spring, 1996 [48] Acoustical Society of America meetings.

APPENDIX I - Sensor Systems in ABM 95

The following table contains a list of the sensor systems deployed during the ABM 95 experiment, along with the institutions responsible for their deployment. As mentioned in the text, only the data from the two hydrophone arrays, the moored sonobuoys, and the 6-element land microphone array (indicated by asterisks in the table) are discussed in this paper.

Sensor Systems Deployed in ABM 95

	Sensor System	Institution
*	2 64-Element hydrophone arrays	Marine Physical Lab/ SIO
	4 Ocean bottom seismometers (OBSs)	Marine Physical Lab/ SIO
*	4 Moored DIFAR (10 Hz - 2.4 kHz) sonobuoys	Marine Physical Lab/ SIO
*	4 Moored Omni (10 Hz - 40 kHz) sonobuoys	Marine Physical Lab/ SIO
*	6-Element land microphone array	Marine Physical Lab/SIO
	Land microphone w/parabolic dish	Marine Physical Lab/SIO
	24-element land geophone array	Marine Physical Lab/SIO
	2 Land microphone/meteorol. station sensor pods	ARL Penn State
	Land geophone array	ARL University of Texas
	2 Ocean bottom E- and M-field sensors	Marine Physical Lab/SIO
	4 Land magnetometers	Naval Comm., Cntrl and Ocean Surv. Cntr
	2 Land E-field sensors	Scripps Institution of Oceanography (SIO)

APPENDIX II - Environmental and Ancillary Data from ABM 95

Below is a list of all the environmental and ancillary information collected during the 1995 experiment. These data are discussed at length in [11].

Environmental and Ancillary Data from ABM 95

Data Type	Sensor System
Basic Weather Data i. wind speed and direction ii. air temperature iii. relative humidity iv. barometric pressure	• 10-m weather station from CCS • 2 miniature ARL/PSU met stations
Water Properties	• 15 CTD casts • inclinometer temperature sensor • CalCOFI report for Apr, 1995 cruise [49]
Ocean Surface Wave Activity	• 2 bottom pressure sensors at moorings 20 m and 300 m offshore • CDIP stations at San Clemente and Oceanside [50] • 2 videocameras
Ocean Currents	• 2 EM current meters at deepest mooring
Water Depth	• shipboard fishfinder during source tows • Navy SEAL survey of Red Beach [51]
Tide Heights	• NOAA stations at La Jolla and Santa Monica, CA • bottom pressure sensors at two offshore moorings
Kelp Canopy Coverage	• Aerial Survey by W. North [52]
Hwy 5 Traffic Activity	• CalTrans vehicle counter [53]
Train Activity	• Amtrak train schedule
Ocean Bottom Geoacoustic Properties	• San Onofre sediment study [54] • TL studies by J. Northrop [55]
Earthquake Activity	• Southern California Earthquake Center Reports [56]

REFERENCES

[1] O. B. Wilson, S. N. Wolf, and F. Ingenito, "Measurements of acoustic ambient noise in shallow water due to breaking surf," J. Acoust. Soc. Am. 78 (1), 190-195 (1985).

[2] E. S. Livingston and B. H. Pasewark, "Surf zone acoustic measurements from DUCK94", J. Acoust. Soc. Am. 98 (5), pt. 2, 2952 (1995).

[3] W. S. Hodgkiss, J. C. Nickles, G. L. Edmonds, R. A. Harriss, and G. L. D'Spain "A large dynamic range vertical array of acoustic sensors," in Proc. of the NATO Workshop, Full Field Inversion Methods in Ocean and Seismic Acoustics, ed. O. Diachok, A. Caiti, P. Gerstoft, and H. Schmidt, Kluwer Acad. Publ., Dordrecht, The Netherlands, 205-210 (1995).

[4] D. E. Ensberg, "Array element localization (AEL) for acoustic arrays deployed during the Adaptive Beach Monitoring Pilot Experiment," MPL TM-449, Marine Physical Laboratory, Scripps Institution of Oceanography, San Diego (1995).

[5] L. E. Horsley, "Modification and deployment techniques for hand-deployed Arctic long-life sonobuoys," IEEE J. Ocean. Engin. 14 (2), 211-220 (1989).

[6] M. B. Bennett, L. A. Thompson, P. T. Eisman, and K. C. Focke, "Moored data buoy for shallow water acoustic studies," in "Shallow water passive technology - broadband correlation studies; SWAMP II operations and preliminary results," ARL Tech. Rept. 92-6, Appl. Research Labs, The University of Texas at Austin, Austin, TX (1992).

[7] Sonobuoy Instruction Manual, NAVAIR 28-SSQ-500-1, (Naval Weapons Support Center, Indiana, 1983).

[8] K. M. McArthur, J. J. Murray, and W. S. Hodgkiss, "A comparison of DIFAR and omnidirectional sonobuoy data with hydrophone array data during the 1995 Adaptive Beach Monitoring Experiment," MPL Tech. Memo. 452, Marine Physical Laboratory, Scripps Institution of Oceanography, San Diego, CA (1996).

[9] "DIFAR Demultiplexer Description and Performance -- Software Version", Greeneridge Sciences, Inc., Santa Barbara, CA, (1995).

[10] D. Swanson, Appl. Research Labs, Penn State, State College, Pennsylvania, private communication (1995).

[11] G. L. D'Spain, R. Shear, R. M. Olivera, J. J. Murray, W. S. Hodgkiss, W. A. Kuperman, and W. K. Melville, "Environmental observations during the 1995 Adaptive Beach Monitoring Experiment," MPL Tech. Memo. 451, Marine Physical Laboratory, Scripps Institution of Oceanography, San Diego, CA (1995).

[12] L. M. Dorman, A. W. Sauter, C. Bradley, S. Wiggins, and J. Porras, "Short-range seismoacoustic propagation on and off the beach," J. Acoust. Soc. Am. 98 (5), pt. 2, 2971 (1995).

[13] W. Brown and T. Cummins, Facilities Maintenance Department, Camp Pendleton, California, private communication (1995).

[14] M. Carver, JMM Operational Services, Avalon, California, private communication (1996).

[15] R. J. Urick, Ambient Noise in the Sea, (Undersea Warfare Tech. Office, Naval Sea Systems Command, Washington, D.C., 1984).

[16] G. L. D'Spain, A. M. Richardson, W. S. Hodgkiss, and L. P. Berger, "Ambient noise vertical and horizontal directionality during SWellEx-1," MPL Tech. Memo. 443, Marine Physical Laboratory, Scripps Institution of Oceanography, San Diego, CA (1994).

[17] G. L. D'Spain, L. P. Berger, A. M. Richardson, G. A. Clapp, and J. Rice, "Late night fish choruses in the shallow waters off San Diego," J. Acoust. Soc. Am. 96 (5), 3270 (1994).

[18] G. A. Clapp, "Periodic variations of the underwater ambient noise level of biological origin off Southern California," NEL Tech. Memo. 1027, U. S. Navy Electronics Laboratory, San Diego, CA (1966).

[19] M. W. Johnson, "Sound as a tool in marine ecology, from data on biological noises and the deep scattering layer," J. Mar. Res. 7 (3), 443-458 (1948).

[20] M. P. Fish and W. Mowbray, Sounds of Western North Atlantic Fishes, (The Johns Hopkins Press, Baltimore, 1970).

[21] W. Cummings, private consultant, unpublished catalog of fish sounds (1994).

[22] G. Goodson, Fishes of the Pacific Coast, (Stanford University Press, Stanford, Calif, 1988), 58-66.

[23] M. P. Fish, "Biological sources of sustained ambient sea noise," in Marine Bio-acoustics, edited by W. N. Tavolga, (Pergammon Press, New York, 1964), 175-194.

[24] W. Evans, Texas Institute of Oceanography, Texas A&M University, private communication (1994).

[25] J. Copeland and A. Moiseff, "The occurrence of synchrony in the North American firefly *Photinus carolinus* (Coleoptera: Lampyridae)," J. Insect Behavior 8 (3), 381-394 (1995).

[26] A. Moiseff and J. Copeland, "Mechanisms of synchrony in the North American firefly *Photinus carolinus* (Coleoptera: Lampyridae)," J. Insect Behavior 8 (3), 395-407 (1995).

[27] "Military specification; Sonobuoy AN SSQ-57B," MIL-S-81478D(AS), Naval Air Engineering Center, Lakehurst, NJ (1990).

[28] M. R. Loewen and W. K. Melville, "An experimental investigation of the collective oscillations of bubble plumes entrained by breaking waves," J. Acous. Soc. Am. 95 (3), 1329-1343 (1994).

[29] F. A. Everest, R. W. Young, and M. W. Johnson, "Acoustical characteristics of noise produced by snapping shrimp," J. Acoust. Soc. Am. 20 (2), 137-142 (1948).

[30] G. L. D'Spain, W. S. Hodgkiss, and G. L. Edmonds, "Energetics of the deep ocean's infrasonic sound field," J. Acoust. Soc. Am. 89 (3), 1134-1158 (1991).

[31] "Underwater noise caused by snapping shrimp," Contract NObs-2074, UCDWR No. U337, University of California, Division of War Research, San Diego, CA (1946).

[32] W. J. North, "Introduction and background" in The Biology of Giant Kelp Beds (Macrocystis) in California, edited by W. J. North, (Verlag Von J. Cramer, Germany, 1971), p. 61.

[33] D. H. Cato and M. J. Bell, "Ultrasonic ambient noise in Australian shallow waters at frequencies up to 200 kHz," DSTO Materials Research Laboratory Rept. No. MRL-TR-91-23, Defence Science and Technology Organisation, Ascot Vale, Victoria, Australia (1992).

[34] W. W. L. Au, "The acoustics of snapping shrimp in Kaneohe Bay," J. Acoust. Soc. Am. 99 (4), pt. 2, 2533 (1996).

[35] J. E. Duffy, "Eusociality in a coral-reef shrimp," Nature 381, 512-514 (1996).

[36] M. B. Priestley, Spectral Analysis and Time Series (Academic Press, San Diego, 1989), pp. 466-468.

[37] H. L. Alder and E. B. Roessler, Introduction to Probability and Statistics (W. H. Freeman and Co., San Francisco, 1968) 4th ed., p. 303.

[38] M. R. Loewen and W. K. Melville, "Microwave backscatter and acoustic radiation from breaking waves," J. Fluid Mech. 224, 601-623 (1991).

[39] C. C. Mei, The Applied Dynamics of Ocean Surface Waves, (World Scientific, Singapore, 1989).

[40] R. M. Kennedy and T. V. Goodnow, "Measuring the vertical directional spectra caused by sea surface sound," IEEE J. Ocean. Engin. 15 (4), 299-310 (1990).

[41] R. M. Kennedy, S. A. L. Glegg, and P. Elisseeff, "Acoustic radiation due to wave-breaking," NUWC-NL Tech. Doc. 10,057, Naval Undersea Warfare Center Detachment, New London, Conn. (1992).

[42] R. M. Kennedy, "Sea surface dipole sound source dependence on wave-breaking variables," J. Acoust. Soc. Am. 91 (4), pt. 1, 1974-1982 (1992).

[43] J. E. Piercy and G. A. Daigle, "Sound propagation in the open air," Chapt. 3 in Handbook of Acoustical Measurements and Noise Control, edited by Cyril M. Harris, (McGraw-Hill, New York, 1991), 3rd ed.

[44] B. Kinsman, Wind Waves, Their Generation and Propagation on the Ocean Surface, (Dover Publ., New York, 1984), pp. 560-575.

[45] "Acoustics -- Attenuation of sound during propagation outdoors -- Part 2: General method of calculation," ISO/DIS 9613-2.2, International Organization for Standardization, CH-1211 Geneva 20, Switzerland (1994).

[46] "Acoustics -- Attenuation of sound during propagation outdoors -- Part 1: Calculation of the absorption of sound by the atmosphere," ISO/DIS 9613-1, International Organization for Standardization, CH-1211 Geneva 20, Switzerland (1993).

[47] G. L. D'Spain, W. S. Hodgkiss, L. P. Berger, and W. A. Kuperman, "Features of the seismoacoustic ambient noise field in a near-shore environment," J. Acoust. Soc. Am. 98 (5), pt. 2, 2952, (1995).

[48] G. L. D'Spain, W. S. Hodgkiss, W. A. Kuperman, and L. P. Berger, "Surf-generated noise and biological sounds in the near-surf-zone environment," J. Acoust. Soc. Am. 99 (4), pt. 2, 2453 (1996).

[49] The Marine Life Research Group, Scripps Institution of Oceanography, World Wide Web home page at the URL http://www-mlrg.ucsd.edu/mlrghome.html, data retrieved in Fall, 1995.

[50] The Coastal Data Information Program, Scripps Institution of Oceanography, World Wide Web home page at the Uniform Resource Locator (URL) http://splash.ucsd.edu/homepage.html, work supported by U.S. Army Corps of Engin. and State of Calif., data retrieved in Summer, 1995.

[51] Red Beach survey, SEAL team V, 25 July, 1994.

[52] W. J. North, Kerckhoff Marine Lab, California Institute of Technology, Corona del Mar, California, unpublished data (1995).

[53] R. J. Triplett, California Department of Transportation, San Diego, California, unpublished data (1995).

[54] San Onofre Sediment Dynamics Group, "Sediment Dynamics of the Area off San Onofre, California", R. Kolpack, ed. and project manager, submitted to Environmental Research, Southern California Edison Company, P.O. Box 800, Rosemead, CA (1990).

[55] J. Northrop, "Low-frequency sound propagation off Mission Beach, California", J. Acoust. Soc. Am., 67 (5), 1598-1602 (1980).

[56] The Southern California Earthquake Center, California Institute of Technology, World Wide Web home page at the URL http://scec.gps.caltech.edu, data retrieved in Summer, 1995.

[57] H. Cox, R. M. Zeskind, and M. M. Owen, "Robust Adaptive Beamforming," IEEE Transactions of Acoustics, Speech and Signal Processing ASSP-35 (10), (1987).

[58] R. Heitmeyer, B. Pasewark, and E. Livingston, Naval Research Laboratory, Washington DC, private communication (1995).

FIGURE CAPTIONS

Fig. 1 Map of the Southern California Bight region. The location of the ABM 95 experiment site, at 33.3° N, 117.5° W, is marked by a small box on the coast.

Fig. 2 The part of the Camp Pendleton chart where the Adaptive Beach Monitoring Pilot Experiment was conducted. The coastline runs northwest-southeast in the upper right corner of the figure. Highway 5, a major freeway between San Diego and Los Angeles, runs subparallel to the coastline to the northeast. Las Pulgas beach, also referred to as "Red Beach", is indicated by a circled "RB" in the figure. The circled "LHA"to the northwest of Red Beach indicates the location of a helicopter landing pad. At the southeastern end of the figure, the major LCAC (Landing Craft, Air Cushioned) offshore transit lane runs perpendicular to shore. Also, the broad diagonal line in the southwest corner shows the along-shore LCAC transiting lane. The dotted line cutting a diagonal across the figure signifies the offshore boundary of the AAV (Autonomous Amphibious Vehicle) training area. The grid squares on the chart are each 1000 m on each side. Superimposed on the map are the locations of 3 moored AN/SSQ-53D ("DIFAR") sonobuoys (plotted as solid triangles), 4 moored AN/SSQ-57B omnidirectional sonobuoys (plotted as solid circles), and the two 64-element bottom hydrophone arrays (plotted as two straight lines 3.4 km off Red Beach). The dashed lines radiating towards the coast from the array position indicate the directions of the main lobe and the 3 dB down points at 195 Hz and 370 Hz for the landward endfire beam of the 35-element subarray discussed in Sect. IV. On shore, a solid square marks the location of the data acquisition van, placed on a 10-m tall bluff at the northern end of Red Beach. The 6-element microphone array was placed on the surf side of the bluff, about 22.3 m from the van. The scattered, irregular, black patches to the west of the "LAS PULGAS BEACH" label indicate the distribution of the kelp canopy coverage as determined from an aerial survey conducted one month prior to the start of ABM 95.

Fig. 3 A plan view of the element positions of the two 64-element bottom hydrophone arrays. The coastline is located 3.4 km to the NE (bearing of 51°). The line array on the right hand side of the figure is approximately parallel to the coast and the other array is nearly perpendicular to it. A 35-element subsection of the array perpendicular to the coast is used to perform endfire beamforming for surf noise identification (re Sect. IV); its elements are highlighted with "x"'s.

Fig. 4 A drawing of the 6-element, lapel microphone array. Three metal rods were held rigidly in mutually orthogonal directions by a small poly-vinyl chloride (PVC) block, with the vertical rod driven into the ground several cm to provide a stable mounting for the microphones. The two elements on the vertical rod, drawn with circles, have a nominal sensitivity of −165 (±3) dB re 1 V/μPa, whereas the other four microphones, indicated by asterisks, are 7 dB less sensitive with a response of −172 (±4) dB re 1 V/μPa. The outputs from the 6 microphones were fed through single-channel audio amplifiers and recorded onto DAT tape using a bandwidth of 20 kHz.

Fig. II.1 A sound speed profile derived from the downcast CTD data taken at 17:32 GMT, JD 145.

Fig. II.2a The average sound speeds at 1 ("1"), 5 ("5"), 10 ("A"), 15 ("E"), and 20 ("2") m depths calculated from the CTD casts. The one point at 5 m depth on JD 161 was obtained from temperature measurements made during the low frequency source tows. The tick marks on the horizontal axis occur at 12:00 GMT on each even-numbered Julian day.

Fig. II.2b The hourly-averaged air temperature as a function of time, from the 10-m weather station data.

Fig. II.3a The ocean surface wave peak period band as a function of time obtained from the Coastal Data Information Program bottom pressure sensor array at San Clemente, about 10 km upcoast from the ABM 95 site [50].

Fig. II.3b The ocean surface wave significant wave angle which specifies the predominant direction the waves are traveling *TO*, also from the Coastal Data Information Program bottom pressure sensor array at San Clemente [50]. The horizontal dashed line at 51° indicates the direction normal to Red Beach.

Fig. II.4 A map of the Southern California Bight region showing the predictions of the Southern California Swell Model for 23 Aug, 1995, from the Coastal Data Information Program World Wide Web site [50]. The ABM 95 experiment site is 33.3° N, 117.5° W.

Fig. II.5a Tide heights, referenced to an arbitrary level, as a function of time. These data were collected by a bottom pressure sensor at the deepest oceanography mooring at the ABM 95 site, about 300 m offshore.

Fig. II.5b The hourly traffic counts along Highway 5 in the north-bound (solid curve) and south-bound (dashed curve) directions. The data were obtained from a California Department of Transportation (CalTrans) sensor just north of Oceanside Harbor exit [53].

Fig. III.1 A 30-min spectrogram, from 0 to 750 Hz, estimated using the data from a single element of the bottom hydrophone array. The starting time of the data are 06:51 GMT (23:51 local PDT), JD 148. The spectrogram was calculated by dividing the time series into consecutive, nonoverlapped, 8192-point (5.46-sec) blocks and incoherently averaging the three 50-%-overlapped, 4096-point fft's within each block. A Kaiser-Bessel window with $\alpha = 2.5$ was used to window each segment before fft'ing.

Fig. III.3 A frequency-versus-angle beamforming plot using the horizontal bottom hydrophone array data. The time of data recording is 06:51 GMT (just prior to local midnight) on JD 148. The vertical axis runs from 10 Hz to 329 Hz. The horizontal axis goes from −180° (south) through the westerly directions to 0° (north) and then through the easterly directions back to the south at +180°. The elevation angle is fixed at 5° up from the horizontal direction. The contours superimposed on the plot occur in 5 dB increments. The beamforming result was created by coherently processing both line arrays' data. The element data were fast-Fourier transformed and the white-noise-constrained adaptive beamforming algorithm [57] with a constraint of 14.5 dB was applied to each frequency bin. The constraint is 6 dB down from ten times the logarithm, base 10, of the number of array elements, which equals the white noise gain in conventional plane wave beamforming.

Fig. III.4 White-noise-constrained adaptive beamforming results over elevation angle and azimuth at 170 Hz. The elevation angles span the range from −90° (vertically downward), through 0° (horizontal), to +90° (vertically upward). The processing method and the other features of the plot are the same as in Fig. III.3.

Fig. III.5 A single-array-element spectrogram covering the 5-min period starting at 01:43 GMT (18:43 local PDT), JD 152. The fft length is 1024 points, giving a frequency resolution of 1.5 Hz.

Each spectral estimate (horizontal line) of the figure is obtained by incoherently averaging two nearly statistically independent fft's, giving a temporal resolution of 1.02 sec.

Fig. III.6 Five 2D pressure spectral density estimates from a single element of the hydrophone array. The vertical axis covers the 50-105 dB re 1 $\mu Pa^2/Hz$ range and the horizontal axis again goes from 0 to 750 Hz. Each spectral estimate was obtained by incoherently averaging sufficient 512-point fft's (frequency resolution of 2.93 Hz) to provide over 60 degrees of freedom, yielding a 90 % confidence interval of −1.2 dB to +1.4 dB. The labels for each of the curves are explained in the text.

Fig. III.7 A calibrated time series of 9 secs of data, sampled at 1.5 kHz, from a single bottom hydrophone array element. These data, collected at 01:44 GMT, JD 152, form the very dark, broadband stripe at 1.7 min in Fig. III.5.

Fig. III.8 A 3-hour spectrogram over the 0 to 750 Hz band starting at 10:33 GMT (03:33 local PDT), JD 156. To create this figure, the processed results for six consecutive 30-min spectrograms were concatenated together. The processing method and the single bottom array element are the same as in Fig. III.1.

Fig. III.9 The occurrence and character of the croaker choruses over the 2.5-week array recording period. The information in this plot was obtained from qualitative assessment of consecutive, half-hour, single-array-element spectrograms. The results for each day of the experiment, starting at the top with JD 144 and ending at the bottom on JD 164, is represented by a horizontal band. Time of day increases from left to right, starting at local noon (19:00 GMT) on each day. The chorus amplitudes are classified as "Light", "Medium", and "Heavy" (i.e., loud) and the periods without choruses as "Background". Times when the broadband spectral levels are very high, but do not display a cycling chorus behavior (discussed in the text) are labeled "Continuous". The "Decaying" periods around sunrise are those when the chorus amplitudes are decreasing and the inter-chorus period is increasing with time. The times of local sunset and sunrise are given by vertical white lines in the plot.

Fig. III.10 A plot of 9.38 sec of calibrated, single-hydrophone-array-element time series collected at 04:34 GMT, JD 156. The first 670 msec of the time series is the uppermost line of the plot, the second 670 msec is the second line, and so on, down the page. The vertical scale for each of the 14 lines, from -50 to +50 Pa, is given for the lowermost line in the figure.

Fig. III.11 A calibrated spectrogram from a single element of the bottom hydrophone array. The start time of the 5-min data recording period is 20:36 GMT (13:36 local PDT), JD 154. Time increases downward along the vertical axis, from 0 to 5 min, and the frequency ranges from 0 to 750 Hz along the horizontal axis. The spectrogram was calculated using a 4096-point fft, yielding a frequency resolution of 0.37 Hz. The individual fft's were weighted with a Kaiser-Bessel window of $\alpha = 2.5$. Sequential fft's were overlapped by 50 percent, giving a temporal resolution of 1.37 sec. The time period used to estimate the spectra and spectral ratios in Fig. IV.A.2a,b is indicated on the right hand side of the plot.

Fig. III.12 A 3-sec calibrated time series (upper plot) and spectrum of the first arrival (lower plot) for a pulse pair extracted from Fig. III.11. The time series were obtained by forming a time-delay-and-sum beam in the broadside direction using a straight subsection of the bottom array oriented parallel to the coast (the easterly array in Fig. 3). Before plotting, the beam data were bandpass filtered between 35 Hz and 375 Hz and desampled by a factor of 2 (to a 750-Hz sampling rate). The 0.2-sec section of the time series between the two vertical dotted

lines in the upper plot were used in calculating the spectrum in the lower plot.

Fig. III.13 The variation in amplitude and occurrence of the biological pulses of unknown origin over the course of the experiment. This plot was created in a way similar to Fig. III.9, by visual examination of single-element spectrograms.

Fig. III.14 Three spectral density estimates from each of the two moored omnidirectional sonobuoys closest to the coast. The inshore buoy, whose three spectra are plotted with thin lines, transmitted its data on radio frequency sonobuoy channel 24. The farther offshore buoy transmitted on channel 25 and its spectra are plotted with thick lines. The time periods for these estimates were 30 sec in duration, taken at the same time of day, 00:00 GMT (17:00 local PDT), on three consecutive days, JD 145, 146, and 147. The spectra have been corrected for the prewhitening in the sonobuoy data acquisition system [27], but are otherwise uncalibrated because of significant clipping of the data. The fft length was 8192 points, giving a frequency resolution of 10.3 Hz with the data sampling rate of 84.7 kHz. Each spectral estimate contains over 1200 degrees of freedom.

Fig. III.15 A plan view of the experiment site showing the track of the deployment ship (solid line) as it headed to the southwest just after deploying the two nearest-to-shore sonobuoys. The size of this plot is 3.3 km north/south by 4.3 km east/west and is approximately the same scale as Fig. 2. The omnidirectional sonobuoy location is plotted with a circle and the adjacent triangle marks the position of the moored DIFAR sonobuoy. The location of the DIFAR buoy 2.4 km offshore is indicated by a second triangle. The solid diagonal line in the upper right corner of the plot shows the location of the coastline, and the data acquisition van next to the beach is plotted as a square. Radiating from each of the two DIFAR buoy locations are three dotted lines. The directions of these lines were calculated by first integrating the horizontal acoustic intensity spectra (re Fig. III.16) from 1.5 to 2.4 kHz for several different time periods. The average, and plus/minus one standard deviation, of the directions towards an acoustic source determined by these integrated intensity spectra are plotted as the dotted lines.

Fig. III.16 The pressure spectral density estimate (upper plot) and the corresponding horizontal active acoustic intensity spectrum (lower plot) estimated from the nearest-to-shore DIFAR sonobuoy data. Both spectra were estimated over the same 6-sec period of time at 21:28 GMT, JD 132, by incoherently averaging 29 2048-point fft's with 50 % overlap. These processing parameters provide a frequency resolution of 2.4 Hz, and a 90 % confidence interval of +1.6 dB to −1.2 dB for the pressure spectral density estimate. The confidence interval on the acoustic intensity estimate is dependent upon the coherence between the omnidirectional and the directional components of the DIFAR buoy. The horizontal axes for both plots are in linear frequency units from 0 to 2.4 kHz. In the upper plot, the vertical axis is in units of dB re 1 $\mu Pa^2/Hz$ and the vertical axis in the lower plot is in units of dB re 1 $\mu Watt/m^2/Hz$. The horizontal intensity magnitude for a given frequency bin in the lower plot can be obtained by measuring the length of that bin's vector along the y axis, starting at −80 dB re 1 $\mu Watt/m^2/Hz$. The direction in which the vector points indicates the direction of net acoustic energy flux, referenced to the compass in the upper right-hand corner of the plot. The intensity spectrum has been corrected for the magnetic variation of 14° east. Additional information on these types of plots can be obtained in [30].

Fig. IV.A.1a A calibrated spectrogram of the landward endfire beam formed using a 35-element subsection of the bottom hydrophone array oriented perpendicular to the coast. The time period on the vertical axis is the same as in Fig. III.11. However, the horizontal frequency axis now runs from 0 up to 400 Hz since the array element spacing is such that spatial aliasing occurs above

400 Hz. The method of spectrogram calculation is the same as in Fig. III.11.

Fig. IV.A.1b A calibrated spectrogram of the seaward endfire beam formed using a 35-element subsection of the bottom hydrophone array oriented perpendicular to the coast. The axes and the method of calculation are the same as in Fig. IV.A.1a.

Fig. IV.A.2a The spectral density estimate of the landward endfire beam averaged over the 12-sec period indicated on the right hand side of Figs. IV.A.1a and b. The vertical axis ranges from 45 to 95 dB re 1 $\mu Pa^2/Hz$ and the horizontal axis goes from 0 to 400 Hz. The linear regression fit to the spectral levels from 250 to 390 Hz is plotted as a solid line.

Fig. IV.A.2b The ratio of the landward-to-seaward endfire beam spectral levels averaged over the same 12-sec period as in Fig. IV.A.2a. The vertical axis spans values from - 10 to + 15 dB, with negative values (values below the horizontal dashed line) indicating higher spectral levels in the seaward than the landward direction. The horizontal axis is the same as in Fig. IV.A.2a. The horizontal dotted line at + 2.53 dB marks the 95 % confidence level for the spectral ratio estimates, i.e., given that the data are Gaussian distributed, then if the spectral levels in the landward direction are, in fact, equal to or lower than those in the seaward direction, then only 5 % of the estimates, on average, should fall above the dotted line. The solid straight line from 250-390 Hz is the linear regression fit over this band.

Fig. IV.A.3a A 2.5-week time series, from JD 147 to JD 165 of the linear regression fits to the landward spectral density levels over the 250-390 Hz band, evaluated at 300 Hz. The vertical axis covers the 15 dB range from 50 to 65 dB re 1 $\mu Pa^2/Hz$, and the horizontal axis goes from 12:00 GMT, JD 141 to 12:00 GMT, JD 169 (tick marks occur at 12:00 GMT on the even-numbered Julian days).

Fig. IV.A.3b The time series of the slopes of the best-fit regression lines to the landward endfire spectral levels from 250-390 Hz. The vertical axis is from - 0.05 to + 0.01 dB re 1 $\mu Pa^2/Hz$ per Hz, with negative slope values signifying decreasing spectral levels with increasing frequency. The horizontal axis is the same as in Fig. IV.A.3a.

Fig. IV.A.3c The time series of the 250-390 Hz linear regression fits to the landward/seaward spectral ratios, evaluated at 300 Hz. The vertical axis runs from - 4.0 dB to + 15.0 dB, with the horizontal dashed line marking the 0.0 dB level. Values greater than 0 dB indicate levels that are higher in the landward than the seaward direction. The horizontal axis is the same as in Fig. IV.A.3a,b.

Fig. IV.A.3d The corresponding time series of the slopes of the regression fits to the landward/seaward spectral ratios over 250-390 Hz. The vertical axis ranges from - 0.03 to + 0.10 dB per Hz, with positive values indicating increasing landward/seaward spectral ratios with increasing frequency.

Fig. IV.A.3e Time series of the ocean surface wave significant wave height (average height of highest third of the waves) recorded by the Coastal Data Information Program station at San Clemente. The vertical axis ranges from 0.2 to 2.8 m, and the horizontal axis is the same as in Figs. IV.A.3a-d. The three asterisks in the plot show the significant wave height for the three time periods considered in reference [1].

Fig. IV.A.3f The spectrogram of the amplitude squared of the ocean surface wave activity over the same time period as in Figs. IV.A.3a-e. The vertical axis spans the periods from 5-23 sec, and the gray scale covers the 15-25 cm^2 range.

Fig. IV.A.3g Time series of the wind speed measured by the 10-m weather station over the same time period as in Figs. IV.A.3a-f. The vertical axis goes from 0 to 10 m/sec (19.4 kts).

Fig. IV.A.4 A comparison of the bottom bathymetry out to 5 km offshore between the Monterey Bay site studied in Ref. [1] (plotted as connected asterisks) and the ABM 95 site (plotted as connected circles). The depth on the vertical axis runs from 0 to 70 m. The Monterey Bay depths were taken from Fig. 1 of [1]. The depths for the ABM site are a combination of the along-coast-averaged SEAL team survey results from 0 to 0.35 km offshore [51] and the shipboard echo-sounder data, corrected to true water depth, collected during the underwater acoustic source tows.

Fig. IV.A.5 A comparison of the bottom bathymetry versus distance offshore out to 370 m between the DUCK 94 and the ABM 95 sites. Depth runs from 0 to 7 m on the vertical axis. The DUCK 94 bathymetry, plotted as connected "+"'s, were obtained from the Naval Research Laboratory [58]. The ABM 95 water depths, plotted with circles, are the along-coast-averaged results from the 1994 SEAL team survey of Red Beach [51].

Fig. IV.B.1 A 5-min normalized spectrogram of the air acoustic data collected by one of the sensors in the 6-element microphone array. The data were collected by the microphone near the top of the vertical support rod in Fig. 4. The spectrogram was calculated using a 4096-point fft, yielding a frequency resolution of 4.88 Hz, with a sequential fft overlap of 50 percent, giving a temporal resolution of 0.10 sec. The data were whitened before plotting using two high-pass RC filters in cascade, both with poles at 1.2 kHz, to give a 12 dB/octave roll-off with decreasing frequency. The vertical axis covers the 0-5 min time period, the horizontal frequency axis runs from 0 to 10 kHz, and the gray scale covers the 0 to - 40 dB range. The two arrows on the right hand side of the plot indicate the two times used to estimate the spectra and spectral ratios presented in Figs. IV.B.2 and IV.B.3.

Fig. IV.B.2 The calibrated received pressure spectral density estimates from two microphones' data. The solid curve is estimated using the data from the same sensor as in Fig. IV.B.1 and the dotted curve is for the microphone on the downcoast side of the horizontal metal rod oriented in the alongcoast direction. The spectra were estimated over a 1.2-sec time period indicated by the lower arrow on the right hand side of Fig. IV.B.1, during a wave breaking event. Averaging 22 realizations of the 2048-pt fft's, overlapped by 50 %, provides a - 1.4 dB to + 1.7 dB confidence interval at the 90 % level for the spectral estimates. The vertical axis runs from - 15 to + 35 dB re 1 $\mu Pa^2/Hz$ and the horizontal frequency axis goes from DC up to 10 kHz.

Fig. IV.B.3 The ratio of the averaged air acoustic spectral density during the wave breaking event indicated by the lower arrow on the right hand side of Fig. IV.B.1 to the spectral density just prior to wave breaking, indicated by the upper arrow in Fig. IV.B.1. The spectral estimates were calculated as described in Fig. IV.B.2's caption. The horizontal dotted line at + 3.2 dB specifies the 95 % confidence level above which the wave breaking spectral levels are statistically greater than those prior to breaking. The vertical axis ranges from 0 to 20 dB and the horizontal axis covers the same 0-10 kHz band as in Figs. IV.B.1 and IV.B.2. The curve fits at the lower frequencies extending up to 4 kHz are the predictions of attenuation due to ground interaction. The solid curves are for a source height of 0.3 m; the upper solid curve is for soft ground and the lower solid curve is for very soft ground. The other dotted and

dashed curves at the lower frequencies are the ground attenuations for other source heights. The curves marked with asterisks extending up to 10 kHz are the predictions of attenuation due to atmospheric absorption, with the upper curve being for 90 % relative humidity and the lower curve for 70 % humidity. Note that the vertical scale for these curve fits is exactly the same as that for the spectral ratio, but runs in the opposite direction. For example, attenuation due to atmospheric absorption at 70 % relative humidity is nearly 0 dB at very low frequencies and increases up to almost 12 dB at 10 kHz.

Fig. IV.B.4 The ratio of the underwater acoustic spectrum estimated during wave breaking to the spectrum estimated shortly after breaking during a quiet period, derived from the spectra in Fig. 4 of [1]. The hydrophone was located 200 m outside the surf zone. The upper plot has a linear frequency scale from 0 - 2000 Hz, whereas the lower plot displays the same ratio on a log frequency axis (the values are Bels re 1 Hz). The vertical axis in both plots runs from 0 to 20 dB.

Fig. IV.B.5 The 1-min-averaged wind speeds (upper plot) and directions (lower plot) recorded by the 10-m weather station during the recording of a microphone array data tape. Both plots' horizontal axes cover the 0 to 120 min period starting at 18:05:00 GMT, JD 164, with the vertical dashed lines indicating the time of recording of the microphone data presented in Figs. IV.B.1-3. The vertical axis in the upper plot of wind speed varies from 0 to 7 m/sec (13.6 kts). The lower plot shows the direction that the wind is blowing *to*, rather than the direction it is coming *from*. The vertical axis covers the true directions from - 90° (due west) to + 90° (due east), with 0° being true north. The horizontal dashed line in the lower plot shows the direction normal to the coastline at Las Pulgas beach.

Fig. IV.B.6 The estimated offshore range of breaking surf from the mean lower low water (MLLW) mark as a function of Julian day. The horizontal axis of this figure from JD 141 to JD 169 is the same as in Figs. IV.A.3a-g. The vertical axis goes from 0 to 225 m and the vertical dashed line signifies the time of recording of the data in Figs. IV.B.1-3. The method of calculation for this estimated range is described in the text.

Fig. IV.B.7 Two microphones' calibrated air acoustic pressure spectra for a breaking wave, corrected for the propagation effects from atmospheric absorption, ground interaction, and geometrical spreading to obtain equivalent point source pressure spectra. The received pressure spectra used in the calculation are those plotted in Fig. IV.B.2. The upper plot shows the corrected spectra on a linear frequency axis from 0 to 10 kHz, with a 0 - 50 dB re 1 $\mu Pa^2/Hz$ range on the vertical axis. The lower figure has a log frequency axis ranging from 0.0 to 1.0 Bels re 1 kHz (i.e., only the data in the upper plot above 1 kHz are plotted), and a 5 - 40 dB re 1 $\mu Pa^2/Hz$ span on the vertical axis.

Southern California Bight Region

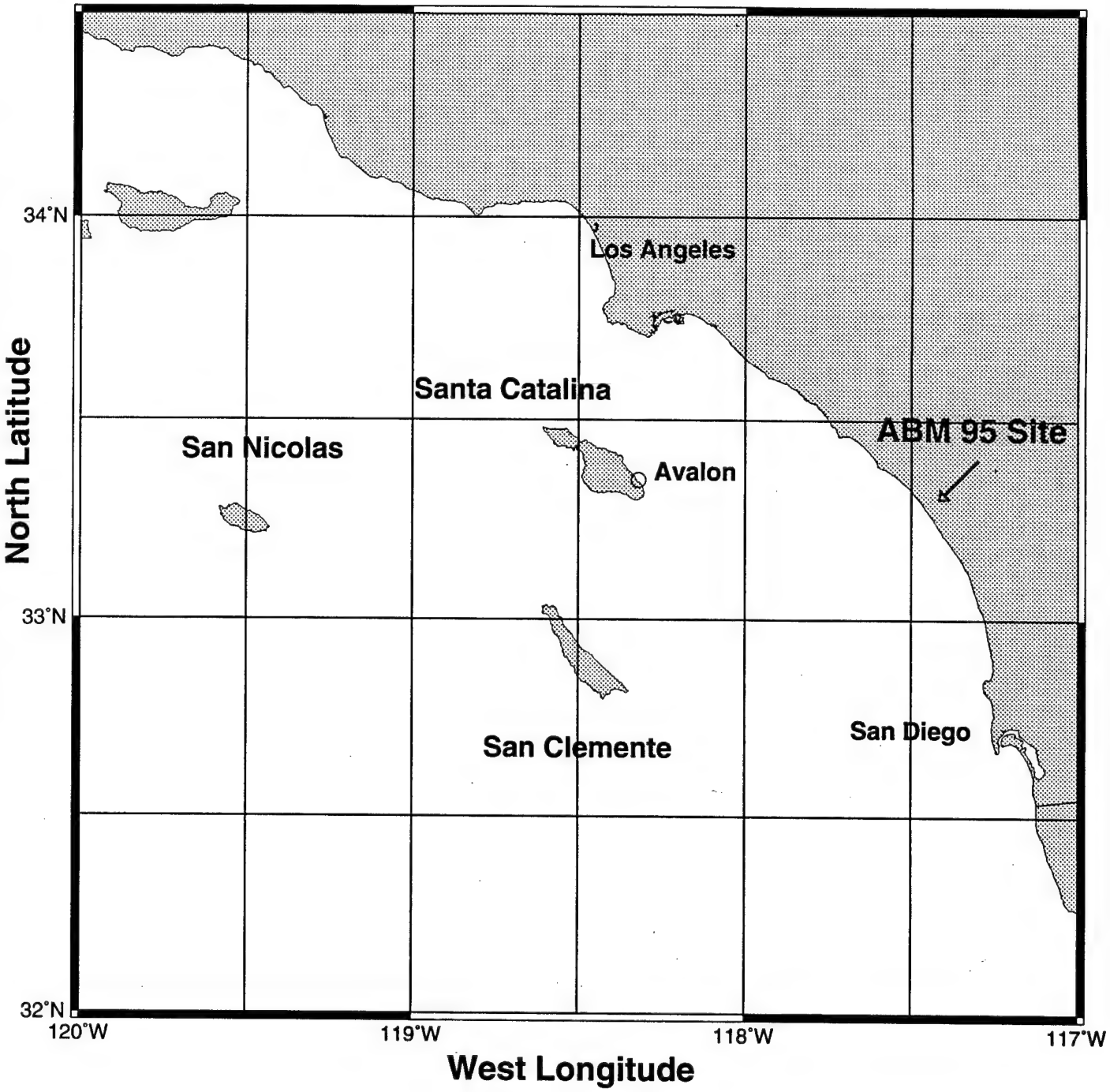

Figure 1

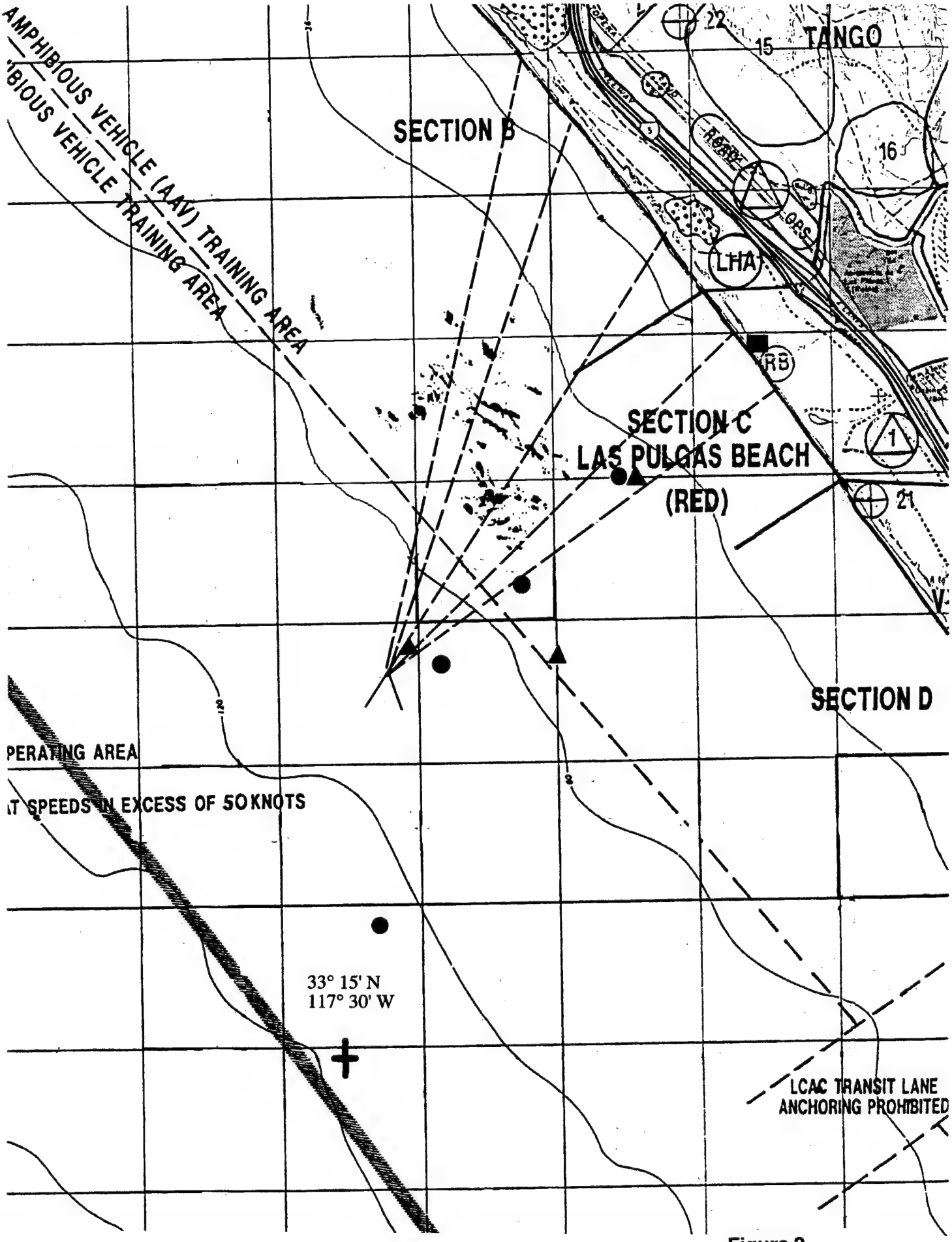
AMPHIBIOUS VEHICLE (AAV) TRAINING AREA
AMPHIBIOUS VEHICLE TRAINING AREA
SECTION B
TANGO
22
15
16
RAMP
LHA
RB
SECTION C
LAS PULGAS BEACH
(RED)
1
21
SECTION D
PERATING AREA
T SPEEDS IN EXCESS OF 50 KNOTS
33° 15' N
117° 30' W
LCAC TRANSIT LANE
ANCHORING PROHIBITED

Figure 2

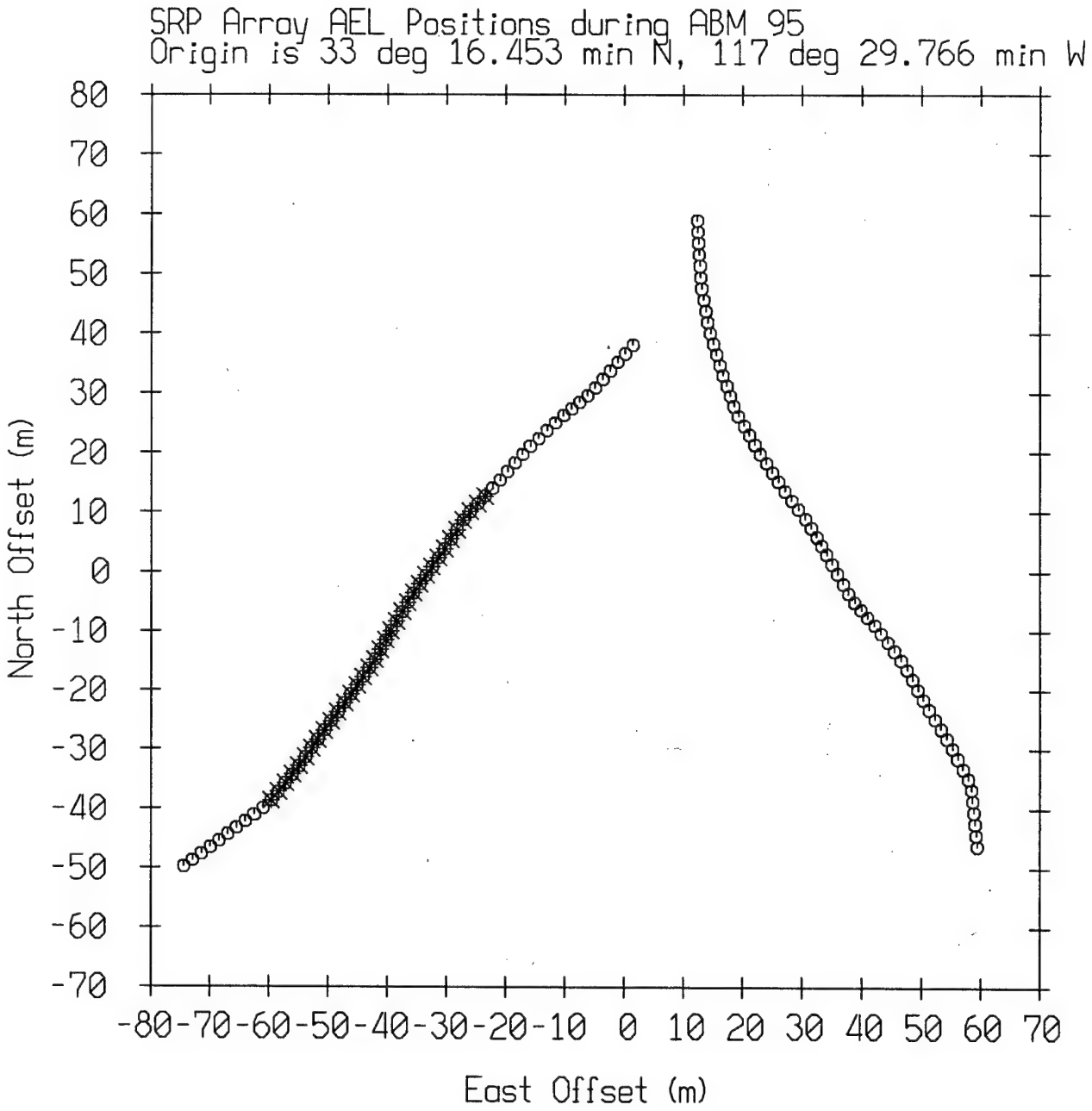
SRP Array AEL Positions during ABM 95
Origin is 33 deg 16.453 min N, 117 deg 29.766 min W
North Offset (m)
80
70
60
50
40
30
20
10
0
-10
-20
-30
-40
-50
-60
-70
-80 -70 -60 -50 -40 -30 -20 -10 0 10 20 30 40 50 60 70
East Offset (m)

Figure 3

6 - Element Microphone Array

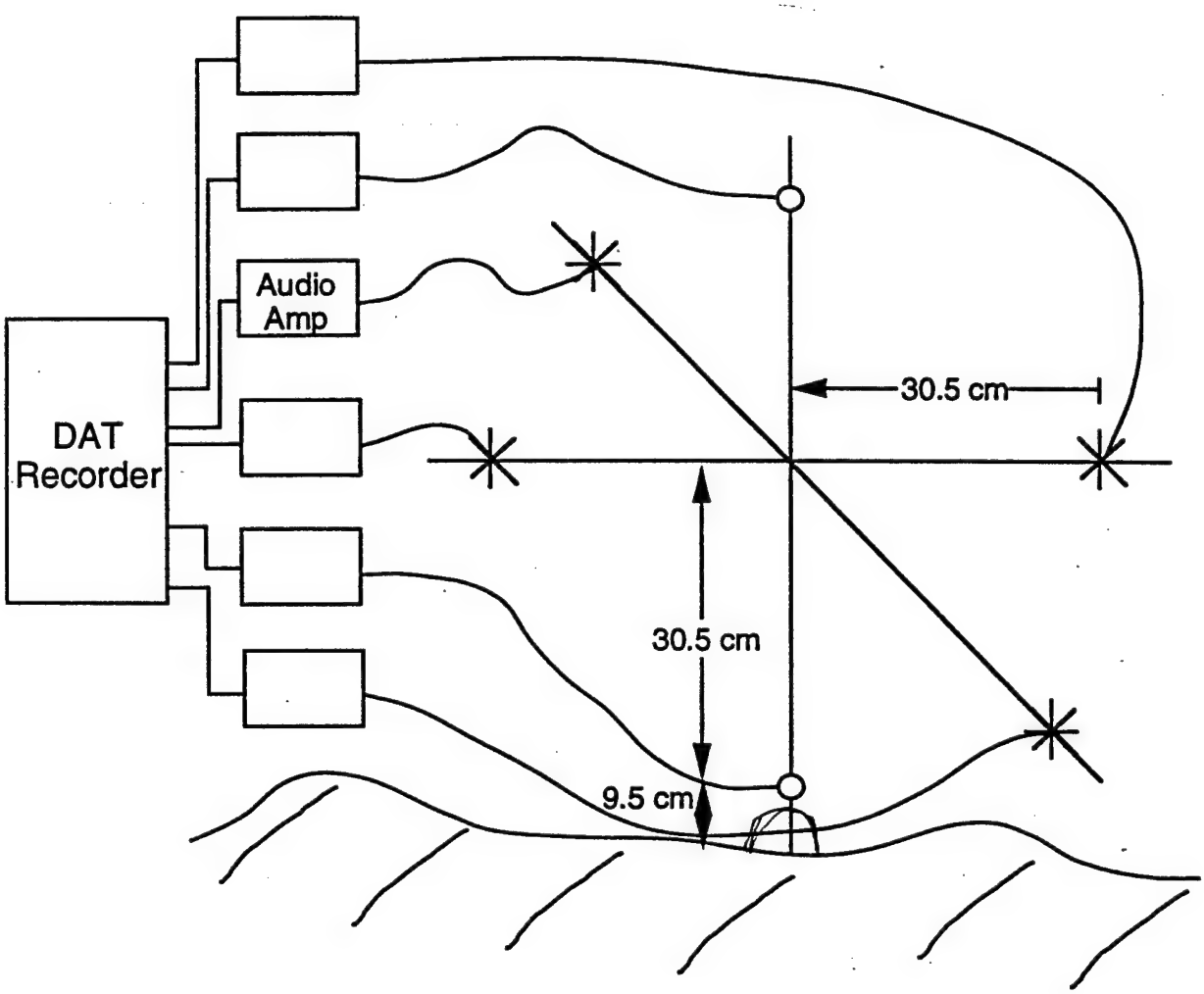

Figure 4

csd 4/10/96

Sound Speed Profile from CTD Data

17:32 GMT, JD 145

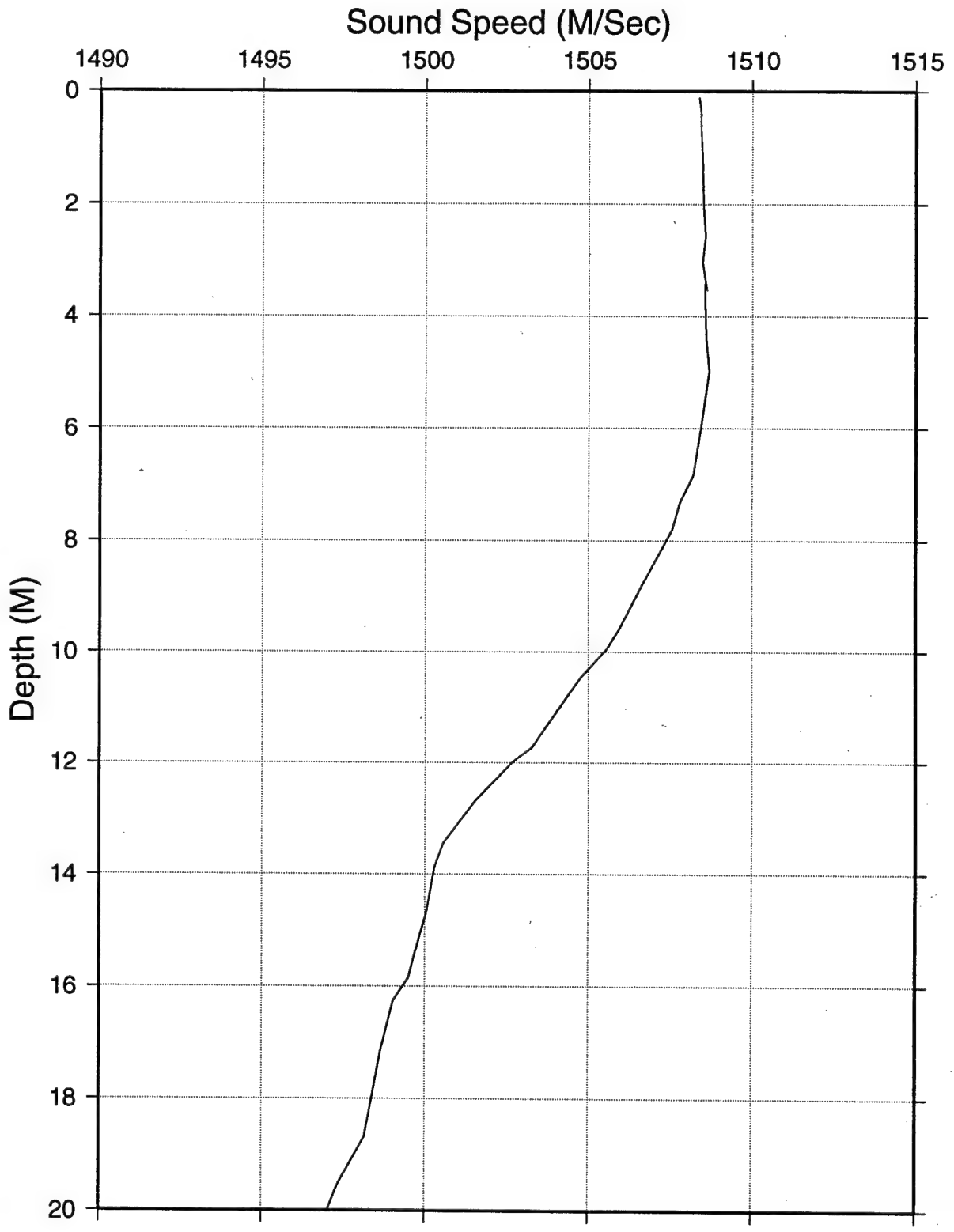

Figure II.1

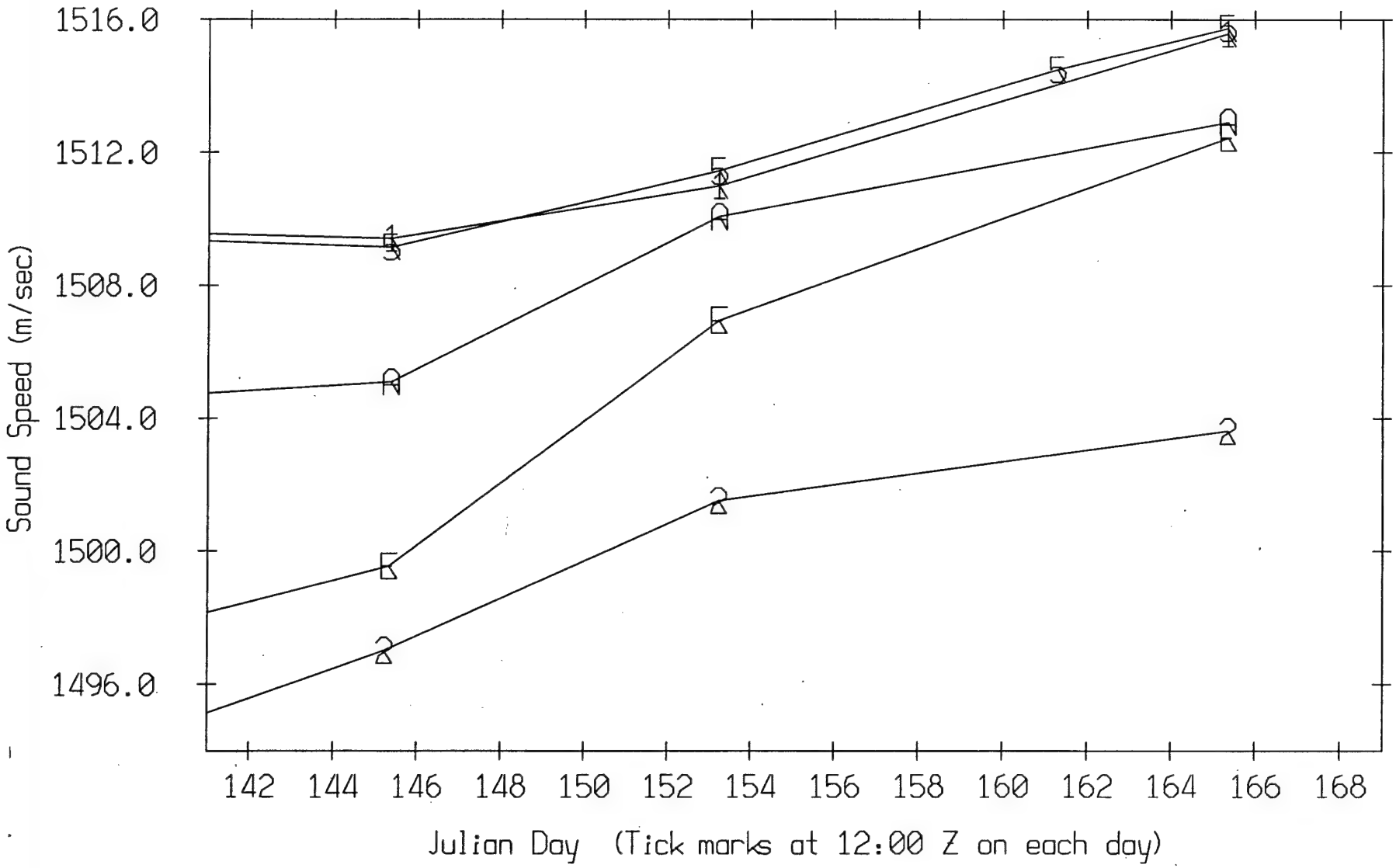
Sound Speed Contours vs Time at Given Depths
1 m ("1"), 5 m ("5"), 10 m ("A"), 15 ("E"), 20 m ("2")
1516.0
1512.0
1508.0
1504.0
1500.0
1496.0
Sound Speed (m/sec)
142
144
146
148
150
152
154
156
158
160
162
164
166
168
Julian Day (Tick marks at 12:00 Z on each day)

Figure II.2a

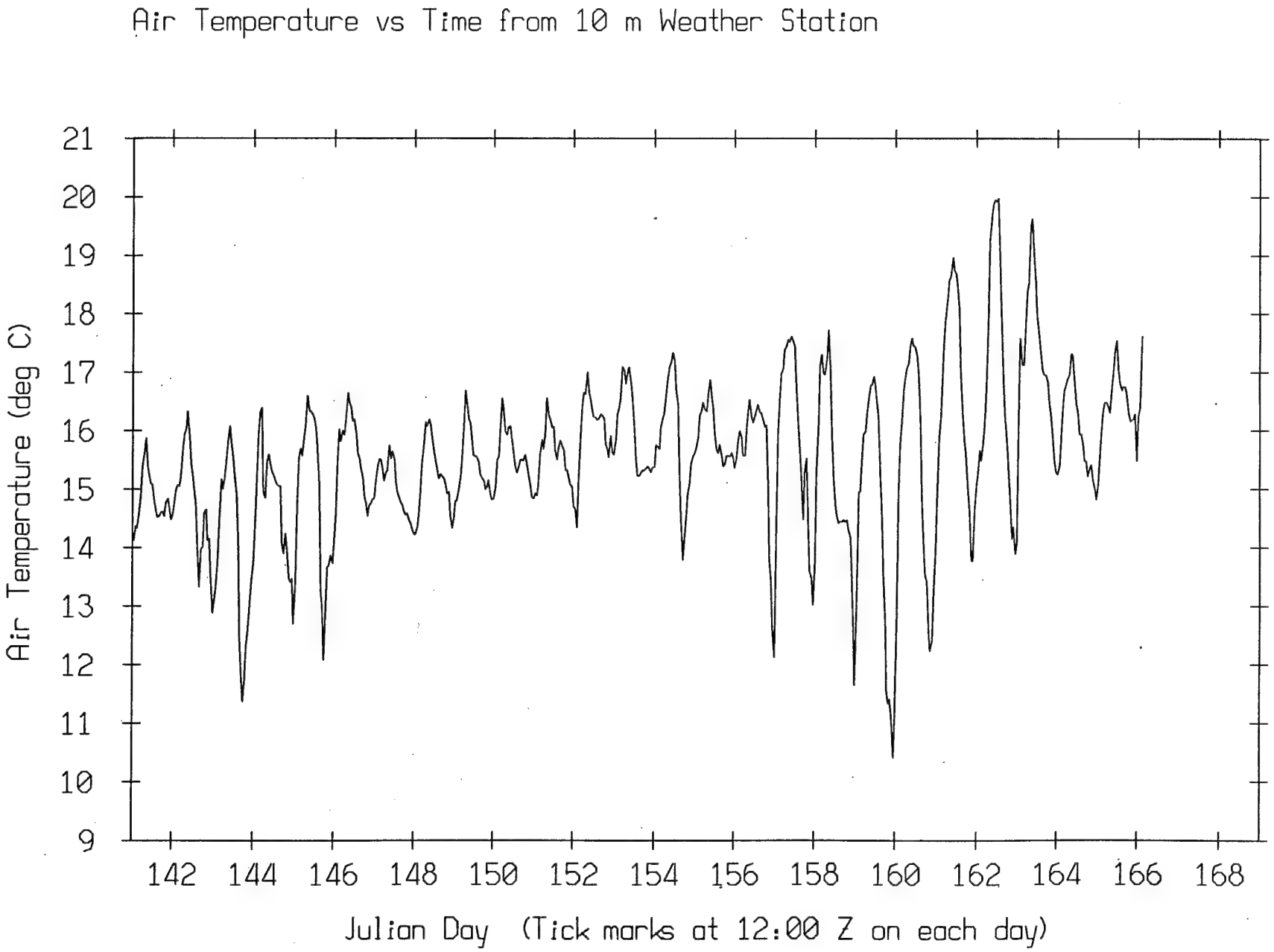
Air Temperature vs Time from 10 m Weather Station
Air Temperature (deg C)
21
20
19
18
17
16
15
14
13
12
11
10
9
142
144
146
148
150
152
154
156
158
160
162
164
166
168
Julian Day (Tick marks at 12:00 Z on each day)

Figure II.2b

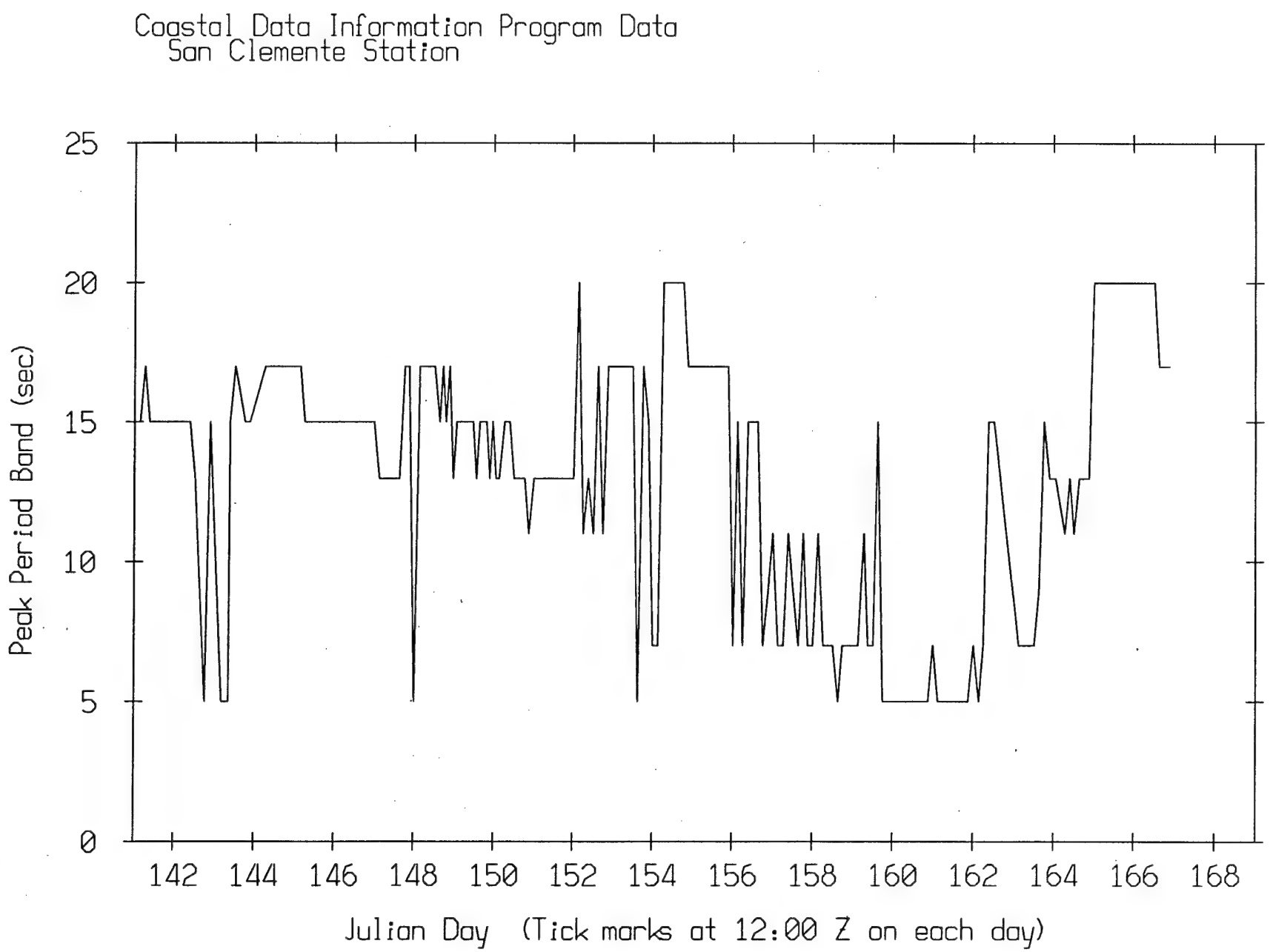
Coastal Data Information Program Data
San Clemente Station
Peak Period Band (sec)
25
20
15
10
5
0
142
144
146
148
150
152
154
156
158
160
162
164
166
168
Julian Day (Tick marks at 12:00 Z on each day)

Figure II.3a

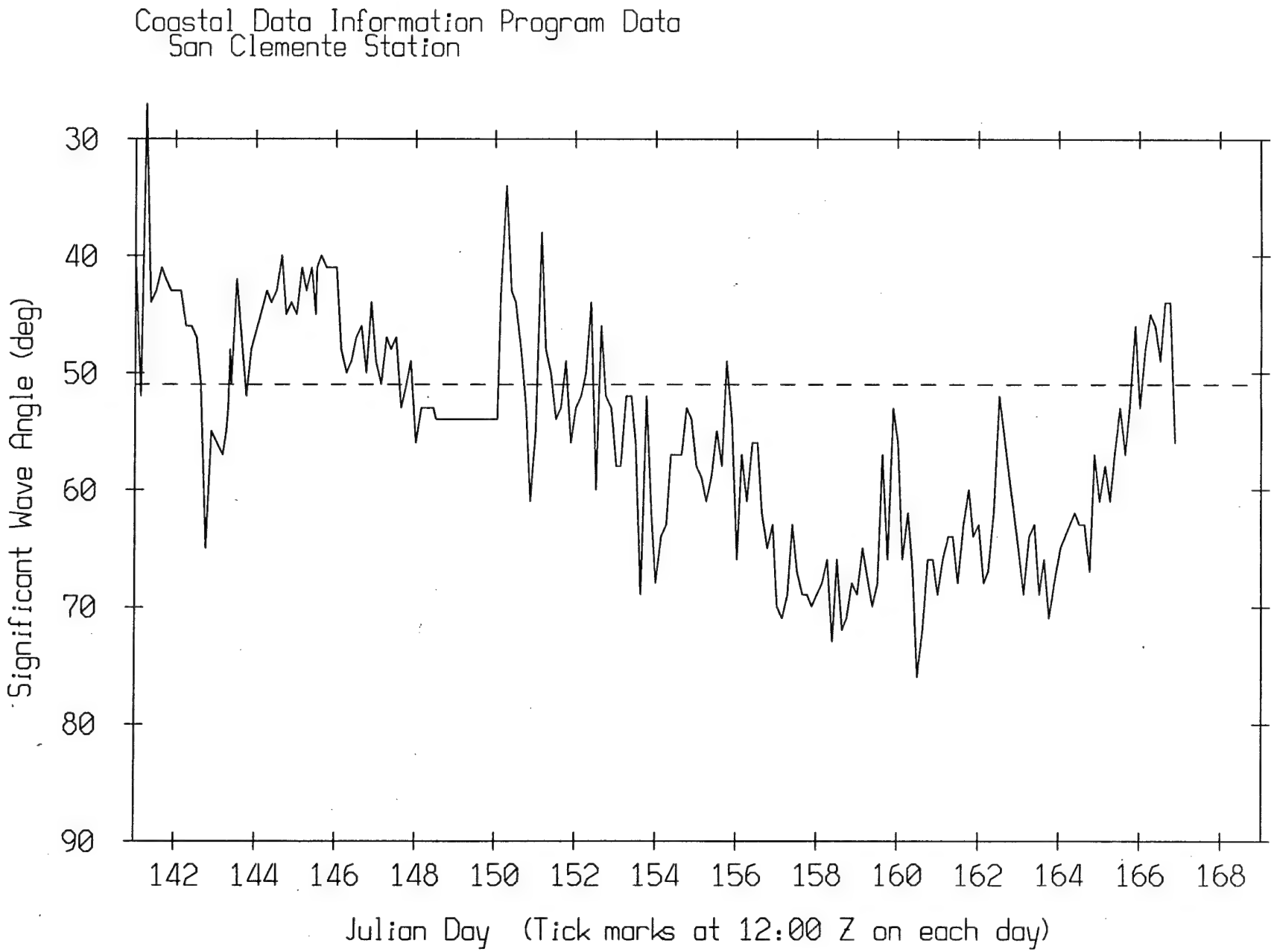
Coastal Data Information Program Data
San Clemente Station
Significant Wave Angle (deg)
30
40
50
60
70
80
90
142
144
146
148
150
152
154
156
158
160
162
164
166
168
Julian Day (Tick marks at 12:00 Z on each day)

Figure II.3b

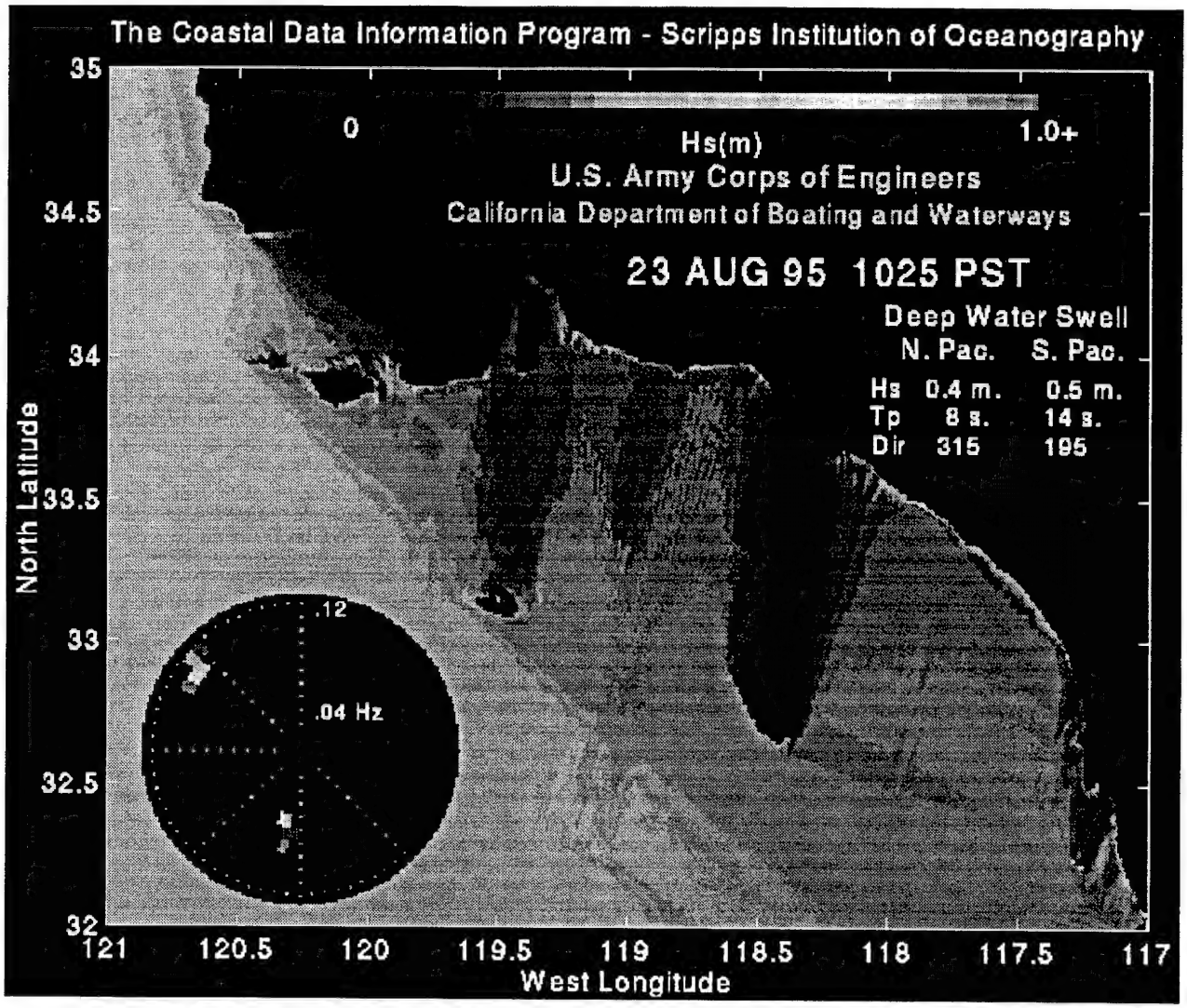
The Coastal Data Information Program - Scripps Institution of Oceanography
0
Hs(m)
1.0+
U.S. Army Corps of Engineers
California Department of Boating and Waterways
23 AUG 95 1025 PST
Deep Water Swell
N. Pac. S. Pac.
Hs 0.4 m. 0.5 m.
Tp 8 s. 14 s.
Dir 315 195
.12
.04 Hz
North Latitude
35
34.5
34
33.5
33
32.5
32
West Longitude
121
120.5
120
119.5
119
118.5
118
117.5
117

Figure II.4

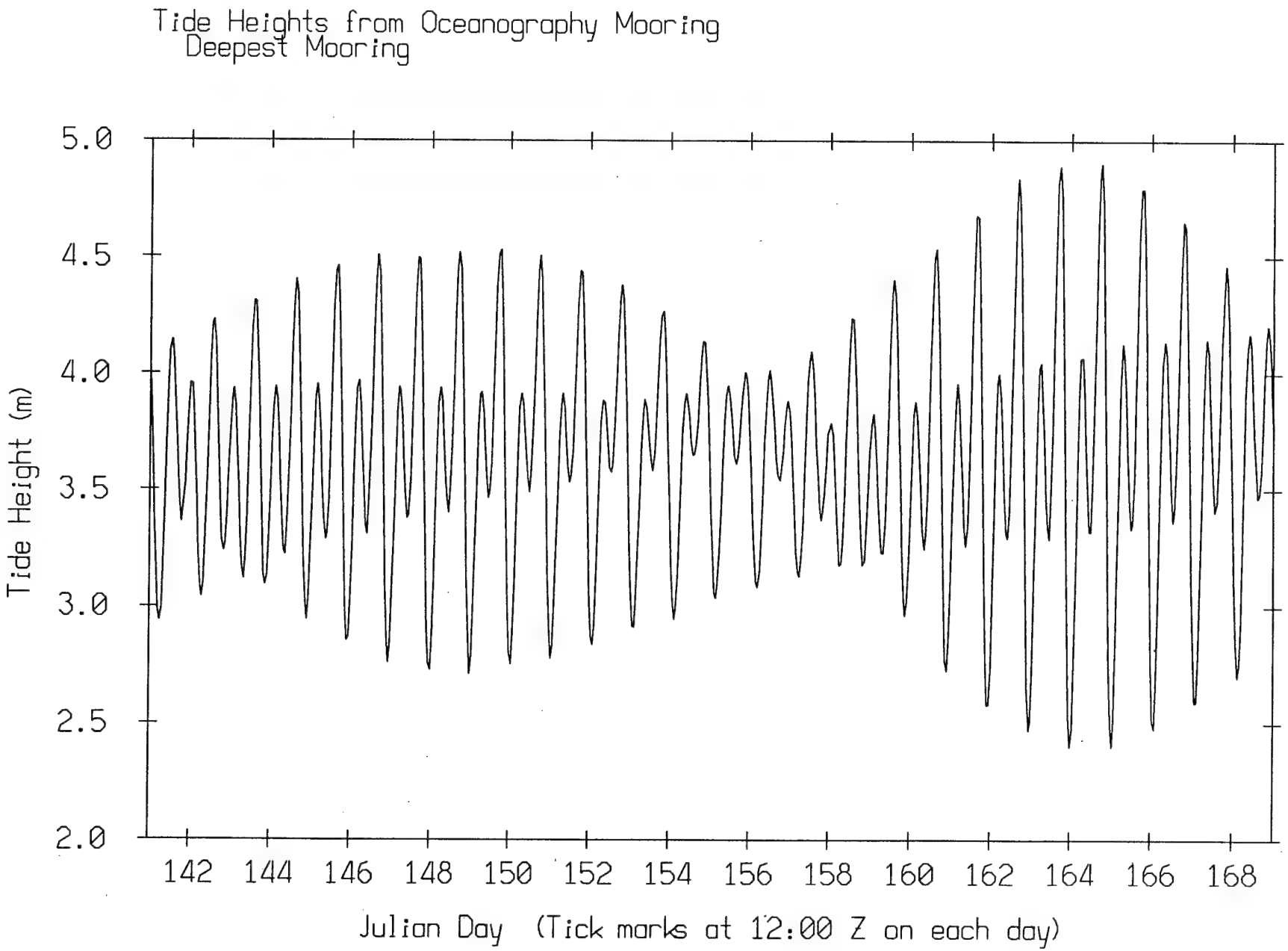
Tide Heights from Oceanography Mooring
Deepest Mooring
5.0
4.5
4.0
3.5
3.0
2.5
2.0
Tide Height (m)
142
144
146
148
150
152
154
156
158
160
162
164
166
168
Julian Day (Tick marks at 12:00 Z on each day)

Figure II.5a

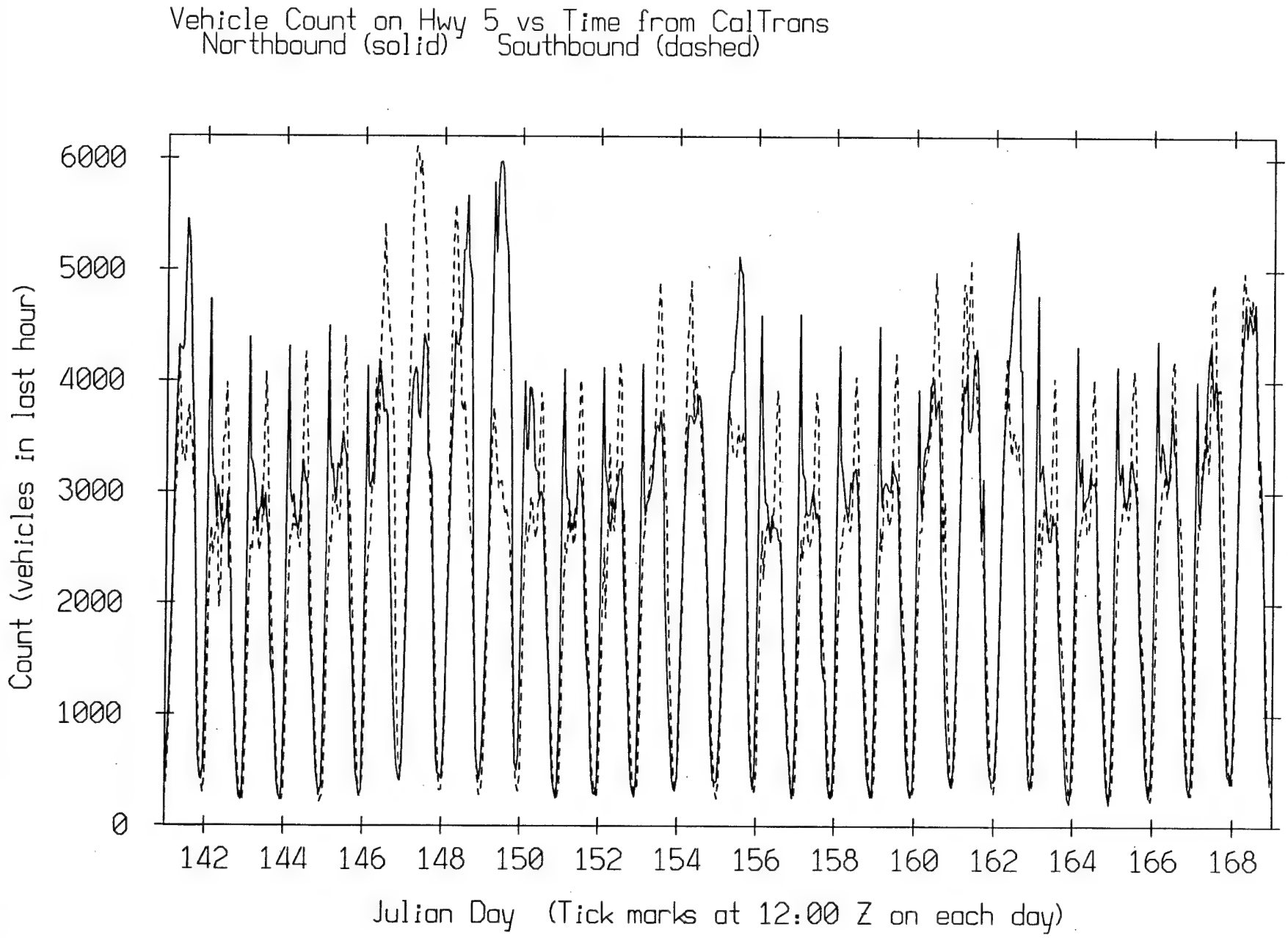
Vehicle Count on Hwy 5 vs Time from CalTrans
Northbound (solid) Southbound (dashed)
Count (vehicles in last hour)
6000
5000
4000
3000
2000
1000
0
142
144
146
148
150
152
154
156
158
160
162
164
166
168
Julian Day (Tick marks at 12:00 Z on each day)

Figure II.5b

ABM SRP NS Array Single Element Gram

JD 148 Start time of tape is 06:51 GMT

Element 8 Offset is 1 point

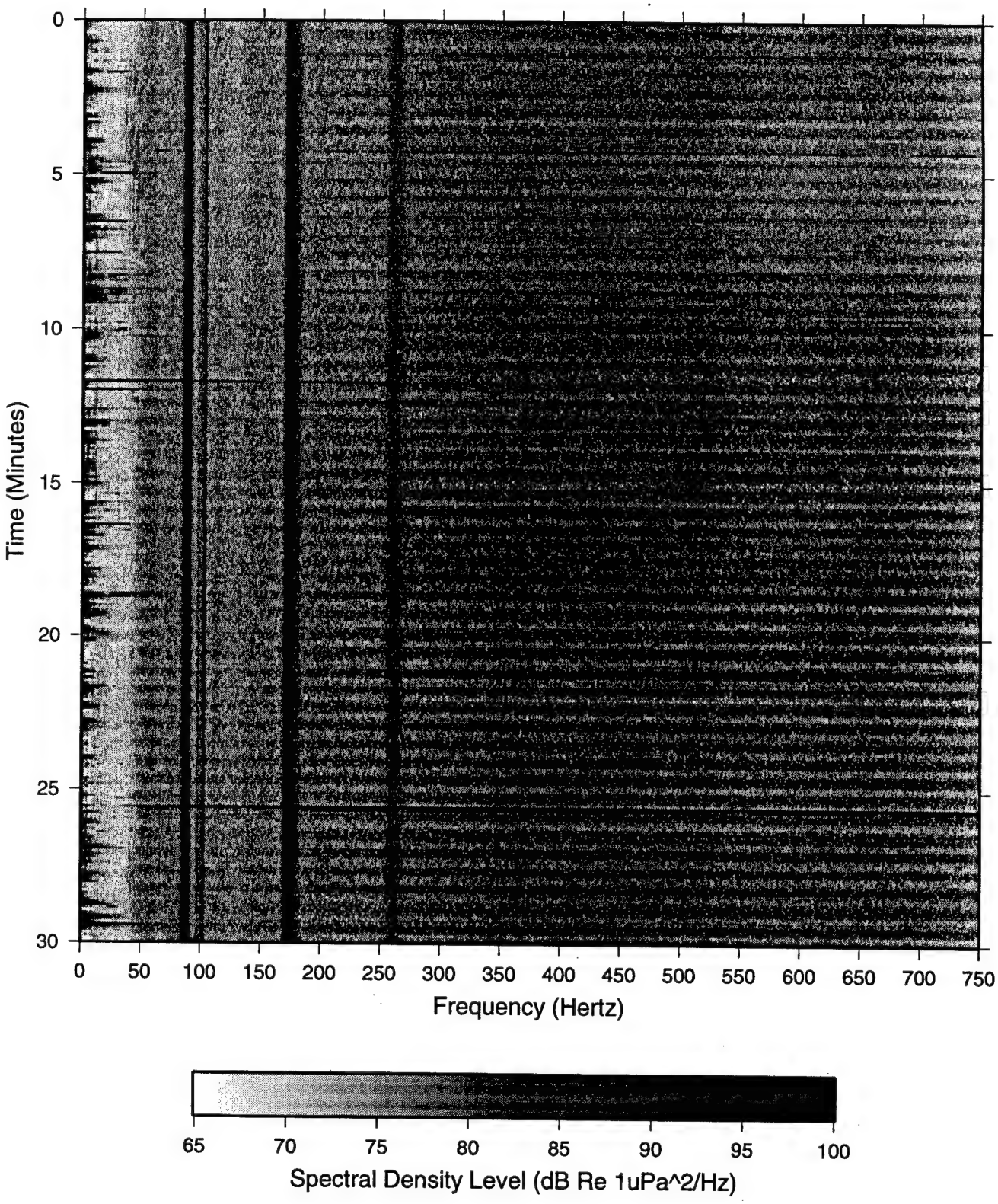

Figure III.1

Water Pumps

ABM SRP NS/EW JD 148 Time 06:51

Adaptive Beamformer (a3) using AEL positions

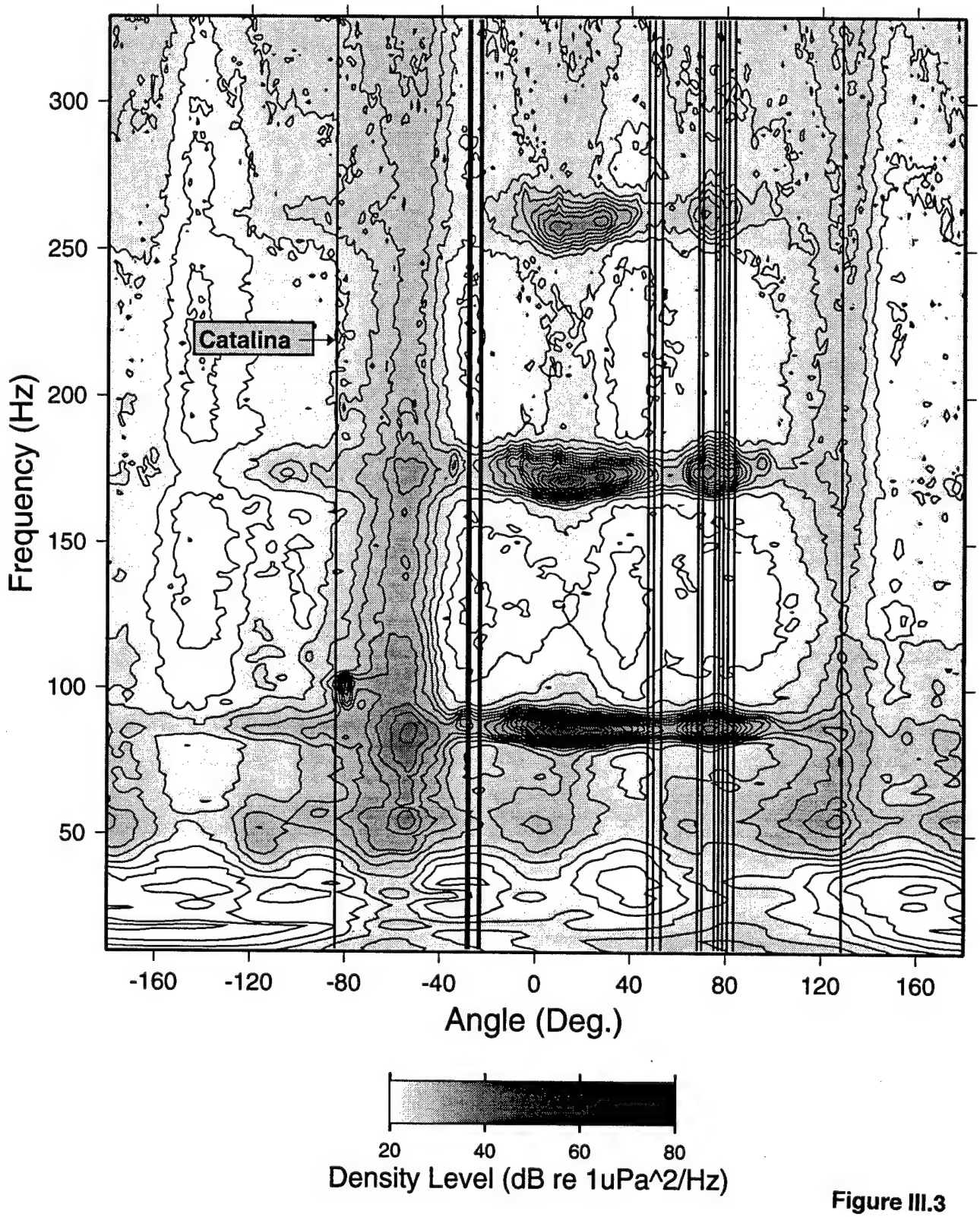

Figure III.3

Water Pumps

ABM SRP NS/EW JD 148 Time 06:51 Frequency = 170 Hz

Adaptive Beamformer (a3) using AEL positions

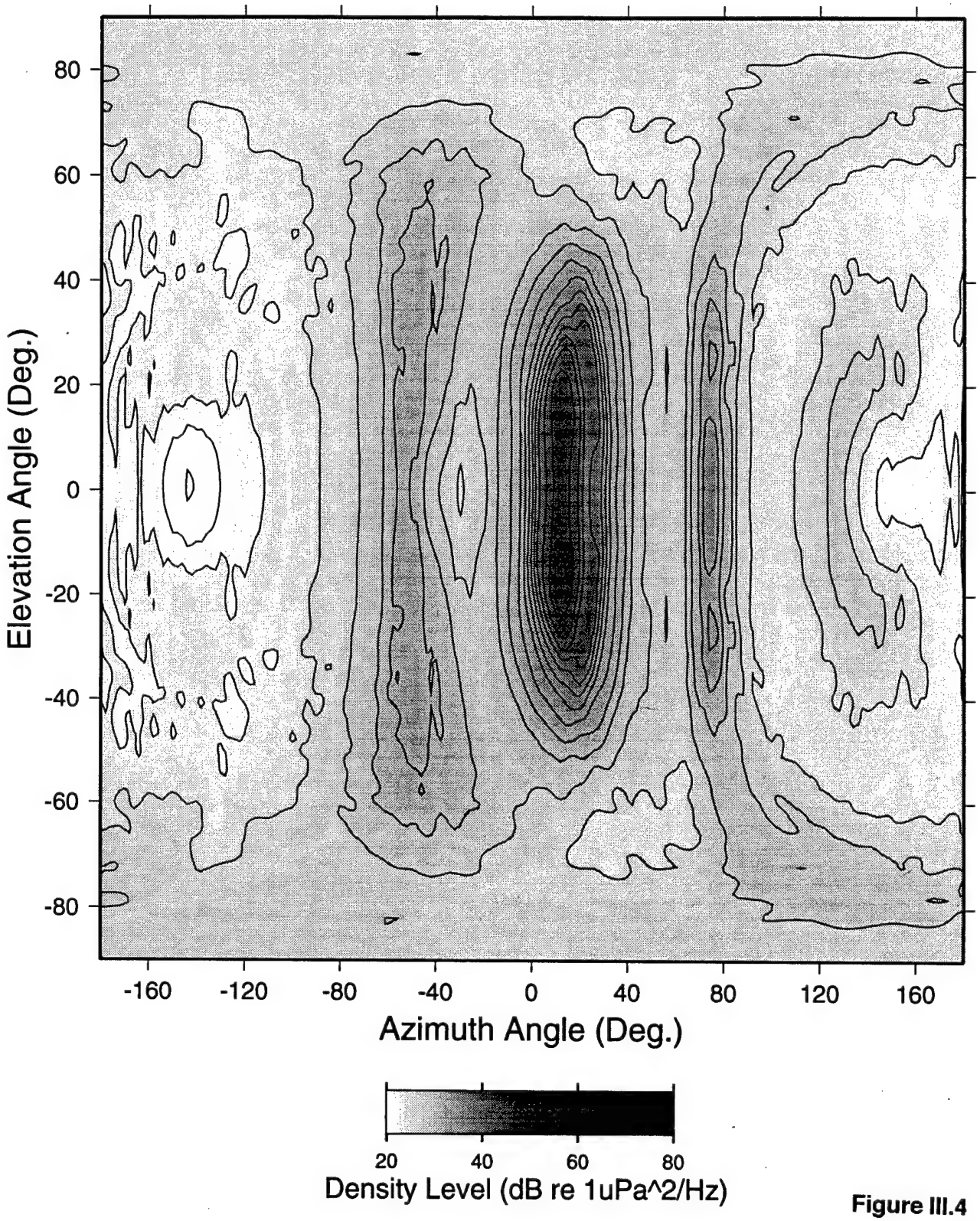

Figure III.4

ABM SRP NS Array Single Element Gram

JD 152 Start time of tape is 01:43 GMT

Element 8 with Zero Offset

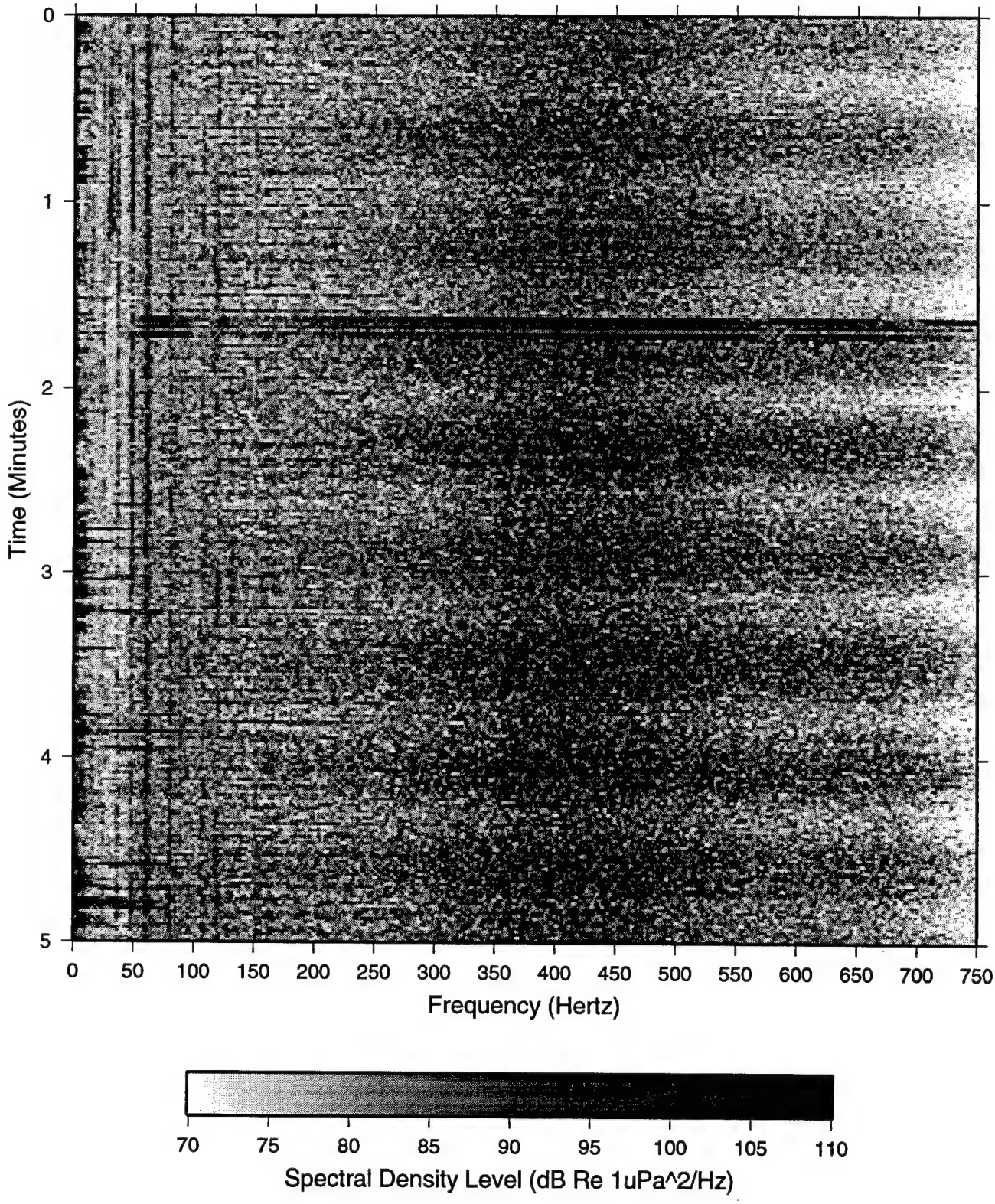

Figure III.5

ABM SRP Croaker Data Element 8 JD 151-152

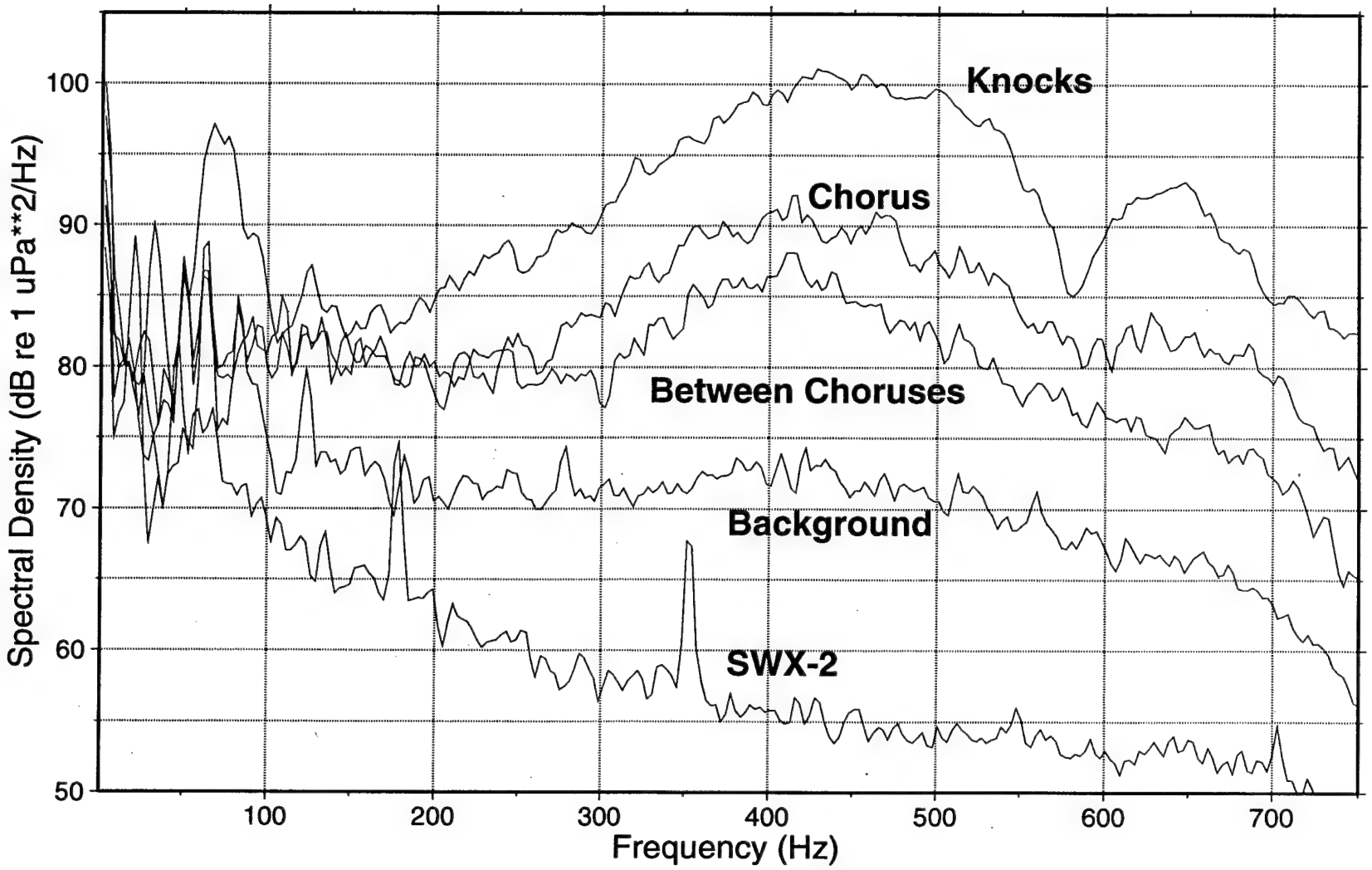

Figure III.6

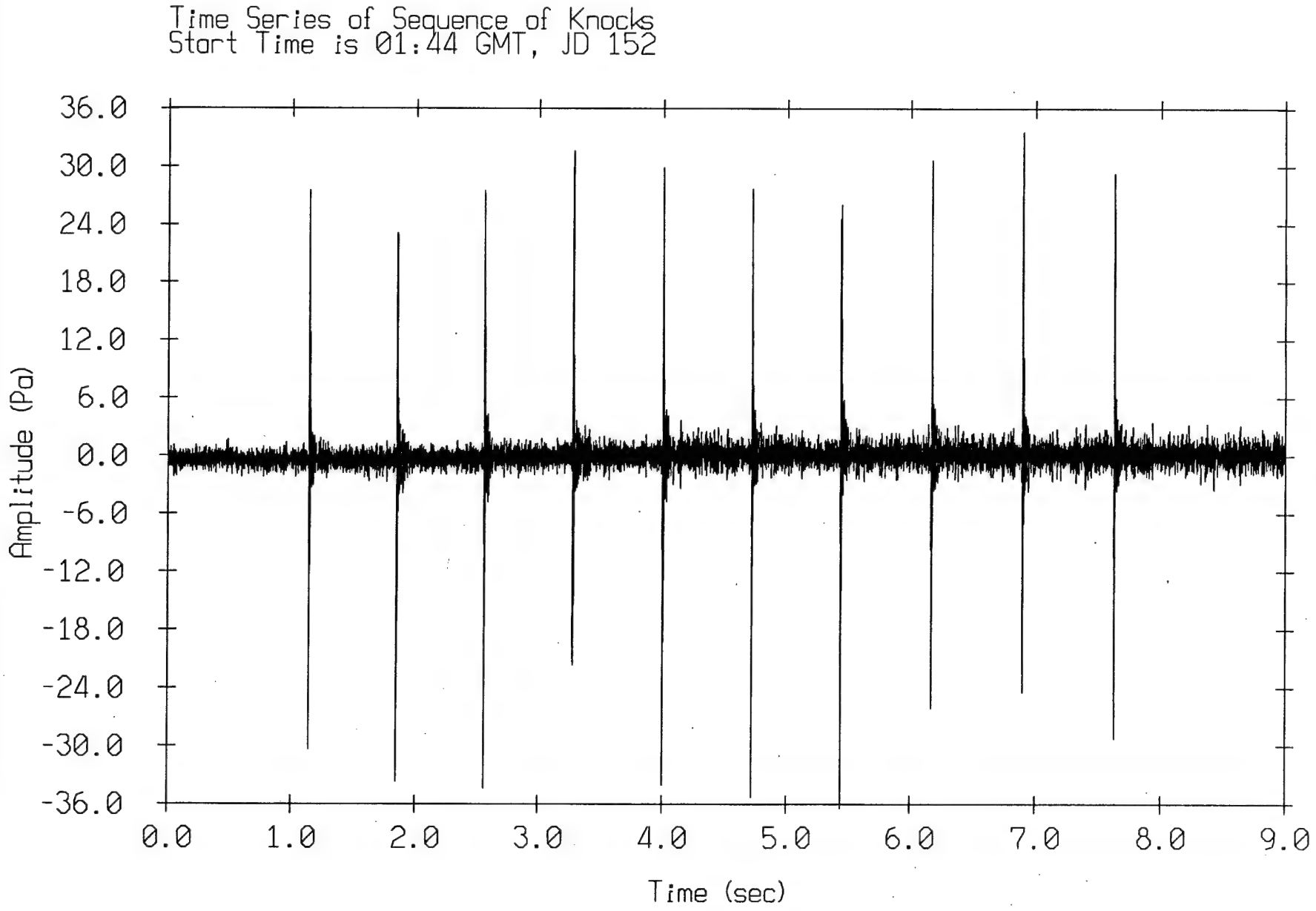
Time Series of Sequence of Knocks
Start Time is 01:44 GMT, JD 152
36.0
30.0
24.0
18.0
12.0
6.0
0.0
-6.0
-12.0
-18.0
-24.0
-30.0
-36.0
Amplitude (Pa)
0.0
1.0
2.0
3.0
4.0
5.0
6.0
7.0
8.0
9.0
Time (sec)

Figure III.7

ABM SRP EW Array Single Element Gram

JD 156 Start time of tape is 10:33 GMT

Element 8 Offset is 1 points

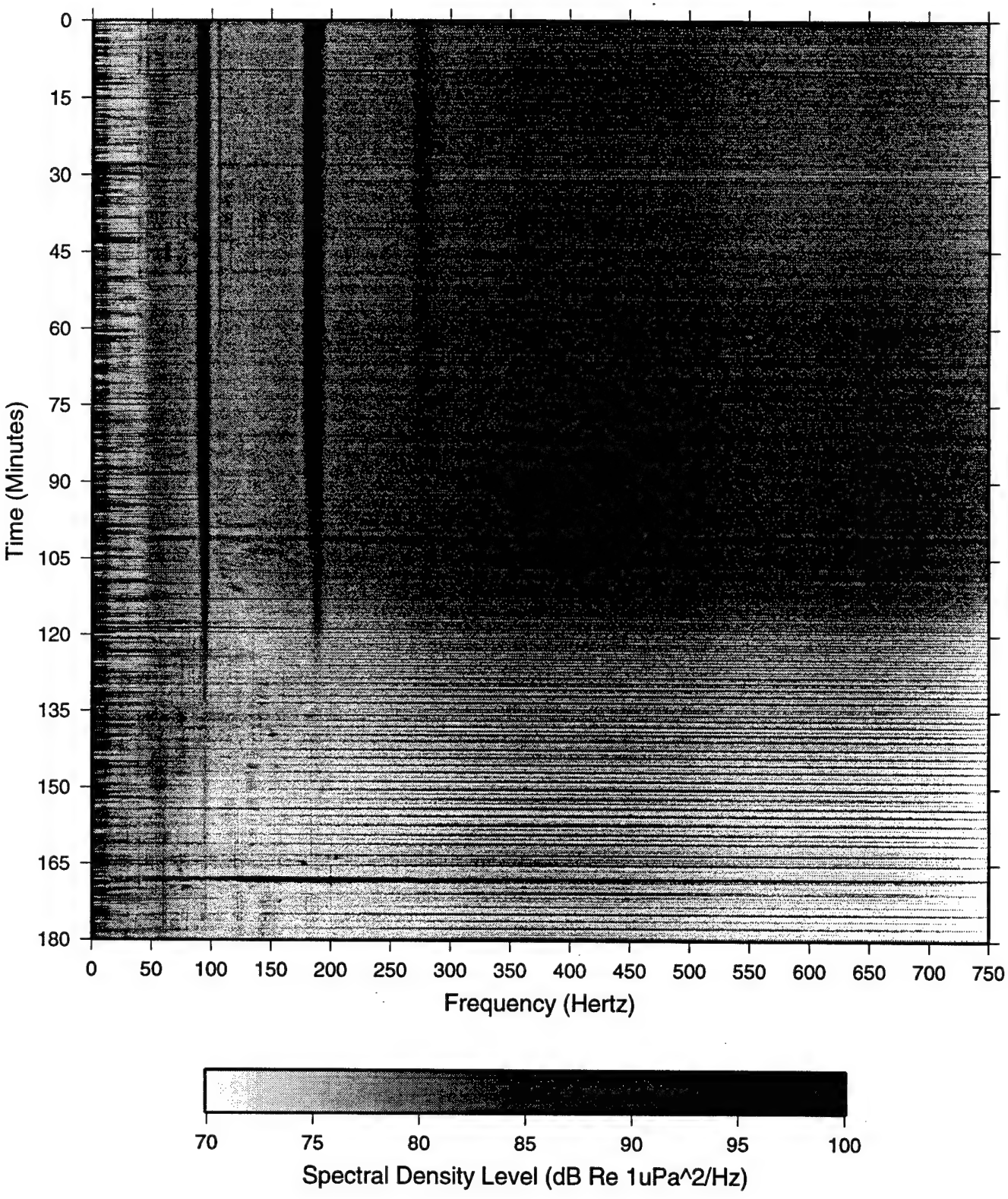

Figure III.8

Diurnal Croaker Variations

JD 144 - JD 164 1995

Day Starts at 12:00 PDT (19:00 GMT)

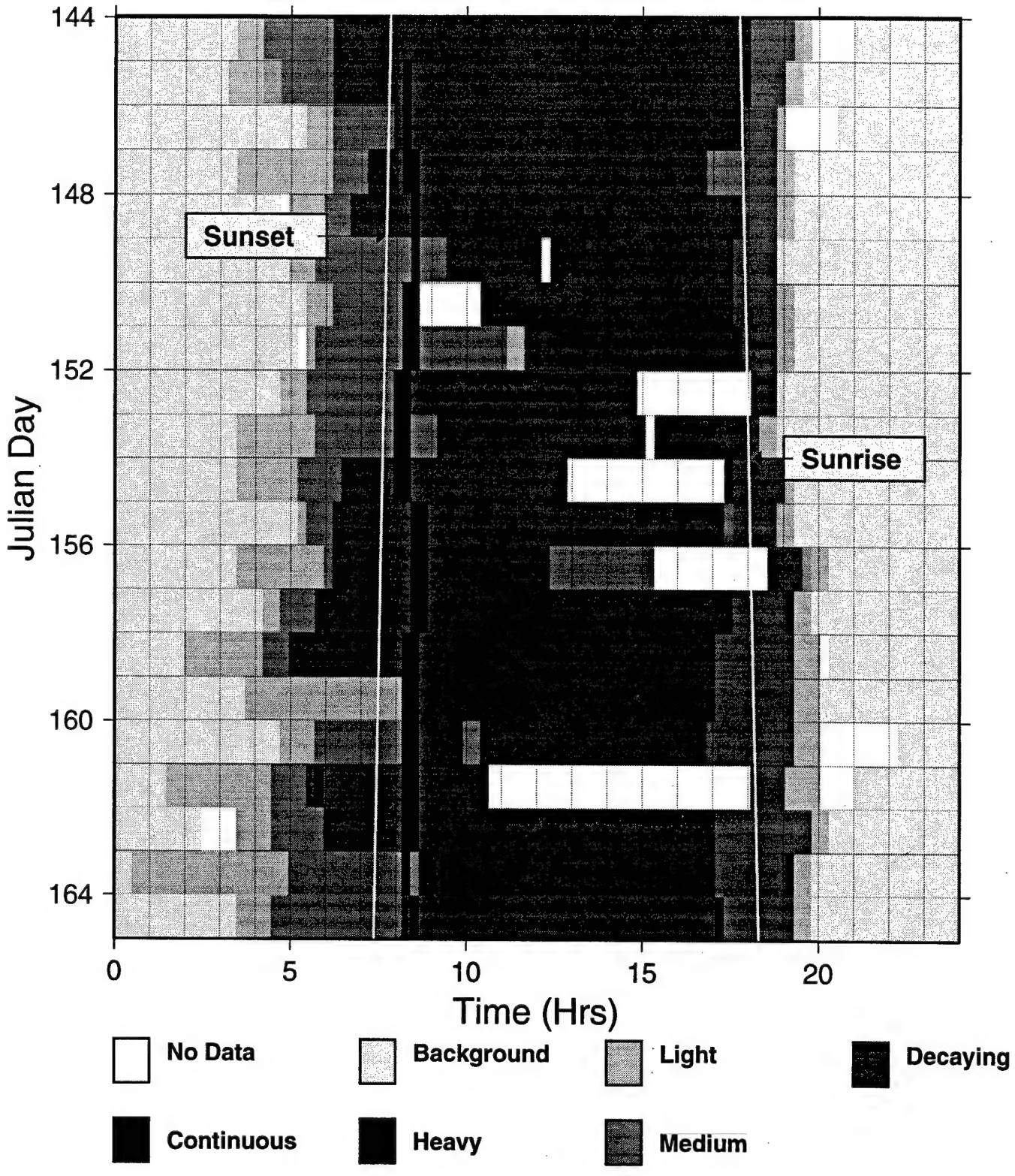

Figure III.9

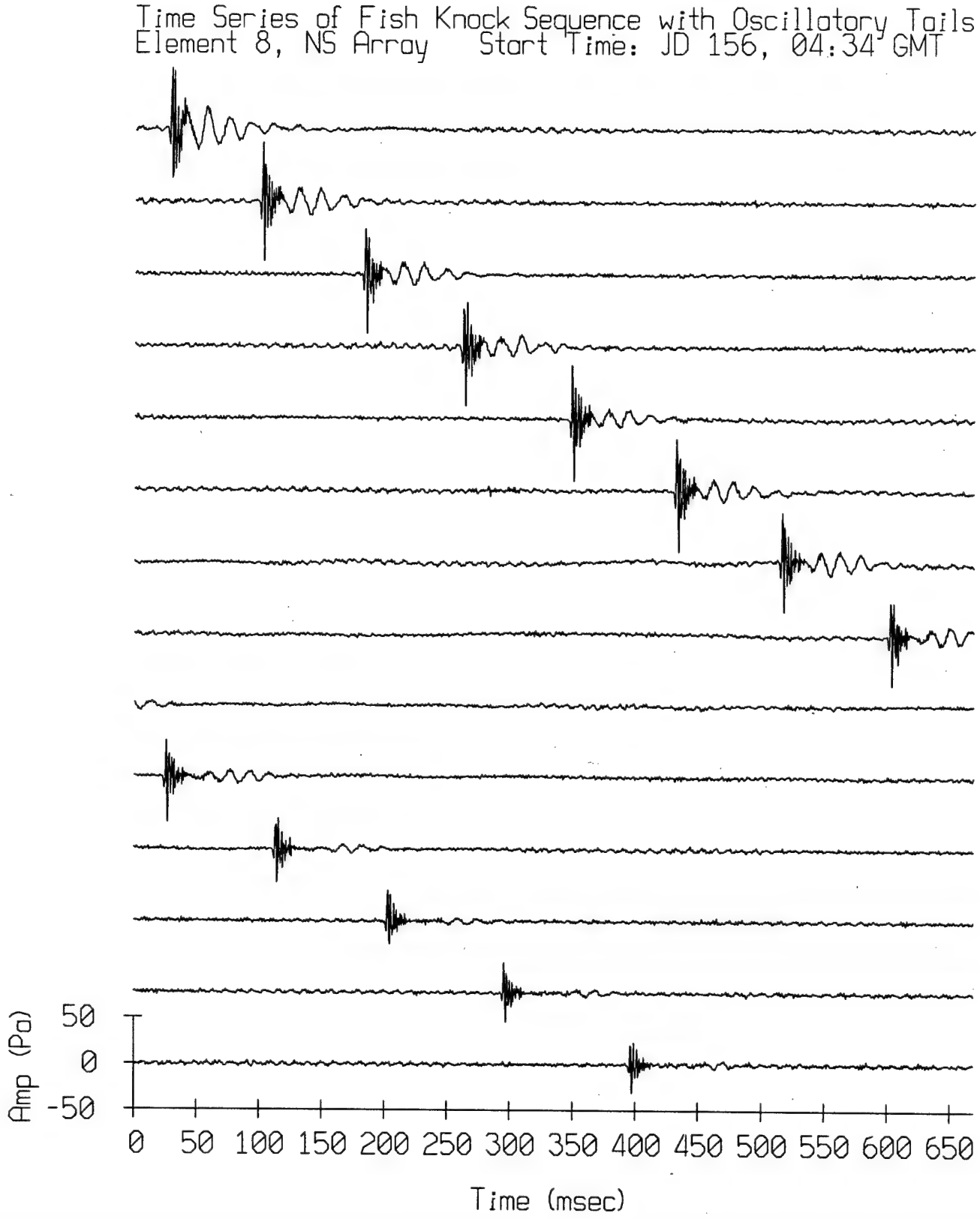

Figure III.10

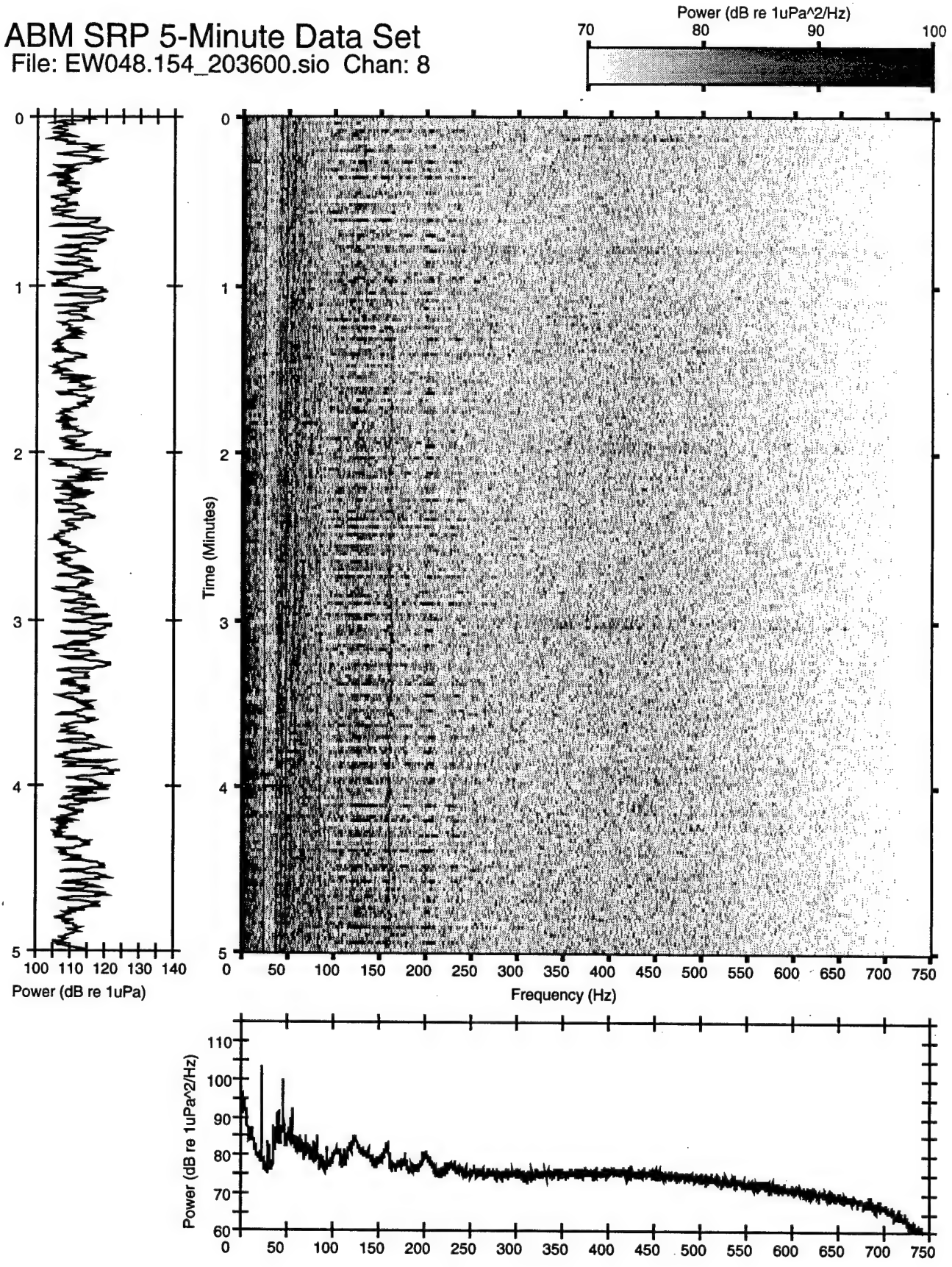

Figure III.11

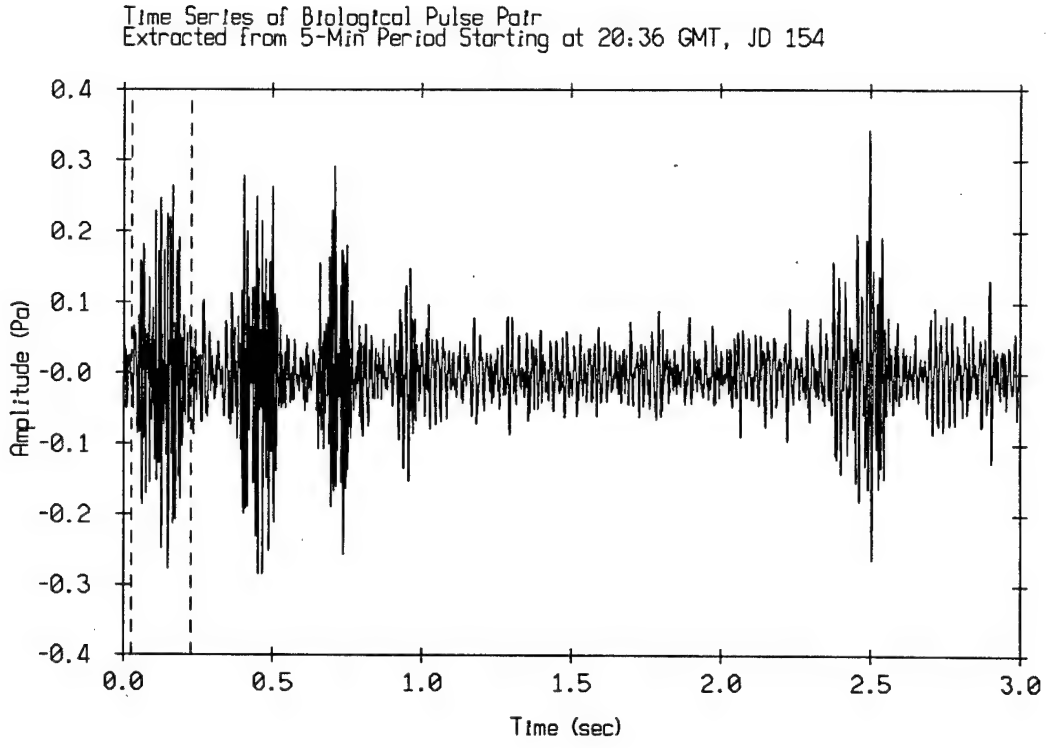

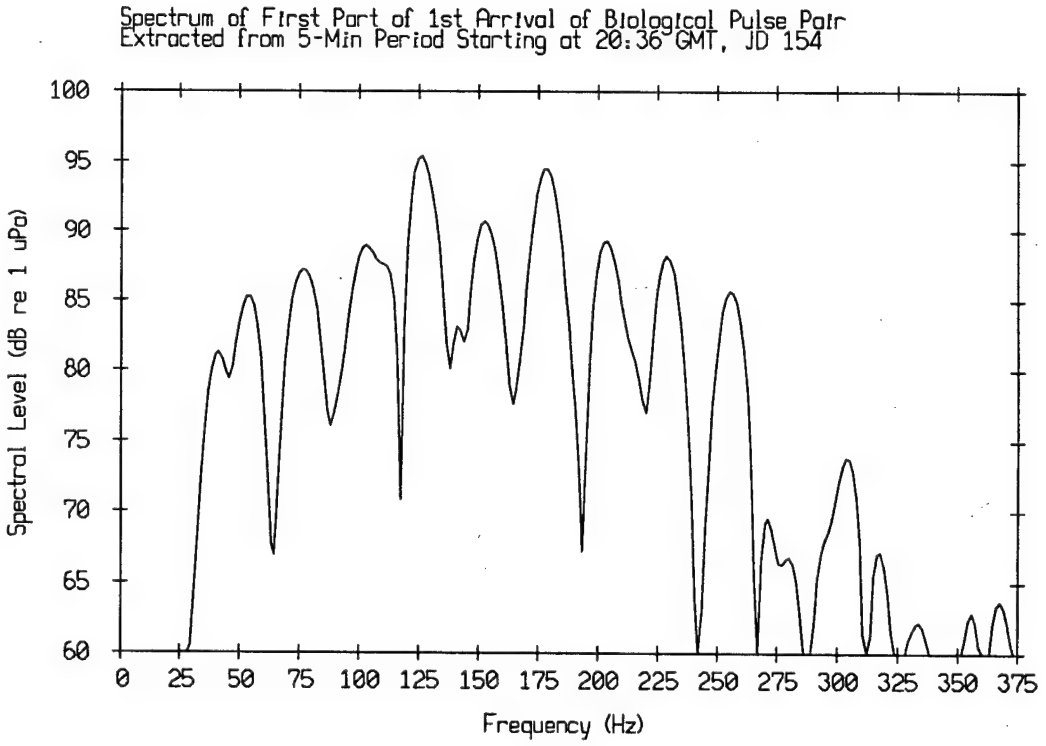

Figure III.12

Biological Pulse Variations

JD 144 - JD 164 1995

Day Starts at 12:00 PDT (19:00 GMT)

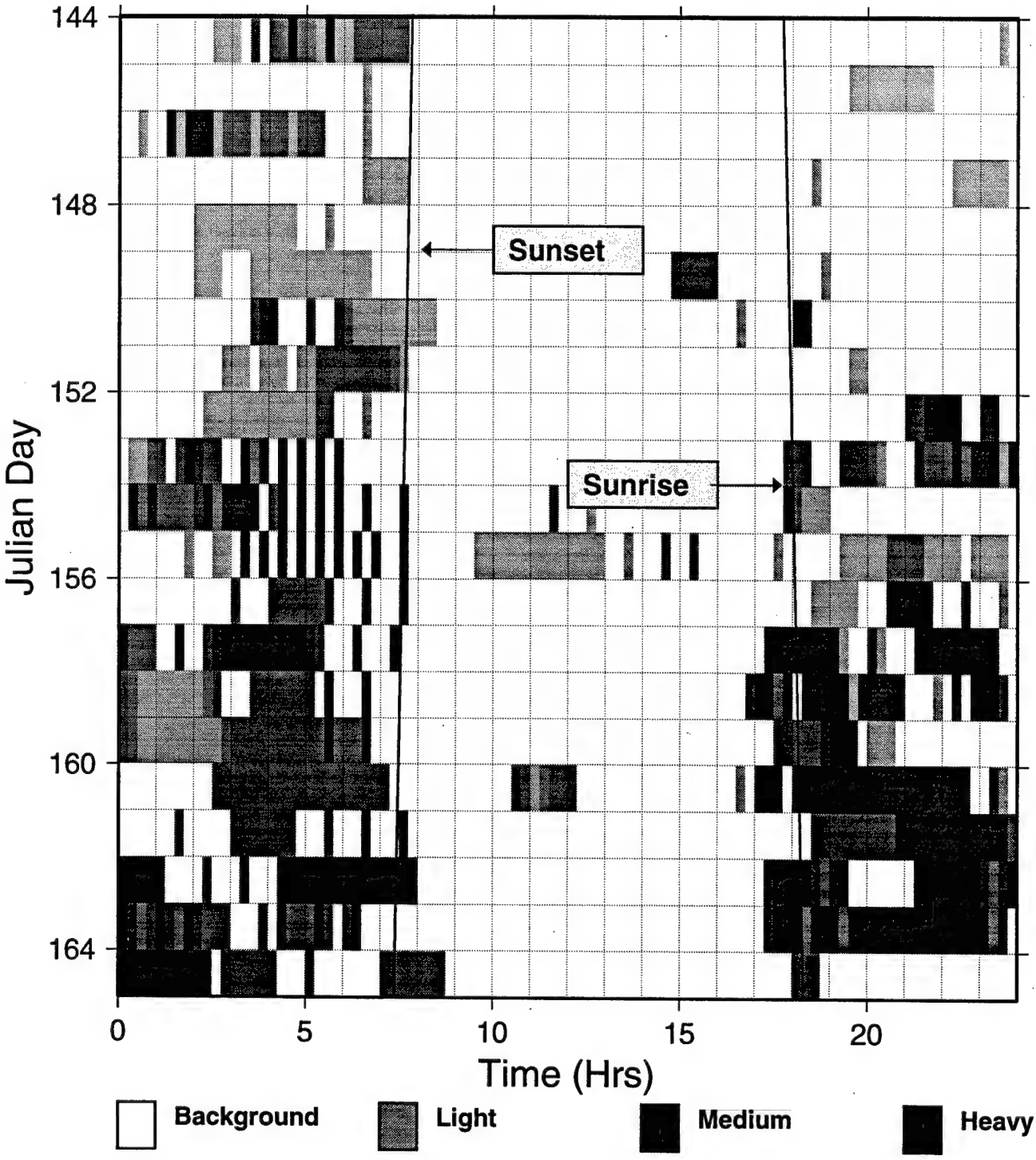

Figure III.13

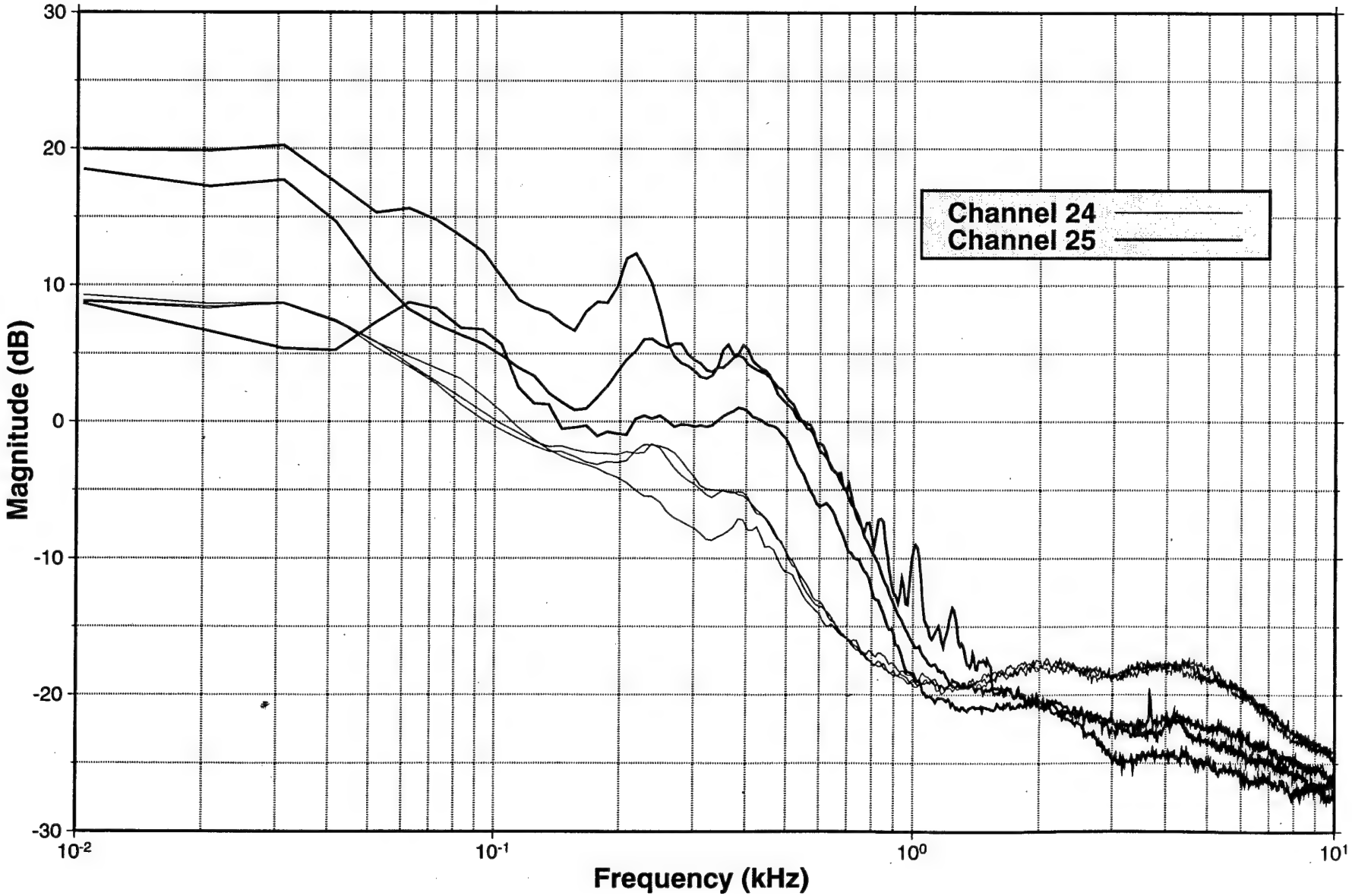

Figure III.14

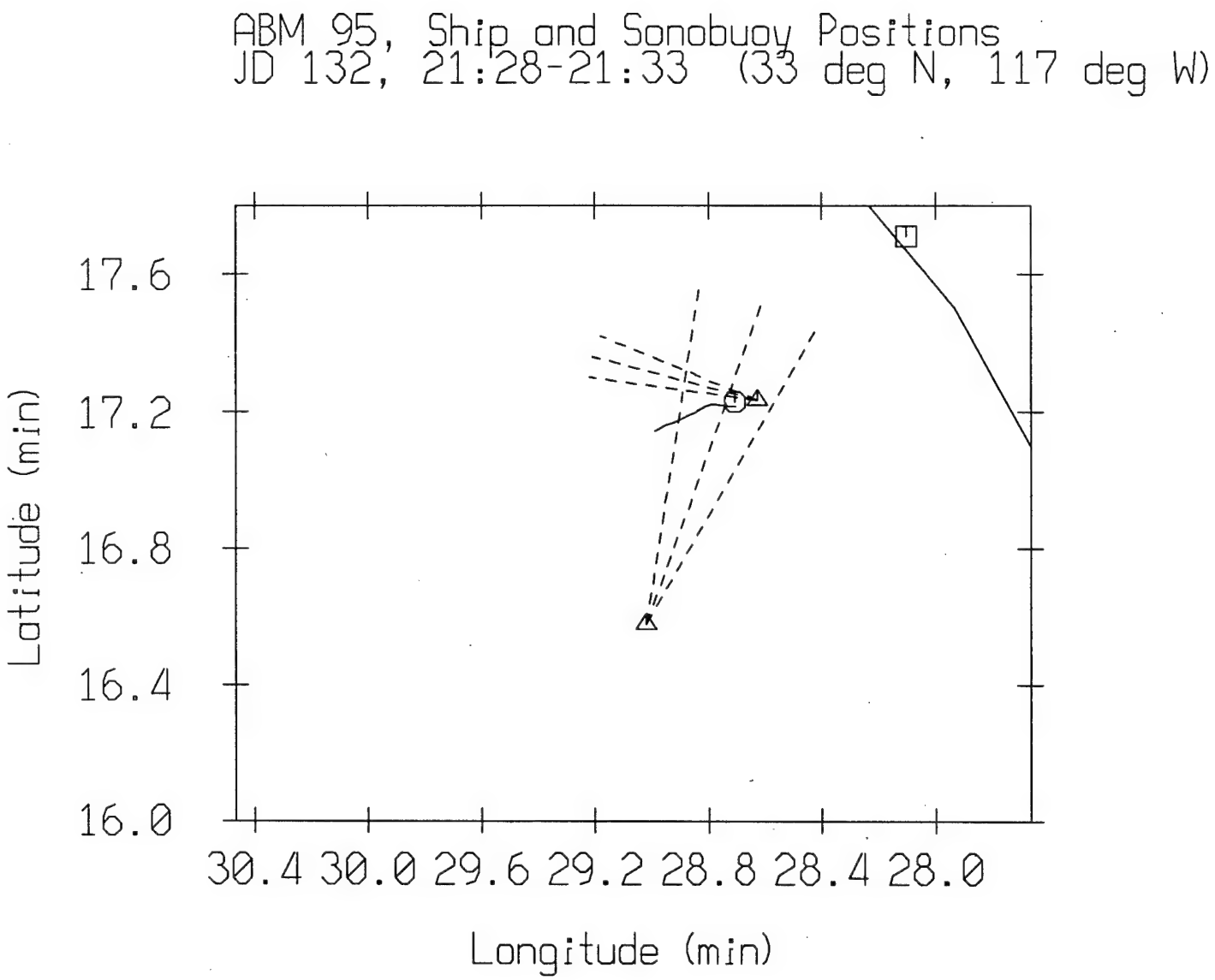

Figure III.15

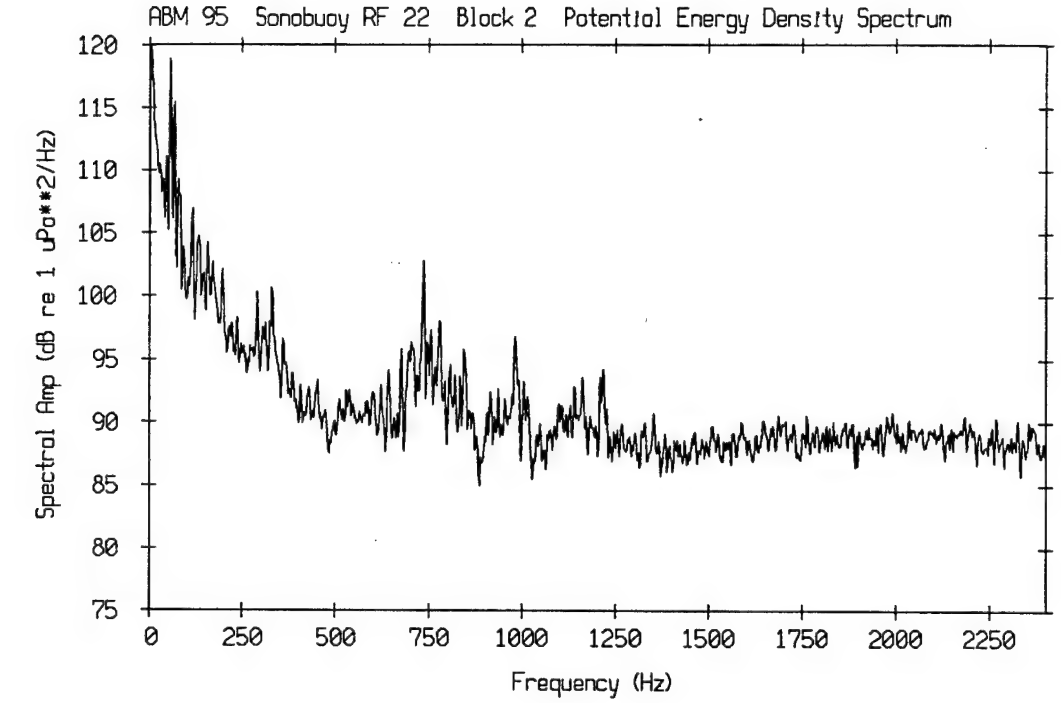

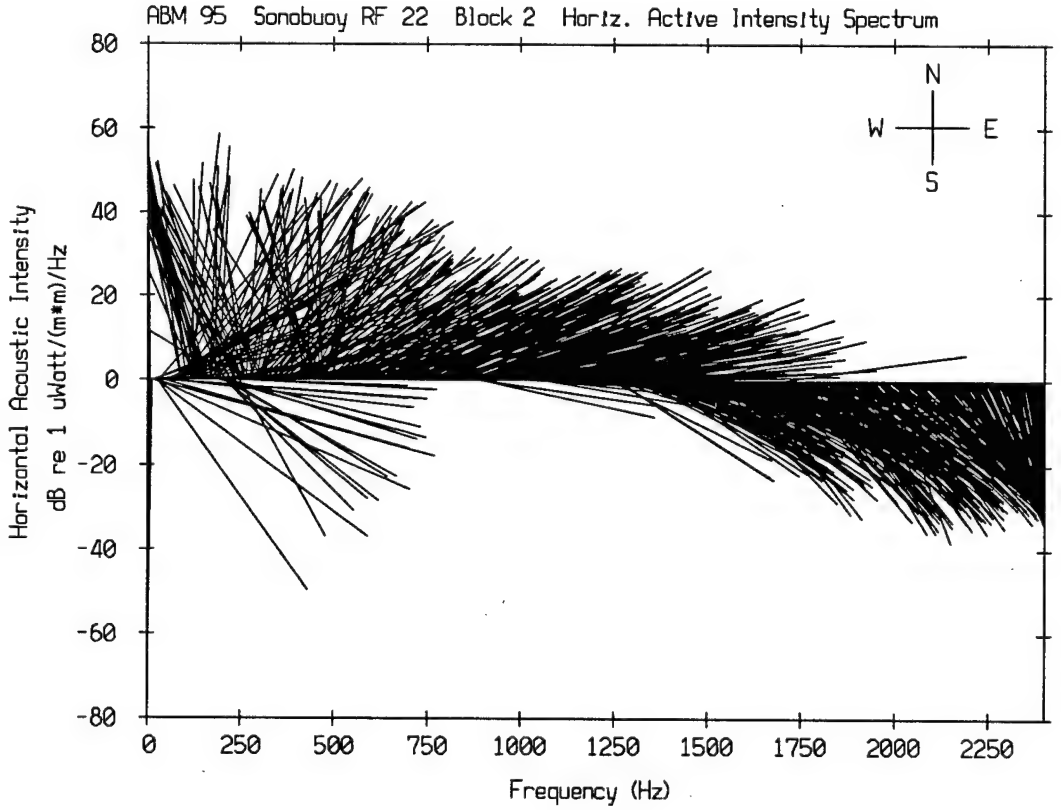

Figure III.16

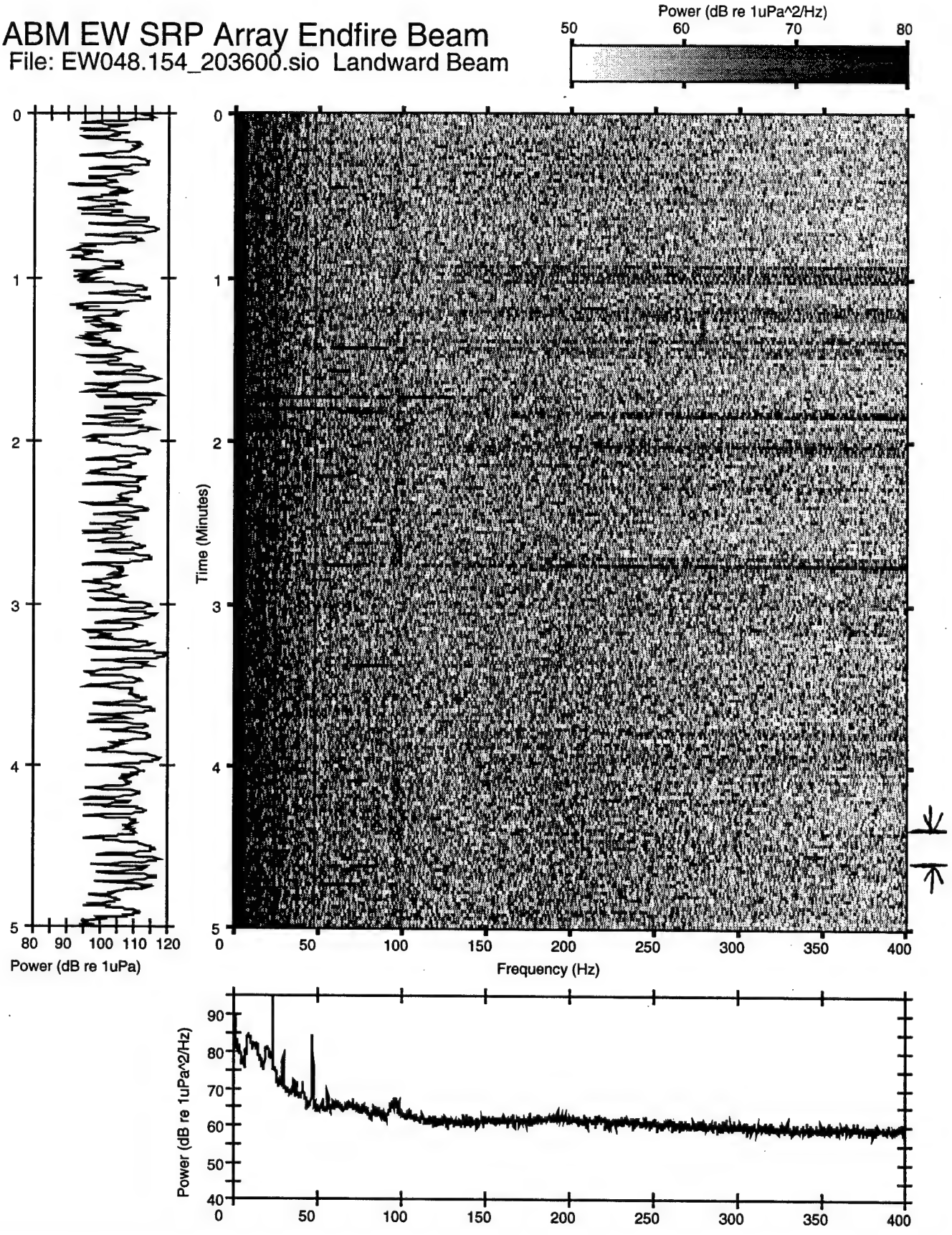

Figure IV.A.1a

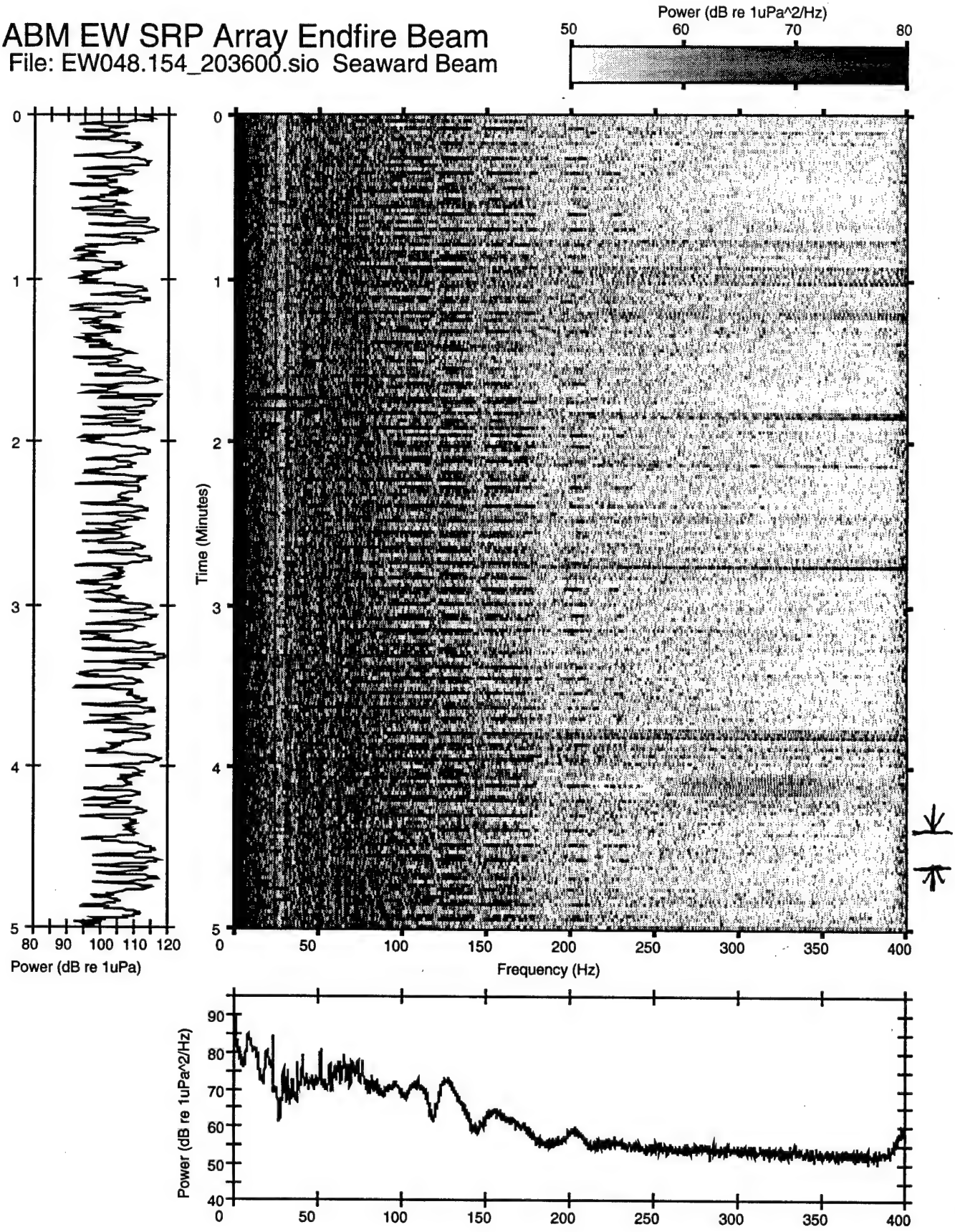

Figure IV.A.1b

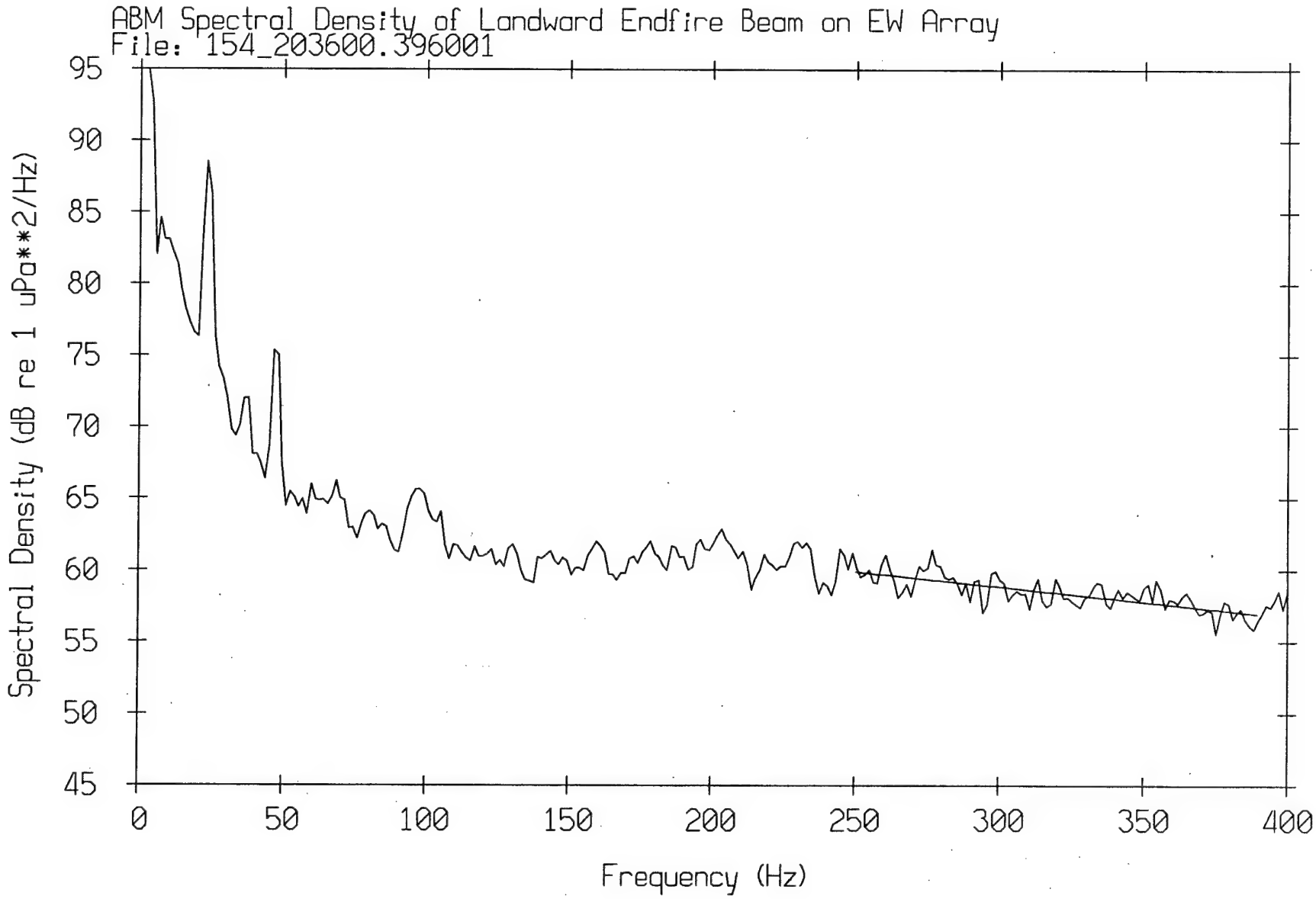

Figure IV.A.2a

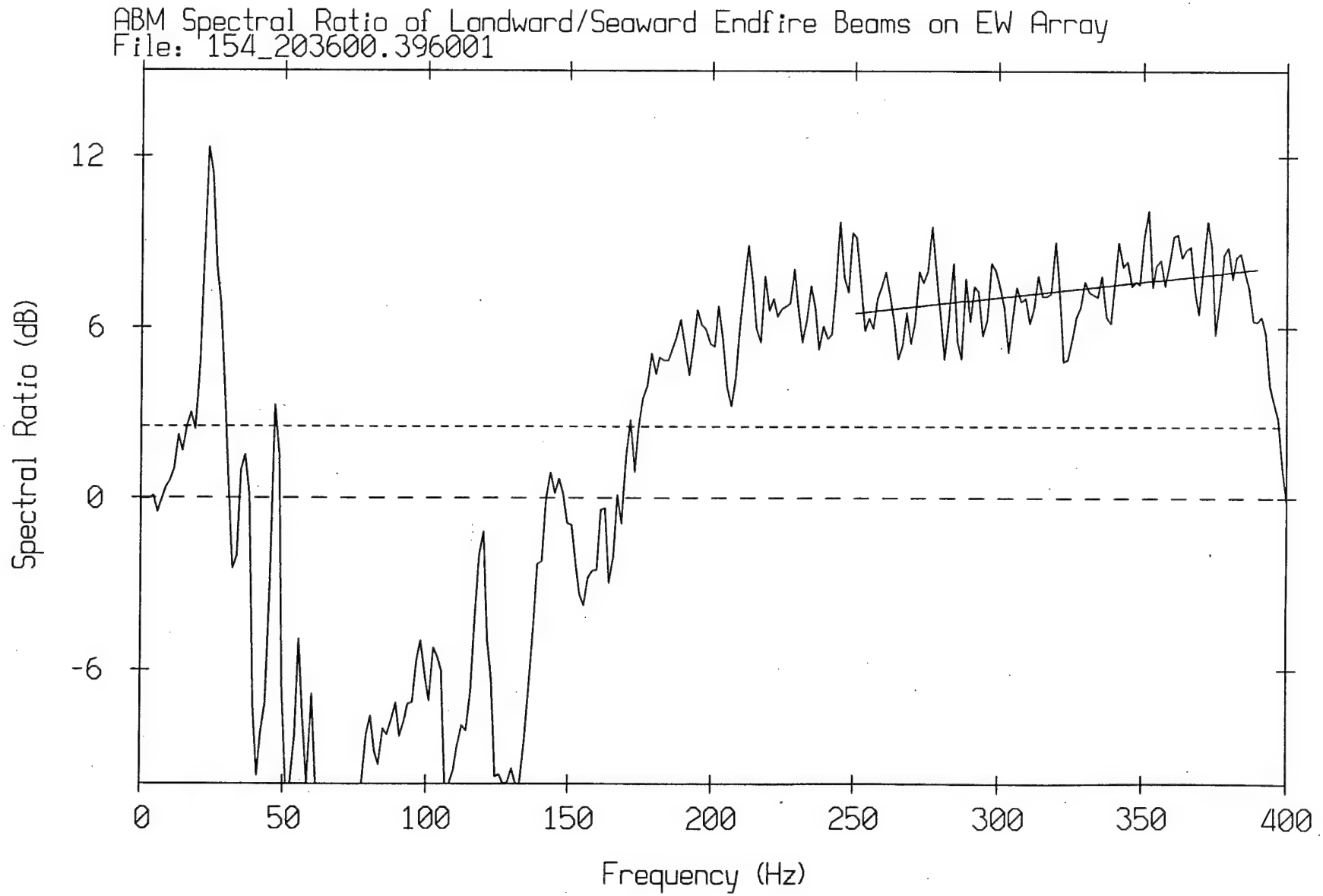

Figure IV.A.2b

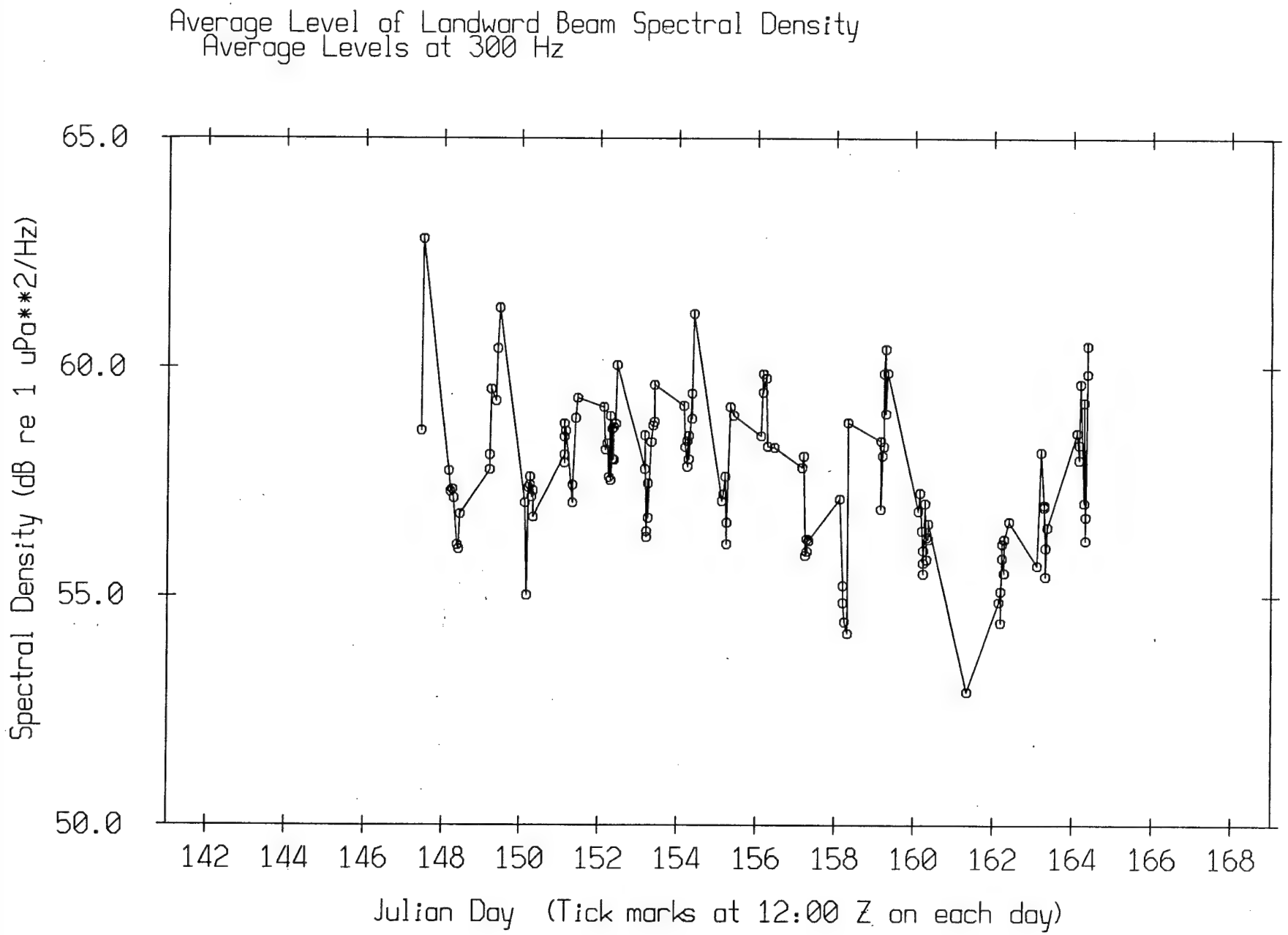

Figure IV.A.3a

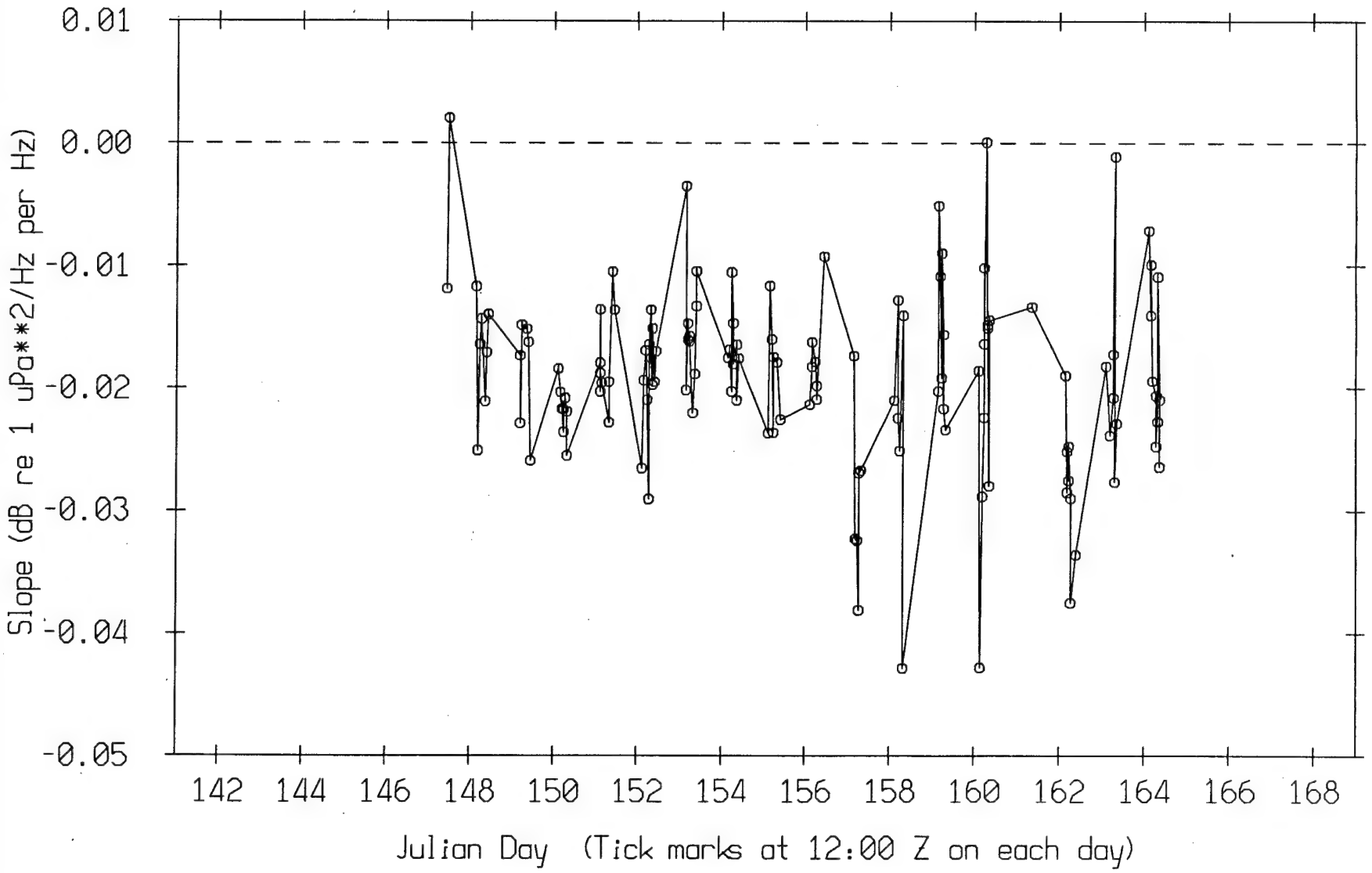

Figure IV.A.3b

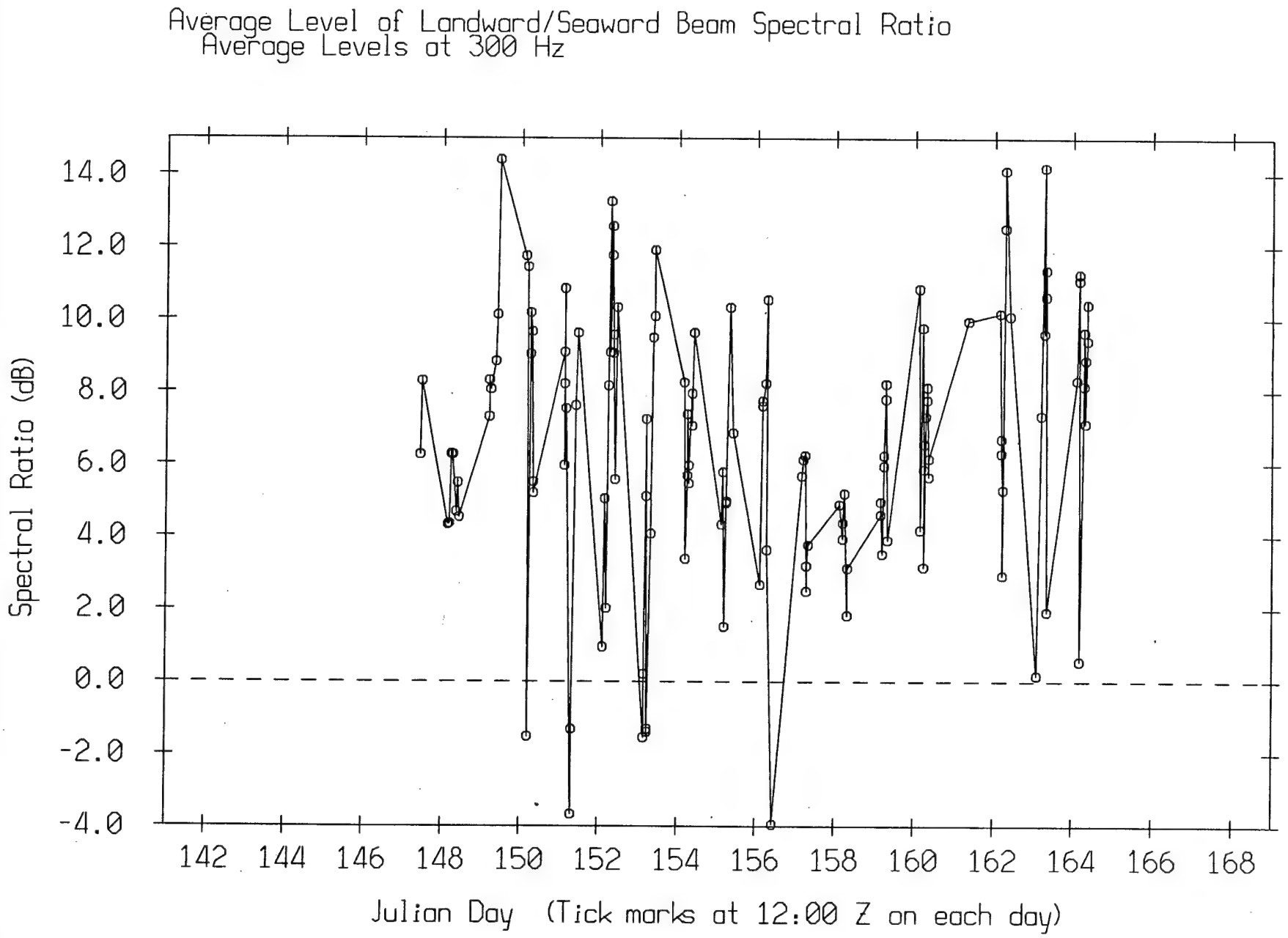

Figure IV.A.3c

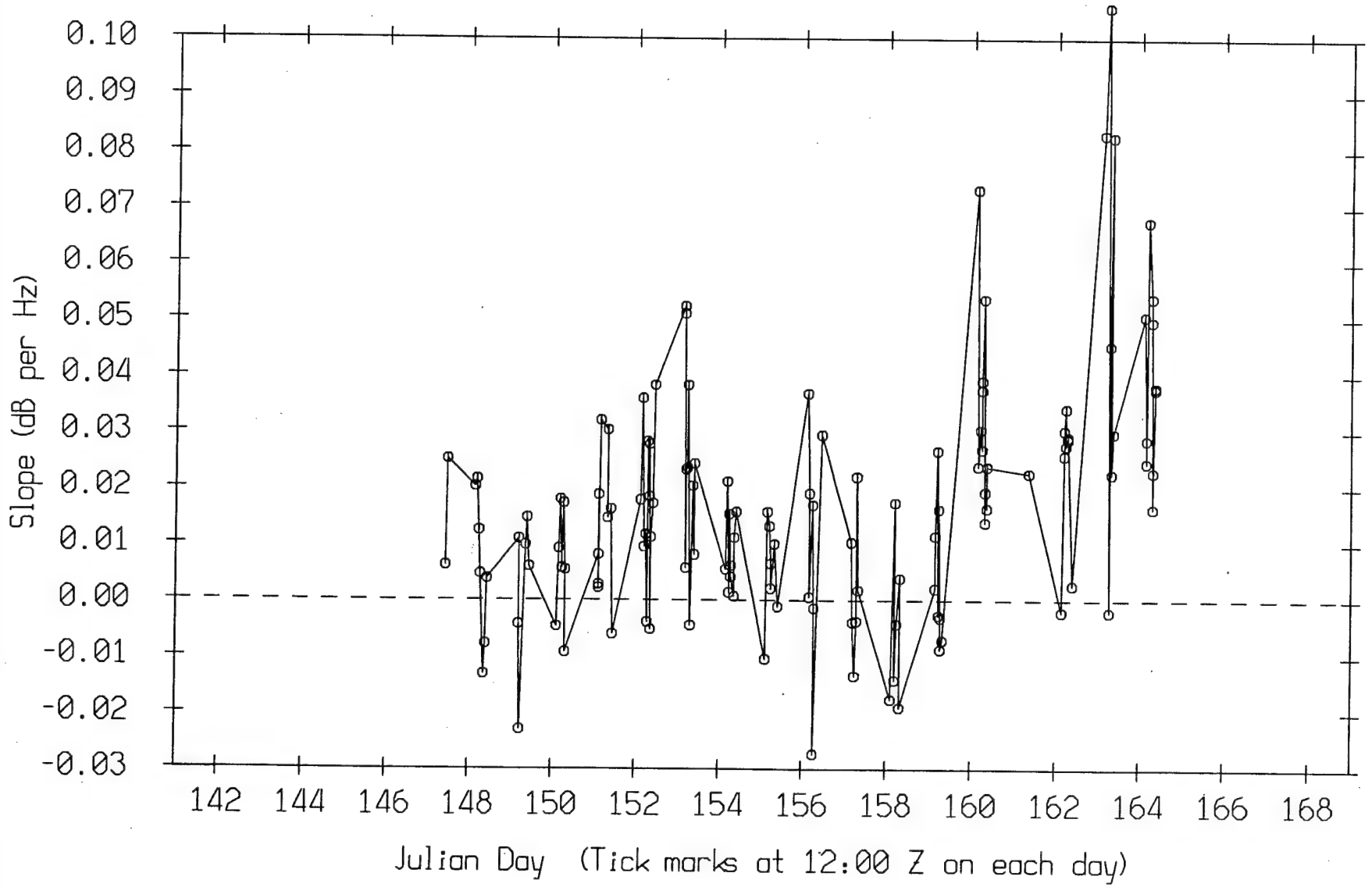

Figure IV.A.3d

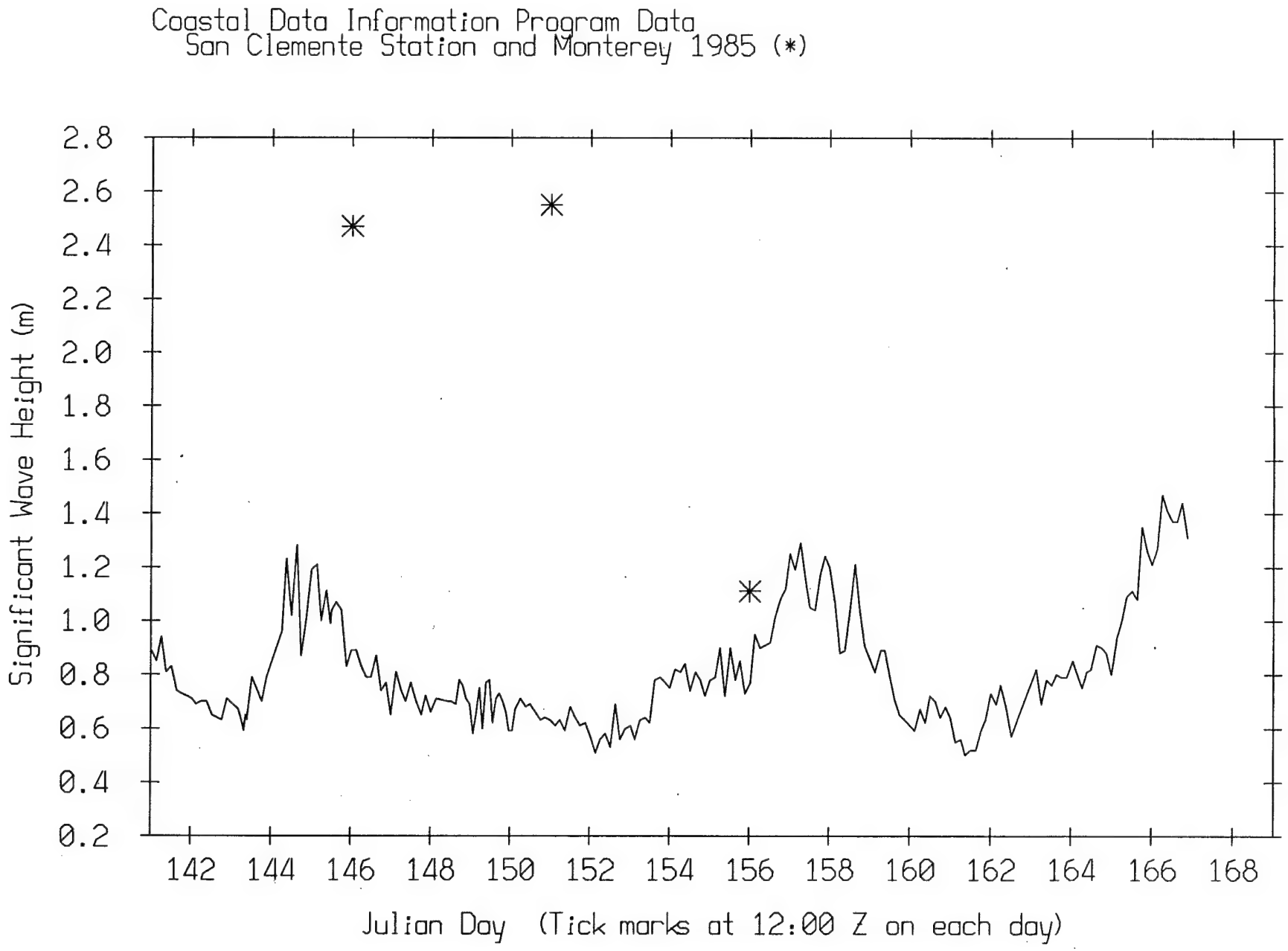

Figure IV.A.3e

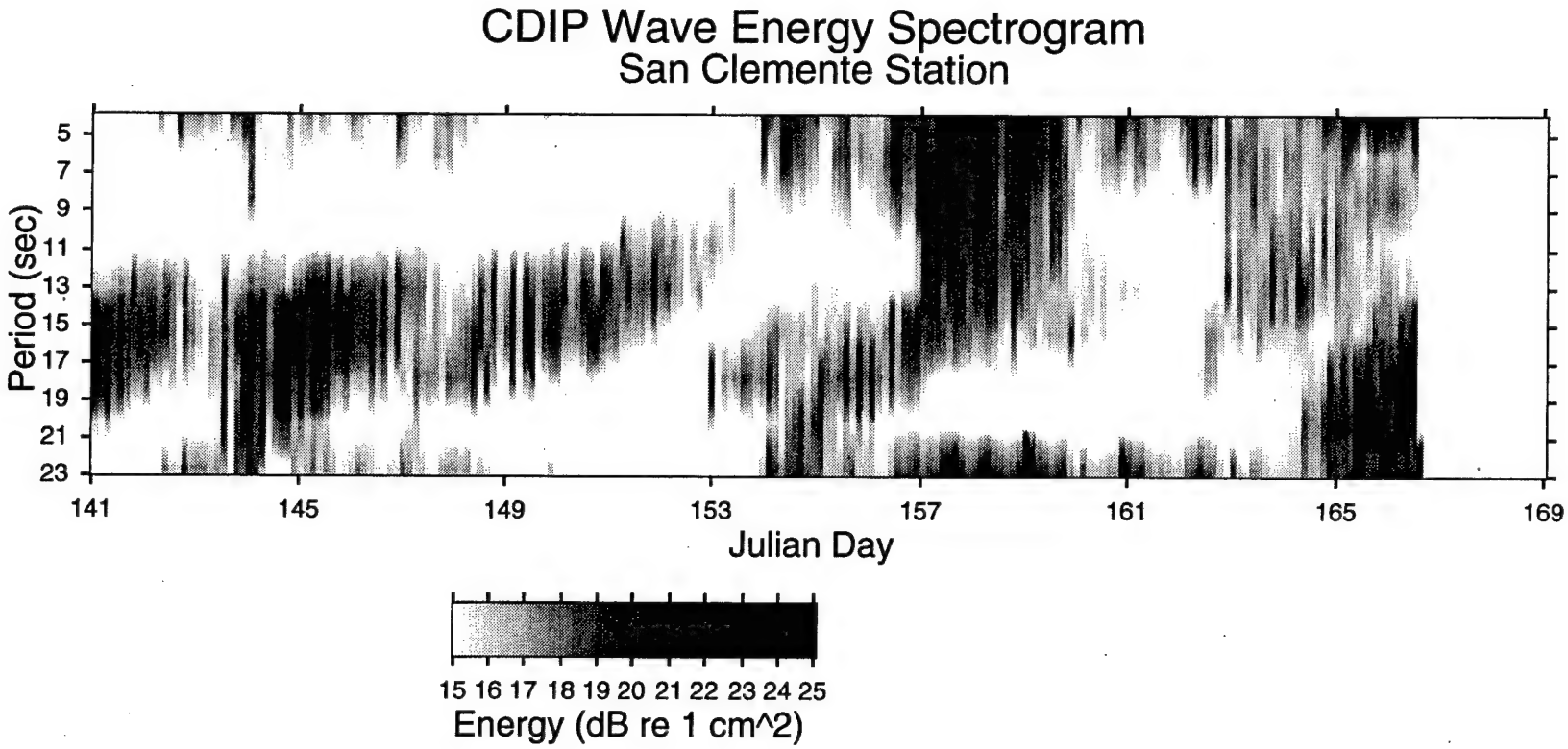

Figure IV.A.3f

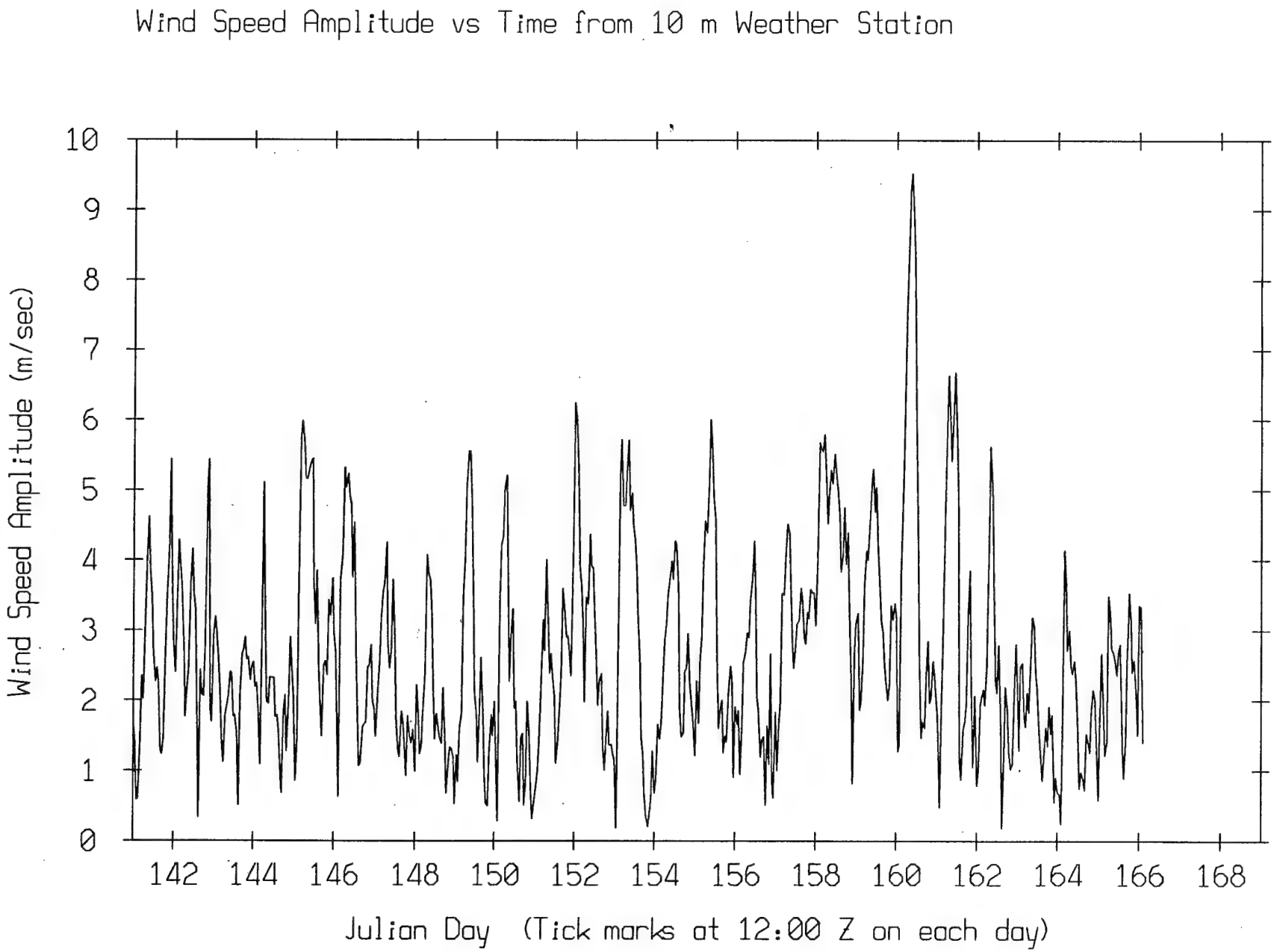

Figure IV.A.3g

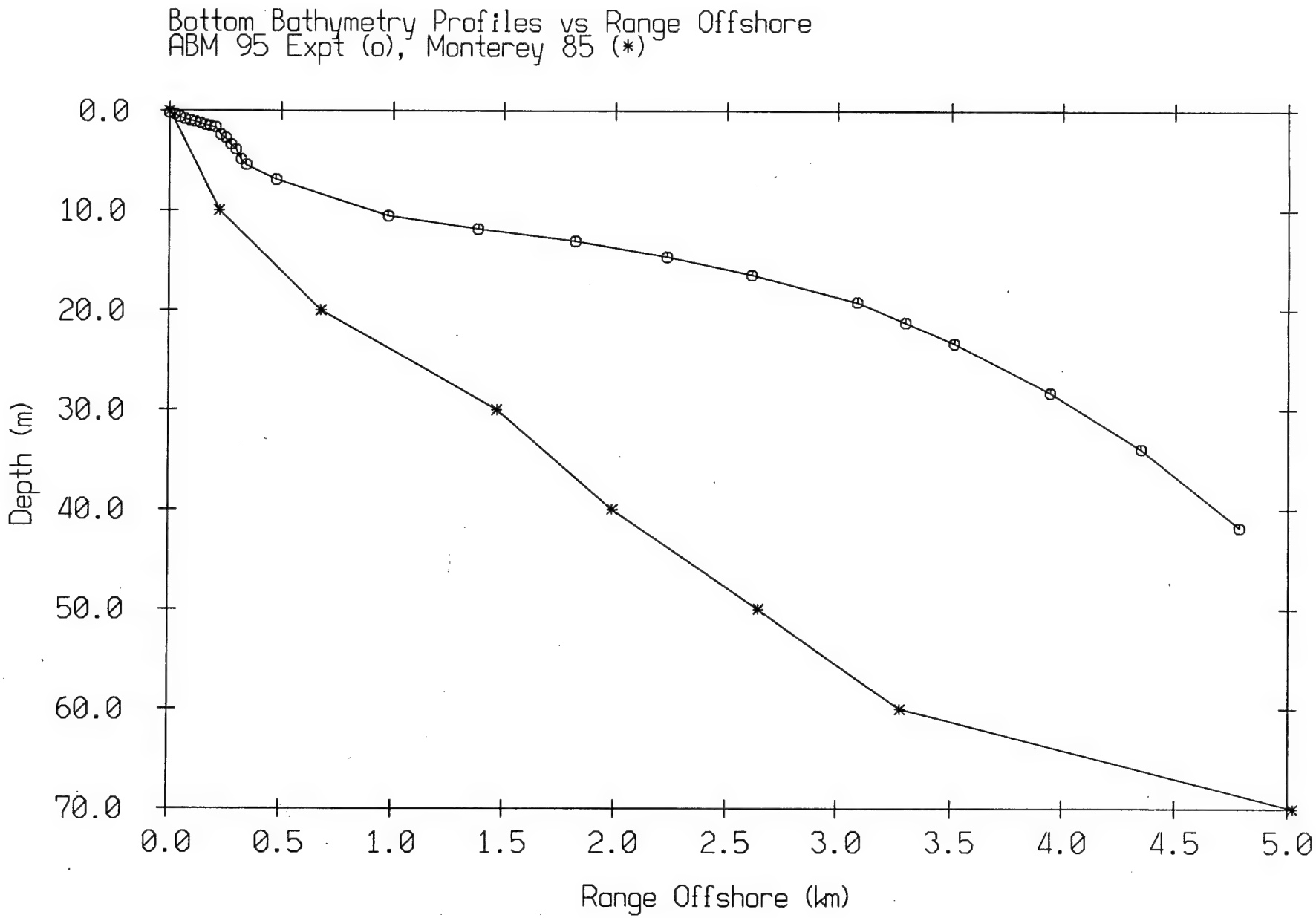
Bottom Bathymetry Profiles vs Range Offshore
ABM 95 Expt (o), Monterey 85 (*)
Depth (m)
0.0
10.0
20.0
30.0
40.0
50.0
60.0
70.0
0.0
0.5
1.0
1.5
2.0
2.5
3.0
3.5
4.0
4.5
5.0
Range Offshore (km)

Figure IV.A.4

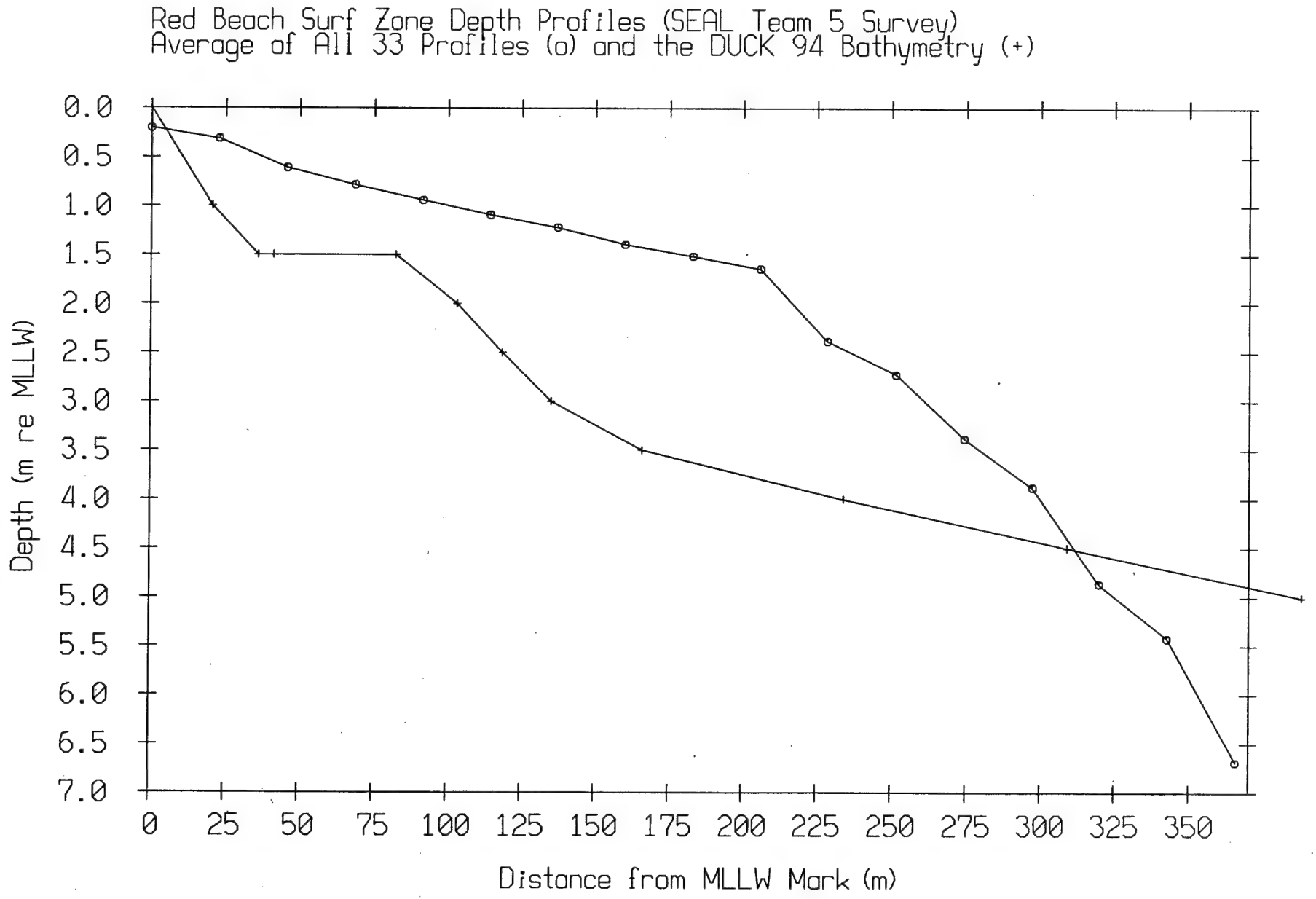
Red Beach Surf Zone Depth Profiles (SEAL Team 5 Survey)
Average of All 33 Profiles (o) and the DUCK 94 Bathymetry (+)
Depth (m re MLLW)
0.0
0.5
1.0
1.5
2.0
2.5
3.0
3.5
4.0
4.5
5.0
5.5
6.0
6.5
7.0
0
25
50
75
100
125
150
175
200
225
250
275
300
325
350
Distance from MLLW Mark (m)

Figure IV.A.5

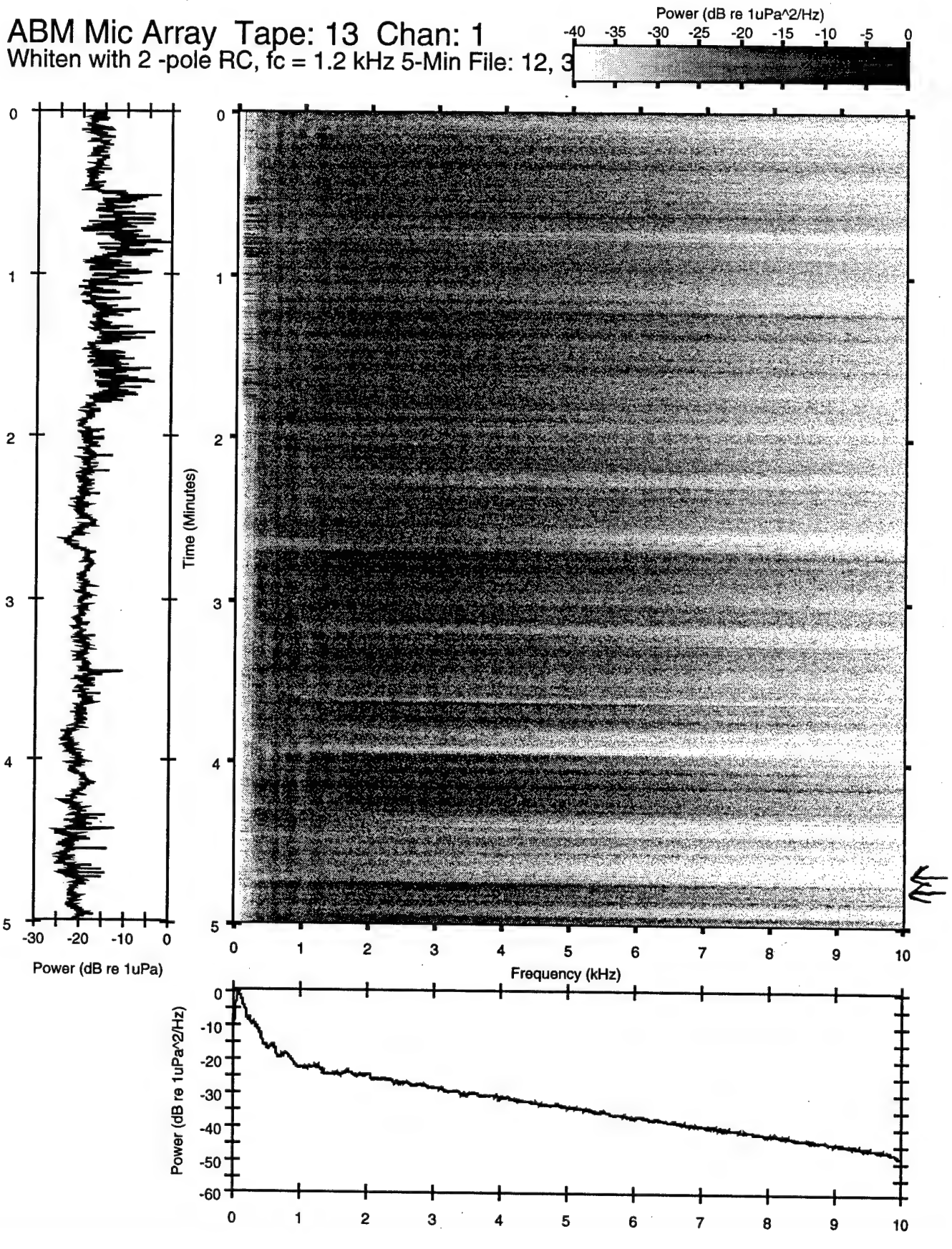
ABM Mic Array Tape: 13 Chan: 1
Whiten with 2 -pole RC, fc = 1.2 kHz 5-Min File: 12, 3
Power (dB re 1uPa^2/Hz)
-40 -35 -30 -25 -20 -15 -10 -5 0
Time (Minutes)
Power (dB re 1uPa)
Frequency (kHz)
Power (dB re 1uPa^2/Hz)

Figure IV.B.1

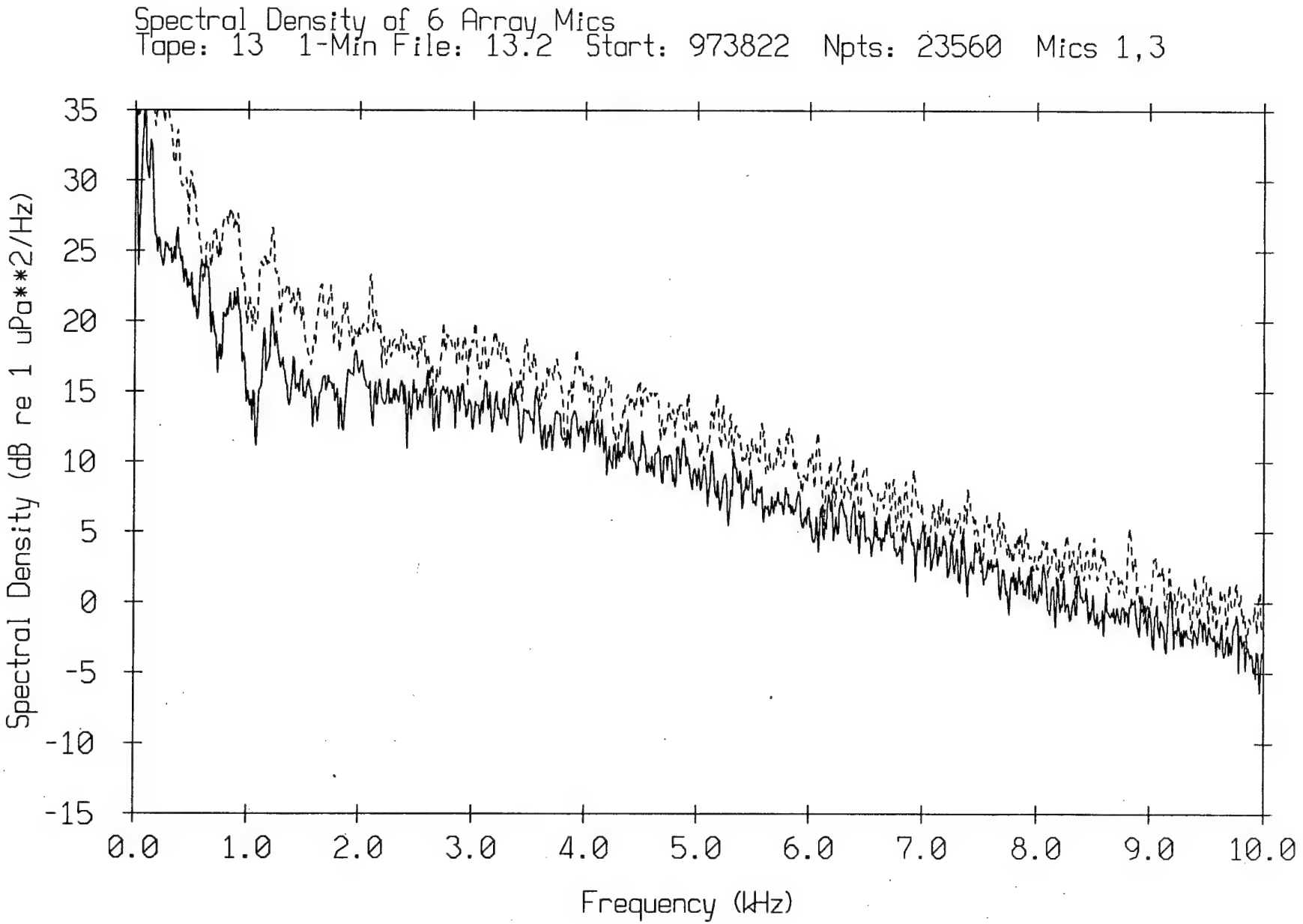
Spectral Density of 6 Array Mics
Tape: 13 1-Min File: 13.2 Start: 973822 Npts: 23560 Mics 1,3
Spectral Density (dB re 1 uPa**2/Hz)
35
30
25
20
15
10
5
0
-5
-10
-15
0.0
1.0
2.0
3.0
4.0
5.0
6.0
7.0
8.0
9.0
10.0
Frequency (kHz)

Figure IV.B.2

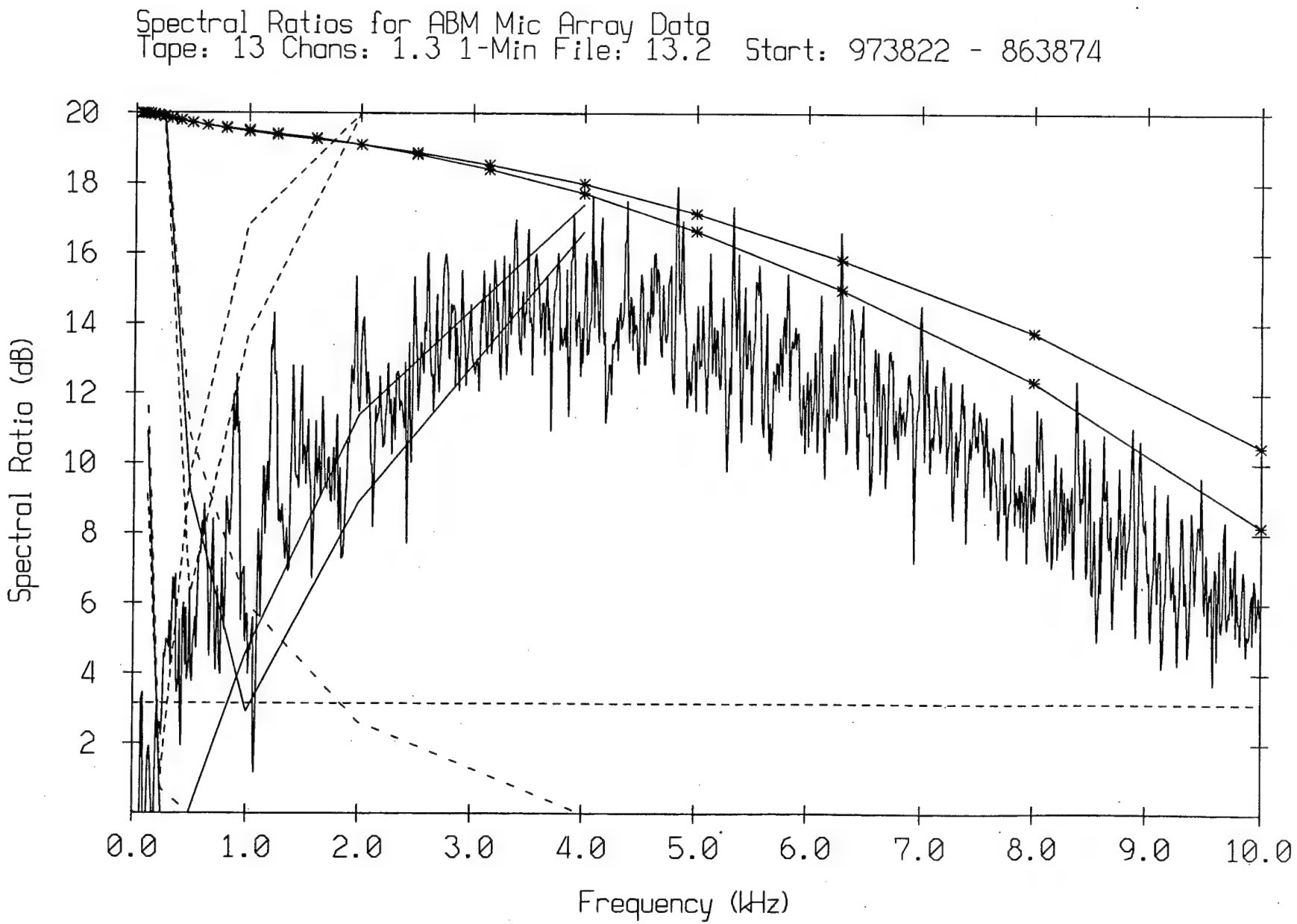
Spectral Ratios for ABM Mic Array Data
Tape: 13 Chans: 1.3 1-Min File: 13.2 Start: 973822 - 863874
Spectral Ratio (dB)
20
18
16
14
12
10
8
6
4
2
0.0
1.0
2.0
3.0
4.0
5.0
6.0
7.0
8.0
9.0
10.0
Frequency (kHz)

Figure IV.B.3

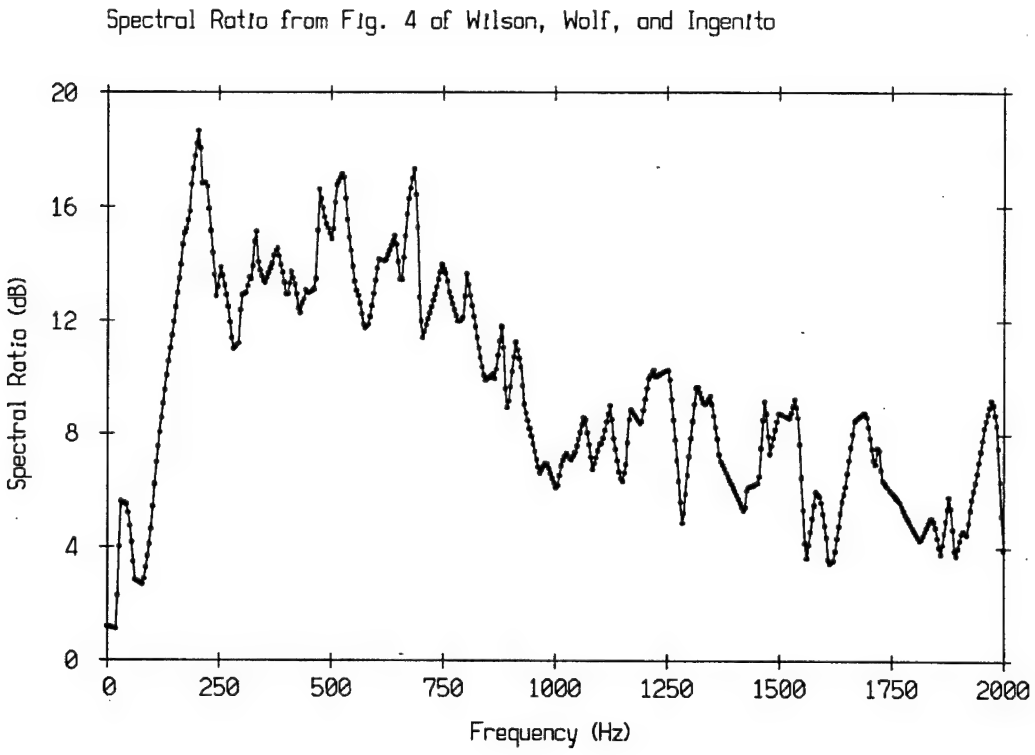
Spectral Ratio from Fig. 4 of Wilson, Wolf, and Ingenito
Spectral Ratio (dB)
20
16
12
8
4
0
0
250
500
750
1000
1250
1500
1750
2000
Frequency (Hz)

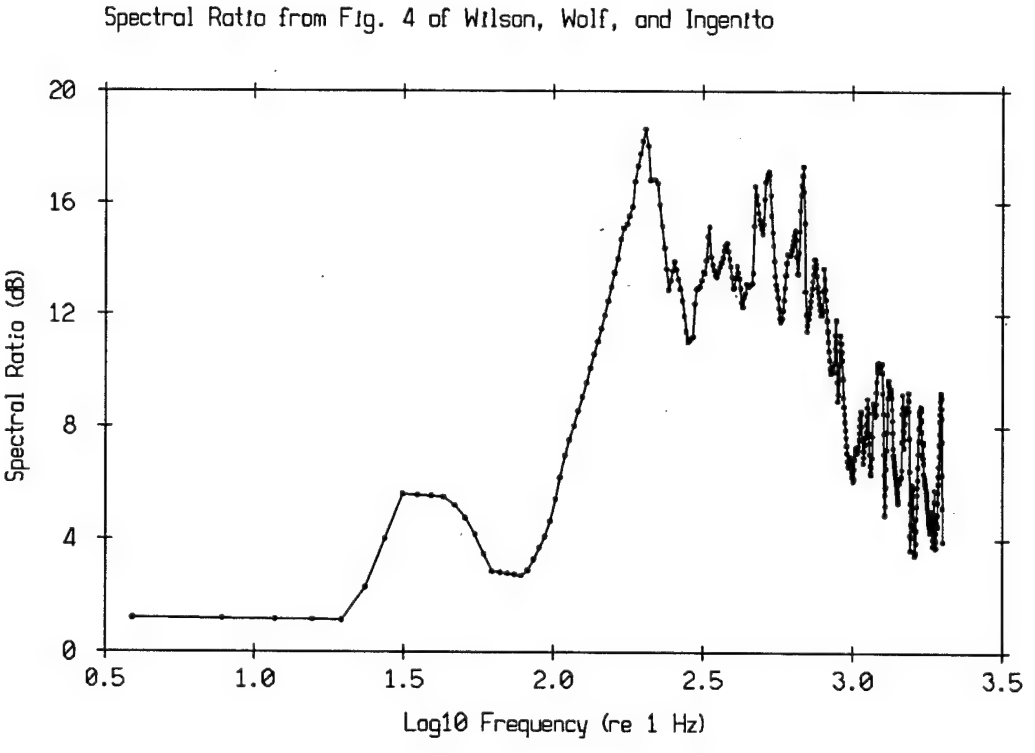
Spectral Ratio from Fig. 4 of Wilson, Wolf, and Ingenito
Spectral Ratio (dB)
20
16
12
8
4
0
0.5
1.0
1.5
2.0
2.5
3.0
3.5
Log10 Frequency (re 1 Hz)

Figure IV.B.4

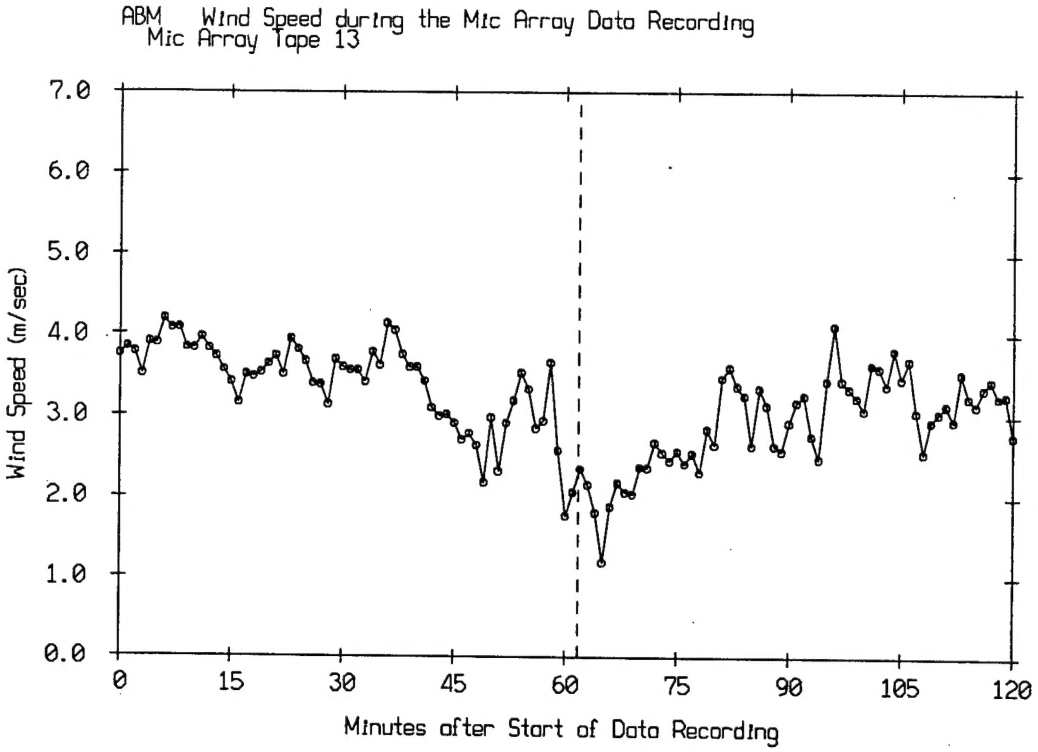
ABM Wind Speed during the Mic Array Data Recording
Mic Array Tape 13
Wind Speed (m/sec)
7.0
6.0
5.0
4.0
3.0
2.0
1.0
0.0
0
15
30
45
60
75
90
105
120
Minutes after Start of Data Recording

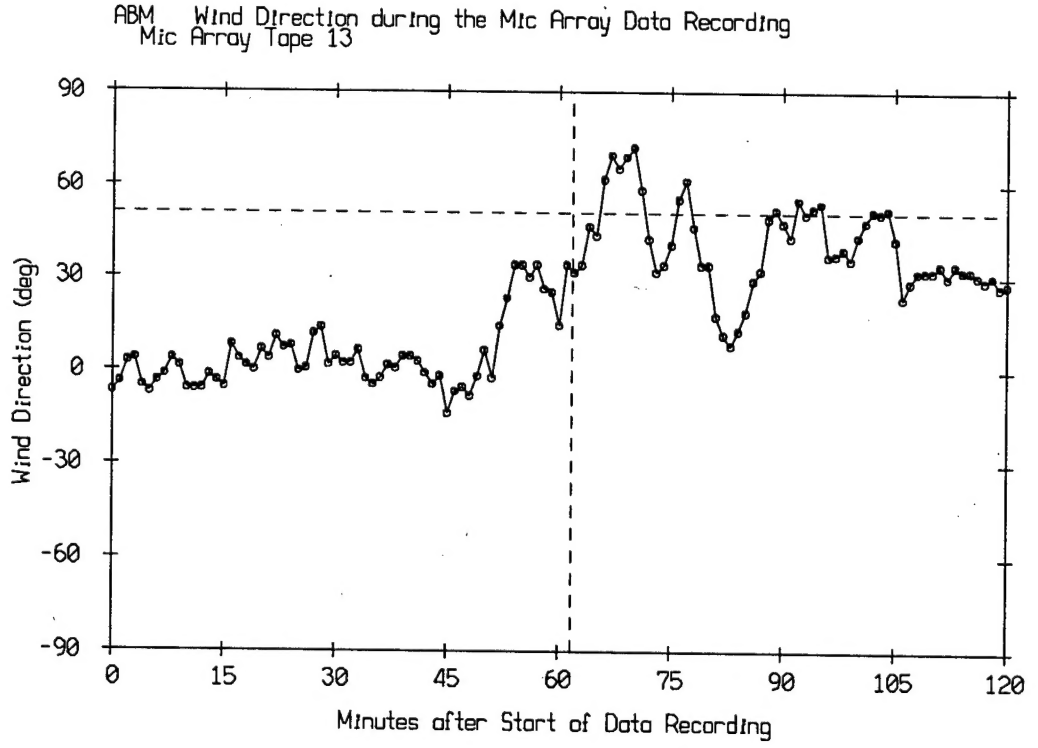
ABM Wind Direction during the Mic Array Data Recording
Mic Array Tape 13
Wind Direction (deg)
90
60
30
0
-30
-60
-90
0
15
30
45
60
75
90
105
120
Minutes after Start of Data Recording

Figure IV.B.5

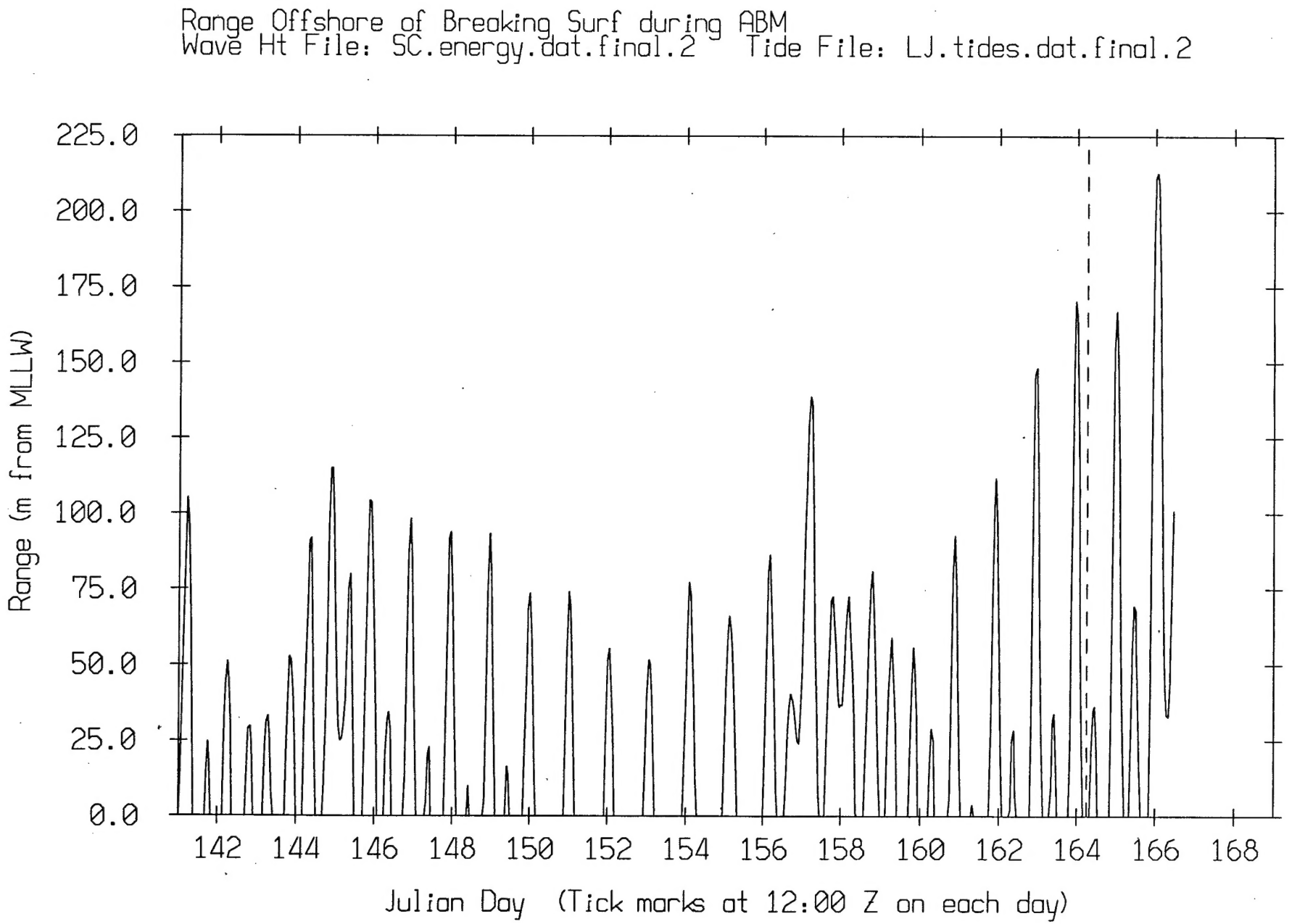
Range Offshore of Breaking Surf during ABM
Wave Ht File: SC.energy.dat.final.2 Tide File: LJ.tides.dat.final.2
Range (m from MLLW)
225.0
200.0
175.0
150.0
125.0
100.0
75.0
50.0
25.0
0.0
142
144
146
148
150
152
154
156
158
160
162
164
166
168
Julian Day (Tick marks at 12:00 Z on each day)

Figure IV.B.6

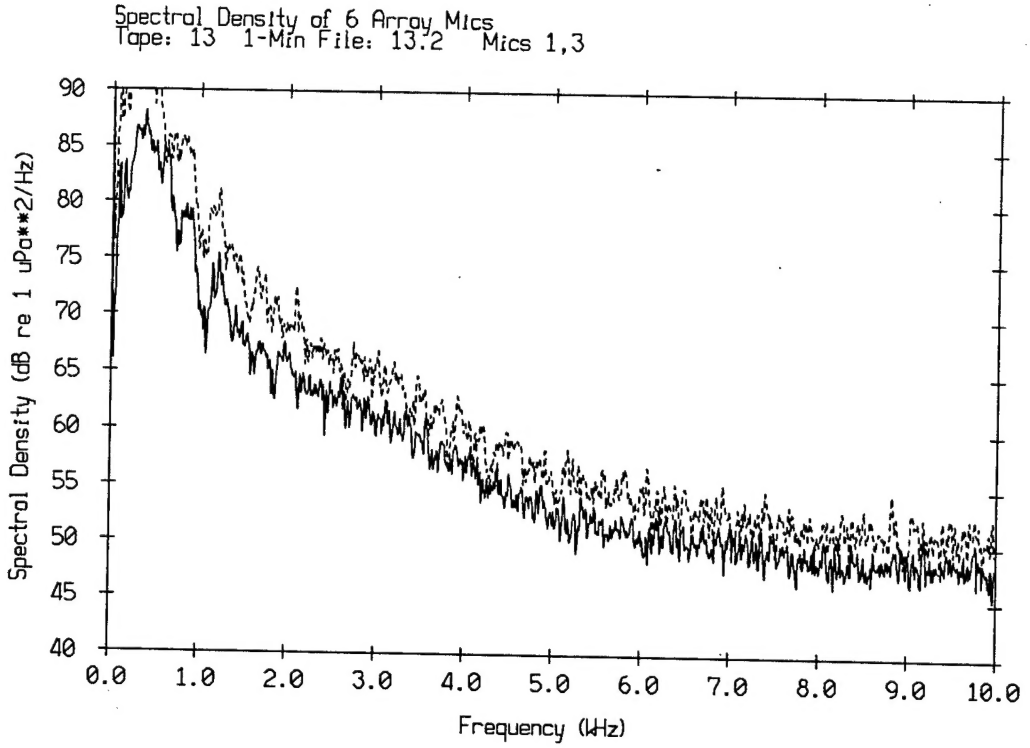
Spectrol Density of 6 Array Mics
Tape: 13 1-Min File: 13.2 Mics 1,3
Spectral Density (dB re 1 uPa**2/Hz)
90
85
80
75
70
65
60
55
50
45
40
0.0
1.0
2.0
3.0
4.0
5.0
6.0
7.0
8.0
9.0
10.0
Frequency (kHz)

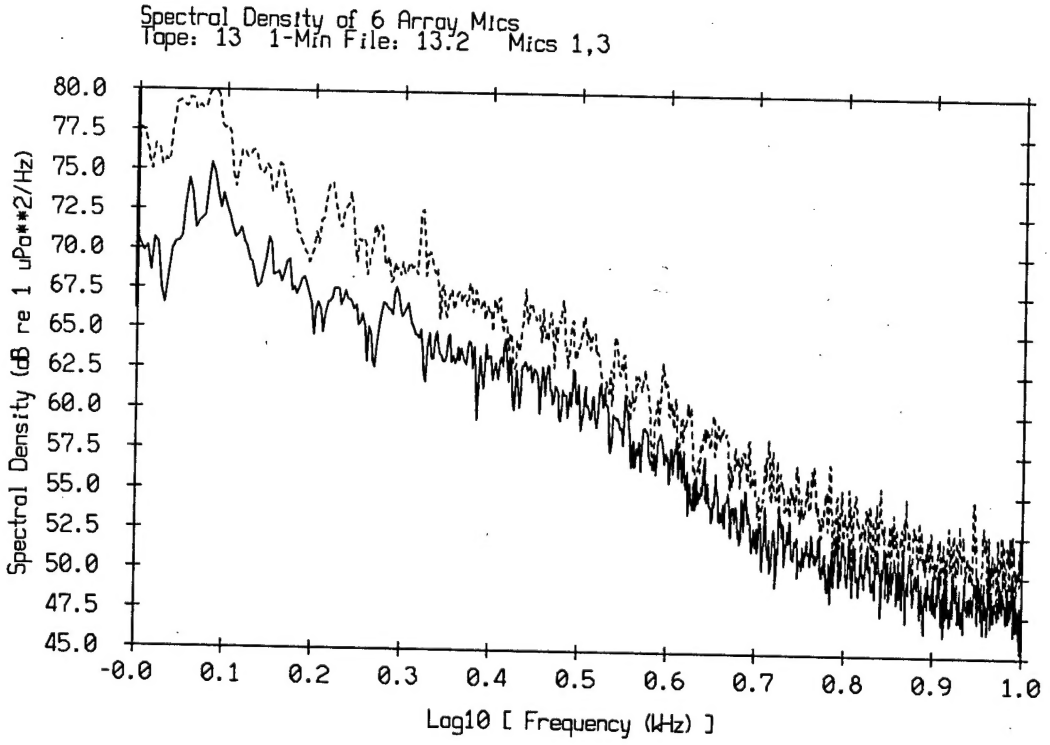
Spectrol Density of 6 Array Mics
Tape: 13 1-Min File: 13.2 Mics 1,3
Spectral Density (dB re 1 uPa**2/Hz)
80.0
77.5
75.0
72.5
70.0
67.5
65.0
62.5
60.0
57.5
55.0
52.5
50.0
47.5
45.0
-0.0
0.1
0.2
0.3
0.4
0.5
0.6
0.7
0.8
0.9
1.0
Log10 [Frequency (kHz)]

Figure IV.B.7

ONR/MPL REPORT DISTRIBUTION

Chief of Naval Research (3)
Ballston Centre Tower One
800 North Quincy Street
Arlington, VA 22217-5660
Attn: Dr. Tommy Goldsberry
Code 321US

Regional Director (1)
ONR Detachment
San Diego Regional Office
4520 Executive Drive, Suite 300
San Diego, CA 92121-3019

Commanding Officer (1)
Naval Research Laboratory
4555 Overlook Avenue, S.W.
Attn: Code 2627
Washington, D.C. 20375-5320

Defense Technical Information Center (4)
8725 John J. Kingman Road
Suite 0944
Ft Belvoir, VA 22060-6218